KARINE ADAMY

Contribution à l'étude théorique et numérique de certains systèmes de mécanique des fluides

Thèses d'Orsay, 2008

<http://www.numdam.org/item?id=BJHTUP11_2008__0745__A1_0>

UNIVERSITÉ PARIS-SUD 11

Faculté des sciences d'Orsay

N° d'ordre : 9055

UNIVERSITÉ PARIS-SUD
FACULTÉ DES SCIENCES D'ORSAY

THÈSE

présentée pour obtenir

LE GRADE DE DOCTEUR EN SCIENCES
DE L'UNIVERSITÉ PARIS XI
Spécialité : Mathématiques

par

Karine ADAMY

Sujet :

CONTRIBUTION A L'ETUDE THEORIQUE ET NUMERIQUE DE CERTAINS SYSTEMES DE MECANIQUE DES FLUIDES.

Soutenue le 23 Juin 2008 devant la Commission d'examen :

M. ALOUGES FRANÇOIS	(Examinateur)
M. BONA JERRY	(Examinateur)
M. JAUBERTEAU FRANÇOIS	(Rapporteur)
M. LAMINIE JACQUES	(Examinateur)
M. SAUT JEAN-CLAUDE	(Directeur de thèse)
M. TEMAM ROGER	(Examinateur)

Après avis des rapporteurs : M. JAUBERTEAU FRANÇOIS
M. DOUGALIS VASSILIOS

Remerciements

Je souhaite avant tout remercier mes directeurs de thèse Jean-Claude Saut et Roger Temam pour m'avoir encadrée et aidée à mener à bien ce travail.
J'adresse toute ma gratitude à Jean-Claude Saut qui m'a encadré durant ces deux dernières années pour sa sympathie et sa bonne humeur, sa disponibilité, sa motivation et ses précieux conseils ; il m'a permis de travailler dans un cadre détendu sur des problèmes intéressants et m'a soutenue dans les moments difficiles. J'ai beaucoup appris grâce à lui et ce depuis les cours de DEA et de maîtrise. Un grand merci pour tout !
Je remercie également Roger Temam pour son encadrement durant mes deux premières années de thèse. Il m'a fait partager son expérience et découvrir des thèmes de recherche variés et sa gentillesse, ses nombreux conseils et ses relectures m'ont beaucoup apportés ainsi que les séjours que j'ai effectués grâce à lui à Bloomington et qui m'ont fait découvrir les Etats-Unis.
Merci à Jacques Laminie pour m'avoir fait découvrir la programmation, pour m'avoir formée au Fortran et pour ses précieuses relectures. Ses méthodes de débuggage, son constant optimisme et son humour m'ont bien aidée.
Je remercie chaleureusement Sylvain Faure sans qui la partie numérique n'aurait pu aboutir ; ses nombreuses idées, sa motivation, sa grande disponibilité, ses conseils avisés, et son approche rigoureuse des choses m'ont été d'une grande aide.

Ma reconnaissance va ensuite à François Jauberteau et à Vassilios Dougalis pour avoir accepté de rapporter sur ma thèse et pour l'intérêt qu'ils ont porté à ce travail.
Je remercie François Alouges pour avoir accepté d'être membre de mon jury et pour ses conseils, son soutien et son enthousiasme, qui depuis la maîtrise, m'ont toujours poussé vers l'avant.
Un grand merci à Jerry Bona pour m'avoir fait l'honneur de faire partie de mon jury.

Je souhaite remercier toute l'équipe d'Analyse Numérique et Equations aux Dérivées Partielles d'Orsay qui m'a accueilli, spécialement Patrick Gérard. Merci à Catherine Poupon, Valérie Lavigne et Danièle Le Meur pour leur gentillesse et leur efficacité. J'adresse également mes remerciements aux personnes que j'ai pu côtoyer autour du bureau 256 parmi lesquels Adeline, Aline, Assia, Christine, Juliette, Ludovic, Madalina, Makram, Mahdi et aux doctorants du bâtiment 430 pour leur soutien et l'ambiance sympathique qu'ils ont créée.

Un grand merci à Fabien : sans son aide sincère et son soutien permanent cette thèse n'aurait pu voir le jour. Je suis enfin très reconnaissante envers mes parents et ma soeur Monique pour leur affection, leur présence et leurs encouragements pendant toutes ces années d'étude. Merci également pour tout cela à la famille Marchand. Merci enfin à Lynn Hill, à tous les amis grimpeurs et autres qui m'ont distrait des mathématiques ; à tous ceux que j'oublie et qui je l'espère ne m'en voudront pas...

Table des matières

1 Introduction **7**

1.1 Présentation des systèmes étudiés 8

1.1.1 Les équations de Saint Venant 8

1.1.2 Le système de Boussinesq 11

1.2 Présentation des travaux réalisés 13

1.2.1 Existence de solutions pour le système de Boussinesq sur la demi-droite ou sur intervalle fini 13

1.2.2 Un problème aux limites pour le système de Saint Venant linéarisé 15

1.2.3 Une méthode multi-niveaux pour la résolution numérique du système de Saint Venant 16

2 Existence de solutions pour un système de Boussinesq sur la demi droite et sur un intervalle fini **21**

2.1 Introduction 22

2.2 Local existence for the regularized system 23

2.3 A priori estimates and consequences 24

2.4 Existence of Solutions for the Boussinesq System with Smooth Data 28

2.5 Existence of Solutions to the Boussinesq System 36

2.6 The Boundary Value Problem with a non homogeneous boundary condition . . . 39

2.7 The Boundary Value Problem on [0,1]. 42

2.8 Uniqueness of smooth solutions 43

2.9 Appendix : regularity of solutions 44

2.9.1 Proof of the estimates 45

2.9.2 Regularity of the solutions 48

3 Sur les équations de Saint Venant avec périodicité dans une direction **51**

3.1 Introduction 52

3.2 Functionnal framework and notations 52

3.3 Reminders 55

3.4 Proof of the main results 57

3.4.1 Positiveness of A 57

3.4.2 Positiveness of the adjoint of A 59

3.5 Well-posedness of the problem 61

3.6 The periodic case 61

3.6.1 Positiveness 62
3.6.2 Surjectivity 62

4 Une méthode multi-niveaux pour la résolution des équations de Saint Venant 67
4.1 Introduction 68
4.2 Presentation of the problem 69
4.3 The multilevel method 71
4.3.1 Incremental unknowns 72
4.3.2 Multilevel scheme 75
4.3.3 Central-upwind schemes 77
4.4 Numerical simulations 79
4.4.1 Analytical solutions 79
4.4.2 A turbulence model 94
4.4.3 Concluding remarks 110
4.5 Appendix 110

Chapitre 1

Introduction

L'objet de cette thèse est de fournir une contribution à l'étude théorique et numérique de deux systèmes de mécanique des fluides décrivant la propagation d'ondes de surface : le système de Saint Venant (ou shallow water) et un système de type Boussinesq. Du point de vue numérique il s'agit plus particulièrement d'expérimenter l'utilisation d'une méthode de résolution multi-niveaux pour un système hyperbolique tel que le système de Saint Venant.

1.1 Présentation des systèmes étudiés

1.1.1 Les équations de Saint Venant

Présentation du système

Le système de Saint Venant a été introduit en 1871 dans [24] et décrit des écoulements en eau peu profonde ou plus généralement pour lesquels la longueur d'onde caractéristique du mouvement est grande comparée à la profondeur moyenne. Ce système est utilisé pour modéliser de nombreux phénomènes physiques : écoulements dans des rivières ou baies peu profondes, transport de polluants, flux atmosphériques ou océaniques, ruptures de barrages, tsunamis...
Nous nous intéressons dans cette thèse à sa version bidimensionnelle qui s'écrit :

$$\begin{cases} \dfrac{\partial h}{\partial t} + \dfrac{\partial hu}{\partial x} + \dfrac{\partial hv}{\partial y} = 0, \\ \dfrac{\partial h\mathbf{u_H}}{\partial t} + div(h\mathbf{u_H} \otimes \mathbf{u_H}) + \dfrac{g}{2}\nabla h^2 = 0. \end{cases} \tag{1.1}$$

où $\mathbf{u_H} = (\mathbf{u}, \mathbf{v})$ est la vitesse horizontale du fluide, h la hauteur d'eau totale, g la constante de gravité, en supposant que le fond est plat. Il est possible d'y introduire d'autres termes (force de Coriolis, termes de frottement) suivant les phénomènes physiques spécifiques que l'on souhaite prendre en compte.
Les équations de Saint Venant constituent un système strictement hyperbolique non linéaire de lois de conservation du premier ordre dans les zones où $h \neq 0$. En effet ce système s'écrit sous forme conservative :

$$\frac{\partial \mathbf{Q}}{\partial t} + \frac{\partial F(\mathbf{Q})}{\partial x} + \frac{\partial G(\mathbf{Q})}{\partial y} = 0.$$

où $\mathbf{Q} = (h, q_u, q_v)$ est le vecteur des variables conservatives si $q_u = uh$ et $q_v = vh$, et où

$$F(\mathbf{Q}) = \begin{pmatrix} q_u \\ \frac{q_u^2}{h} + \frac{gh^2}{2} \\ \frac{q_u q_v}{h} \end{pmatrix}, \; G(\mathbf{Q}) = \begin{pmatrix} q_v \\ \frac{q_u q_v}{h} \\ \frac{q_v^2}{h} + \frac{gh^2}{2} \end{pmatrix}, \tag{1.2}$$

Nous pouvons encore l'écrire :

$$\frac{\partial \mathbf{Q}}{\partial t} + A_x(\mathbf{Q})\frac{\partial \mathbf{Q}}{\partial x} + A_y(\mathbf{Q})\frac{\partial \mathbf{Q}}{\partial y} = 0.$$

où A_x et A_y sont les matrices :

$$A_x(\mathbf{Q}) = \begin{pmatrix} 0 & 1 & 0 \\ \frac{-q_u^2}{h^2} + gh & \frac{2q_u}{h} & 0 \\ \frac{-q_u q_v}{h^2} & \frac{q_v}{h} & \frac{q_u}{h} \end{pmatrix}, \quad A_y(\mathbf{Q}) = \begin{pmatrix} 0 & 0 & 1 \\ \frac{-q_u q_v}{h^2} & \frac{q_v}{h} & \frac{q_u}{h} \\ \frac{-q_v^2}{h^2} + gh & 0 & \frac{2q_v}{h} \end{pmatrix}$$

Pour tout vecteur $\xi \in \mathbb{R}^2$, dès que h est non nul, la matrice $A(\xi) = \xi_x A_x(\mathbf{Q}) + \xi_y A_y(\mathbf{Q})$ admet les trois valeurs propres réelles distinctes :

$$\lambda_1(\xi) = \xi_x u + \xi_y v + \sqrt{gh}, \quad \lambda_2(\xi) = \xi_x u + \xi_y v, \quad \lambda_3(\xi) = \xi_x u + \xi_y v - \sqrt{gh}$$

ce qui rend le système strictement hyperbolique (voir [26]).

Dérivation des équations

Nous rappelons ici comment sont obtenues formellement les équations de Saint Venant par intégration verticale des équations d'Euler (voir [30], [21], [27]). Nous considérons un fluide non visqueux incompressible irrotationnel dans un champ gravitationnel constant ; le mouvement du fluide est alors régi par les équations d'Euler :

$$\frac{\partial \mathbf{U}}{\partial t} + (\mathbf{U}.\nabla \mathbf{U}) = -\frac{1}{\rho}\nabla p - g\mathbf{j} \tag{1.3}$$

$$\nabla.\mathbf{U} = \frac{\partial u}{\partial x} + \frac{\partial v}{\partial y} + \frac{\partial w}{\partial z} = 0, \tag{1.4}$$

où les coordonnées en espace sont notées (x, y, z), $\mathbf{j}$ est le vecteur unité dans la direction de z, $\mathbf{U} = (\mathbf{u}, \mathbf{v}, \mathbf{w})$ est le vecteur vitesse, g l'accélération de la pesanteur, ρ la densité supposée constante et p est le champ de pression du fluide.
Nous supposons ici le fond imperméable et plat, et désignons par h_0 la profondeur du fluide au repos et par $z = \eta(t, x, y)$ une paramétrisation de la surface libre du fluide à l'instant t. Les conditions aux bords sur la surface libre et sur le fond s'écrivent :

$$\frac{\partial \eta}{\partial t} + u\frac{\partial \eta}{\partial x} + v\frac{\partial \eta}{\partial y} = w \text{ en } z = \eta(t, x, y), \tag{1.5}$$

$$p = p_0 \text{ en } z = \eta(t, x, y), \tag{1.6}$$

$$w = 0 \text{ en } z = -h_0. \tag{1.7}$$

Le point clé est de faire l'approximation hydrostatique suivante dans la composante verticale de l'équation (1.3) :

$$-\frac{1}{\rho}\frac{\partial p}{\partial z} - g = 0 \tag{1.8}$$

ce qui donne

$$p - p_0 = \rho g(\eta - z).$$

Cela revient à supposer que la composante verticale de l'accélération des particules de fluide a un effet négligeable sur la pression.
Les composantes horizontales de l'équation (1.3) s'écrivent :

$$\frac{\partial \mathbf{u_H}}{\partial t} + u\frac{\partial \mathbf{u_H}}{\partial x} + v\frac{\partial \mathbf{u_H}}{\partial y} + w\frac{\partial \mathbf{u_H}}{\partial z} = -g\nabla_H \eta, \tag{1.9}$$

où $\mathbf{u_H} = (\mathbf{u}, \mathbf{v})$ et $\nabla_H = (\partial_x, \partial_y)$.
D'après (1.9), la dérivée particulaire de $\mathbf{u_H}$ est indépendante de z ; ainsi si nous supposons la vitesse horizontale $\mathbf{u_H}$ indépendante de z initialement, elle le reste et (1.9) fournit la première équation du système de Saint Venant :

$$\frac{\partial \mathbf{u_H}}{\partial t} + u\frac{\partial \mathbf{u_H}}{\partial x} + v\frac{\partial \mathbf{u_H}}{\partial y} + g\nabla_H \eta = 0. \tag{1.10}$$

En intégrant ensuite l'équation de conservation de la masse entre $z = -h_0$ et $z = \eta$, nous trouvons

$$0 = \int_{-h_0}^{\eta} (\frac{\partial u}{\partial x} + \frac{\partial v}{\partial y} + \frac{\partial w}{\partial z})dz = \frac{\partial}{\partial x}(\int_{-h_0}^{\eta} udz) + \frac{\partial}{\partial y}(\int_{-h_0}^{\eta} vdz) + [w]_{-h_0}^{\eta}$$
$$- u(z=\eta)\frac{\partial \eta}{\partial x} - v(z=\eta)\frac{\partial \eta}{\partial y}$$

Cette expression peut être simplifiée grâce aux conditions aux bords :

$$\frac{\partial}{\partial x}(\int_{-h_0}^{\eta} udz) + \frac{\partial}{\partial y}(\int_{-h_0}^{\eta} vdz) + \frac{\partial \eta}{\partial t} = 0.$$

En notant $h = h_0 + \eta$ la profondeur totale de fluide, comme u et v sont supposés indépendants de z, nous obtenons la deuxième équation du système :

$$\frac{\partial h}{\partial t} + \frac{\partial hu}{\partial x} + \frac{\partial hv}{\partial y} = 0. \tag{1.11}$$

Il reste alors à incorporer (1.11) dans (1.10) pour obtenir le système suivant :

$$\begin{cases} \dfrac{\partial h}{\partial t} + \dfrac{\partial hu}{\partial x} + \dfrac{\partial hv}{\partial y} = 0, \\ \dfrac{\partial h\mathbf{u_H}}{\partial t} + div(h\mathbf{u_H} \otimes \mathbf{u_H}) + \dfrac{g}{2}\nabla h^2 = 0. \end{cases} \tag{1.12}$$

L'erreur faite lors de l'approximation hydrostatique (1.8) est d'ordre $\mu = \frac{H^2}{L^2}$ si la longueur d'onde caractéristique de propagation horizontale des ondes est notée L et la profondeur moyenne H. Le cadre de ce modèle est celui d'un écoulement en eau peu profonde ($\mu << 1$) mais de comparativement forte amplitude ($\epsilon = A/H \sim 1$), si A désigne l'amplitude typique de l'écoulement observé). Le nombre $S = \epsilon/\mu >> 1$ appelé nombre de Stokes évalue le rapport entre effets non linéaires (mesurés par ϵ) et effets dispersifs (mesurés par μ) ; dans ce cadre, les effets dispersifs sont peu importants et l'écoulement est fortement influencé par les effets non linéaires.

1.1.2 Le système de Boussinesq

Présentation

Les travaux réalisés dans cette thèse portent sur le système de Boussinesq dit classique, dérivé par Boussinesq en 1871 dans [5] :

$$\begin{aligned} &\frac{\partial \eta}{\partial t} + \frac{\partial u}{\partial x} + \frac{\partial (\eta u)}{\partial x} = 0, \\ &\frac{\partial u}{\partial t} + \frac{\partial \eta}{\partial x} + u\frac{\partial u}{\partial x} - \frac{1}{3}\frac{\partial^3 u}{\partial x^2 \partial t} = 0. \end{aligned} \tag{1.13}$$

où u est la vitesse horizontale du fluide et η la déviation du fluide par rapport à sa position au repos. Il est possible d'obtenir en introduisant des changements de variable toute une classe de systèmes formellement équivalents à (1.13) (voir [3]) :

$$\begin{aligned} &\frac{\partial \eta}{\partial t} + \frac{\partial u}{\partial x} + \frac{\partial (\eta u)}{\partial x} + a\frac{\partial^3 u}{\partial x^3} - b\frac{\partial^3 \eta}{\partial x^2 \partial t} = 0, \\ &\frac{\partial u}{\partial t} + \frac{\partial \eta}{\partial x} + u\frac{\partial u}{\partial x} + c\frac{\partial^3 \eta}{\partial x^3} - d\frac{\partial^3 u}{\partial x^2 \partial t} = 0. \end{aligned} \tag{1.14}$$

où les paramètres a, b, c, d vérifient

$$a+b = \frac{1}{2}(\theta^2 - \frac{1}{3}) \ , \ c+d = \frac{1}{2}(1-\theta^2) \geq 0 \ , \ a+b+c+d = \frac{1}{3} \ , \ \theta \in [0,1].$$

Dans cette écriture u représente la vitesse horizontale du fluide à la hauteur θh_0, h_0 étant la hauteur de fluide au repos. Le système (1.13) correspond à $a = b = c = 0$, $d = 1/3$ et $\theta^2 = 1/3$.

Dérivation

Le système de Boussinesq (1.13) s'obtient également formellement à partir des équations d'Euler avec surface libre (1.3)-(1.7) (voir [3], [30] et [21] pour une justification mathématique rigoureuse). Par rapport au système de Saint Venant on se place ici dans le cadre d'un écoulement en eau peu profonde ($\mu << 1$) et de petite amplitude ($\epsilon << 1$) dans lequel les effets non linéaires et les effets dispersifs s'équilibrent ($S \sim 1$).
Nous reprenons ici les mêmes notations que dans la Section 1.1.1. Le champ de vitesses est supposé irrotationnel, donc il existe une fonction potentiel Φ telle que $\mathbf{U} = \nabla\Phi$. L'équation d'incompressibilité (1.4) entraîne que Φ vérifie l'équation de Laplace :

$$\Delta\Phi = 0. \tag{1.15}$$

Comme dans la Section 1.1.1, on désigne par $z = -h_0$ le fond imperméable et plat et par $z = \eta(t,x,y)$ la surface libre du fluide en contact avec l'air. L'équation de Laplace se complète donc avec les deux conditions aux limites (1.5) et (1.7) :

$$\frac{\partial \eta}{\partial t} + \frac{\partial \Phi}{\partial x}\frac{\partial \eta}{\partial x} + \frac{\partial \Phi}{\partial y}\frac{\partial \eta}{\partial y} = \frac{\partial \Phi}{\partial z} \text{ en } z = \eta(t,x,y), \tag{1.16}$$

$$\frac{\partial \Phi}{\partial z} = 0 \text{ en } z = -h_0. \tag{1.17}$$

et la condition supplémentaire suivante, conséquence de l'intégration de (1.3) en utilisant (1.6) :

$$\frac{\partial \Phi}{\partial t} + \frac{1}{2}|\nabla \Phi|^2 + gz = 0 \text{ en } z = \eta(t, x, y). \tag{1.18}$$

Nous considérons plus particulièrement le cas d'un mouvement constant dans la direction y, les équations deviennent alors :

$$\frac{\partial^2 \Phi}{\partial x^2} + \frac{\partial^2 \Phi}{\partial z^2} = 0 \text{ pour } -h_0 < z < \eta(t, x), \tag{1.19}$$

$$\frac{\partial \Phi}{\partial z} = 0 \text{ en } z = -h_0, \tag{1.20}$$

$$\frac{\partial \eta}{\partial t} + \frac{\partial \Phi}{\partial x}\frac{\partial \eta}{\partial x} = \frac{\partial \Phi}{\partial z} \text{ en } z = \eta(t, x), \tag{1.21}$$

$$\frac{\partial \Phi}{\partial t} + \frac{1}{2}\left(\frac{\partial \Phi}{\partial x}^2 + \frac{\partial \Phi}{\partial z}^2\right) + gz = 0 \text{ en } z = \eta(t, x). \tag{1.22}$$

Pour faire apparaître les différentes échelles, il est utile d' introduire les variables adimensionnées suivantes :

$$x = L\bar{x}, \quad z = h_0(\bar{z} - 1), \quad \eta = A\bar{\eta}, \quad t = L\bar{t}/c_0, \quad \Phi = gAL\bar{\Phi}/c_0,$$

avec $c_0 = \sqrt{gh_0}$. Avec ces nouvelles variables (nous omettrons les barres dans la suite par souci de simplicité), les petits paramètres ϵ et μ définis plus hauts apparaissent dans le système :

$$\mu\frac{\partial^2 \Phi}{\partial x^2} + \frac{\partial^2 \Phi}{\partial z^2} = 0 \text{ pour } 0 < z < 1 + \epsilon\eta(t, x), \tag{1.23}$$

$$\frac{\partial \Phi}{\partial z} = 0 \text{ en } z = 0, \tag{1.24}$$

$$\frac{\partial \eta}{\partial t} + \epsilon\frac{\partial \Phi}{\partial x}\frac{\partial \eta}{\partial x} = \frac{1}{\beta}\frac{\partial \Phi}{\partial z} \text{ en } z = 1 + \epsilon\eta(t, x), \tag{1.25}$$

$$\frac{\partial \Phi}{\partial t} + \frac{1}{2}\epsilon\frac{\partial \Phi}{\partial x}^2 + \frac{1}{2}\frac{\epsilon}{\mu}\frac{\partial \Phi}{\partial z}^2 + gz = 0 \text{ en } z = \eta(t, x). \tag{1.26}$$

L'étape suivante est alors de représenter formellement Φ par un développement asymptotique en z, $\Phi = \sum_{k=0}^{\infty} z^k f_k(t, x)$, qui, injecté dans l'équation de Laplace, donne :

$$(k + 2)(k + 1)f_{k+2}(t, x) = -\mu\partial_{xx} f_k(t, x), \text{ pour } k \geq 0.$$

Compte-tenu de (1.24), on a $f_1(t, x) = 0$ donc

$$f_{2k+1}(t, x) = 0, \quad k \geq 0.$$

Si $F = f_0$ représente le potentiel des vitesses en $z = 0$, nous obtenons donc

$$f_{2k}(t,x) = \frac{(-1)^k}{(2k)!}\frac{\partial^{2k}F}{\partial x^{2k}}\mu^k,$$

soit,

$$\Phi = \sum_{k=0}^{\infty}(-1)^k\frac{z^{2k}}{(2k)!}\frac{\partial^{2k}F}{\partial x^{2k}}\mu^k.$$

Nous reportons alors cette dernière expression avec $z = \eta(t,x)$ dans les deux dernières équations (1.25) et (1.26) en ne gardant que les termes d'ordre 1 en ϵ et μ pour obtenir :

$$\frac{\partial\eta}{\partial t} + \frac{\partial((1+\epsilon\eta)u)}{\partial x} - \frac{1}{6}\mu\frac{\partial^3 u}{\partial x^3} = \mathcal{O}(\epsilon\mu,\mu^2), \tag{1.27}$$

$$\frac{\partial u}{\partial t} + \epsilon u\frac{\partial u}{\partial x} + \frac{\partial\eta}{\partial x} - \frac{1}{2}\mu\frac{\partial^3}{\partial x^2\partial t}u = \mathcal{O}(\epsilon\mu,\mu^2). \tag{1.28}$$

où $u(t,x) = \dfrac{\partial F(t,x)}{\partial x}$ représente la vitesse horizontale au fond $z = 0$. Il suffit ensuite d'introduire les nouvelles variables $x = \mu^{1/2}\tilde{x}$, $t = \mu^{1/2}\tilde{t}$, $\eta = \epsilon^{-1}\tilde{\eta}$, $w = \epsilon^{-1}\tilde{w}$ pour retrouver exactement le système (1.13).
Remarquons que cette méthode permet également de dériver les équations de Saint Venant, en effet négliger les termes d'ordre μ en ne gardant que les termes d'ordre ϵ conduit au système de Saint Venant en dimension un.

1.2 Présentation des travaux réalisés

1.2.1 Existence de solutions pour le système de Boussinesq sur la demi-droite ou sur intervalle fini

Parmi les systèmes de la forme (1.14), l'existence globale de solutions au problème de Cauchy sur $\mathbb{R}$ a été démontrée uniquement dans le cas hamiltonien où $b = d$, $a \leq 0$, $c < 0$ (dans [4]) et pour le système (1.13) dans [25]. Pour les autres systèmes de cette forme, seuls des résultats d'existence locale ont pu être obtenus (voir [3], [4]).
Dans ce chapitre nous nous intéressons à la résolution du problème aux limites pour le système de Boussinesq (1.13) sur $\mathbb{R}^+$ ou sur un intervalle fini de la forme $[0,L]$, plus particulièrement $[0,1]$ pour simplifier les notations. Dans cette partie la hauteur de la surface libre du fluide est notée ρ.
Dans [25], M. Schonbek montre l'existence de solutions faibles au problème de Cauchy en employant une régularisation parabolique de l'équation portant sur la hauteur d'eau ; elle construit une entropie pour la partie hyperbolique du système et obtient ainsi une estimation a priori sur les solutions du problème régularisé qui constitue le point de départ pour la preuve de l'existence globale de solutions. Elle démontre le résultat suivant :

Théorème 1.2.1. *Soient $(\rho_0, u_0 - \bar{u}) \in \Lambda_{\sigma_0} \times H^1$ avec $u_0 - \bar{u}$, $\rho_0 - \bar{\rho}$ à support compact (où $\bar{\rho}, \bar{u}$ sont des constantes réelles) et $\inf_{x\in\mathbb{R}}(1+\rho_0)(x) > 0$. Alors il existe une solution (ρ, u) du système (1.13) telle que $(\rho, u - \bar{u}) \in L^\infty(\mathbb{R}^+; \Lambda_{\sigma_0} \times H^1)$.*

Ici Λ_{σ_0} désigne un espace de Orlicz basé sur la fonction convexe positive σ_0 telle que

$$\sigma_0(\rho) = (1+\rho)(\log(1+\rho) - \log(1+\bar{\rho})) + \bar{\rho} - \rho$$

En effet Λ_{σ_0} est défini par $\Lambda_{\sigma_0} = \left\{\rho;\ \int_{\mathbb{R}^+} \sigma_0(1+\rho)(x)dx < \infty\right\}$.
Nous reprenons ici la méthode proposée dans [25] pour obtenir l'existence de solutions aux problemes aux limites sur $\mathbb{R}^+$ ou sur $[0, L]$ pour (1.13).

Pour le problème aux limites homogène sur $\mathbb{R}^+$ le résultat est le suivant :

Théorème 1.2.2. *Soient $(\rho_0, u_0) \in \Lambda_{\sigma_0} \times H_0^1(\mathbb{R}^{+*})$ vérifiant :*
- $\inf_{x\in\mathbb{R}^+}(1+\rho_0(x)) > 0$
- *il existe $L > 0$ tel que $\rho_0(x) = 0$ pour presque tout $x \geq L$.*

Alors il existe une solution (ρ, u) du système (1.13) avec la donnée initiale (ρ_0, u_0) vérifiant la condition aux limites $u(t, 0) = 0$ pour presque tout $t > 0$.
De plus (ρ, u) appartient à $L^\infty(\mathbb{R}^+; \Lambda_{\sigma_0} \times H_0^1)$.

Nous présentons également un résultat pour le problème aux limites non homogène :

Théorème 1.2.3. *Soient $g \in C^1(\mathbb{R}^+)$ et $T > 0$; soient $(\rho_0, u_0) \in \Lambda_{\sigma_0} \times H_0^1(\mathbb{R}^{+*})$ vérifiant :*
- $\inf_{x\in\mathbb{R}^+}(1+\rho_0(x)) > 0$
- *il existe $L > 0$ tel que $\rho_0(x) = 0$ pour presque tout $x \geq L$.*

et la condition de compatibilité $u_0(0) = g(0)$.
Alors il existe une solution (ρ, u) du système (1.13) avec la donnée initiale (ρ_0, u_0) vérifiant la condition aux limites $u(t, 0) = g(t)$ pour presque tout $t \in [0, T]$.
De plus (ρ, u) appartient à $L^\infty(\mathbb{R}^+; \Lambda_{\sigma_0} \times H^1)$.

Sur l'intervalle $[0, 1]$, nous obtenons la version suivante :

Théorème 1.2.4. *Soient $(\rho_0, u_0) \in \Lambda_{\sigma_0} \times H_0^1(0, 1)$ vérifiant $\inf_{x\in[0,1]}(1+\rho_0(x)) > 0$.*
Alors il existe une solution (ρ, u) du système (1.13) avec la donnée initiale (ρ_0, u_0), vérifiant les conditions aux limites $u(t, 0) = u(t, 1) = 0$ pour presque tout $t > 0$.
De plus (ρ, u) appartient à $L^\infty(\mathbb{R}^+; \Lambda_{\sigma_0} \times H_0^1(0, 1)) \subset L^\infty(\mathbb{R}^+; L^1(0, 1) \times H_0^1(0, 1))$.

Notons que la condition portant sur $\inf_{x\in\mathbb{R}^+}(1+\rho_0(x)) > 0$ est cohérente du point de vue physique puisque $1 + \rho$ représente ici la hauteur d'eau totale.
Les problèmes aux limites étudiés font tous intervenir une condition aux limites portant sur la vitesse du fluide u. Dans [16], les auteurs s'intéressent aux problèmes aux limites pour le système de Boussinesq linéarisé sur $\mathbb{R}^+$ et sur $[0, 1]$ en considérant des données initiales régulières. Ils démontrent que les conditions aux bords rendant le problème bien posé sur $\mathbb{R}^+$ (respectivement $[0, 1]$) sont $u(t, 0) = 0$, $\rho(t, 0) = 0$ ou $u_x(t, 0) = 0$ (respectivement $u(t, 0) = u(t, 1) = 0$, $\rho(t, 0) = \rho(t, 1) = 0$ ou $u_x(t, 0) = u_x(t, 1) = 0$). La méthode présentée ici ne semble pas pouvoir fonctionner avec des conditions portant sur ρ ou u_x.

Dans [1], C. Amick étudie la régularité et l'unicité des solutions faibles de M. Schonbek pour le problème de Cauchy : pour des données C^∞ à support compact, il montre que les solutions

faibles de [25] sont infiniment différentiables sur $\mathbb{R}^+ \times \mathbb{R}$. Dans la suite de ce chapitre nous présentons un résultat d'unicité pour des solutions au problème aux limites sur $\mathbb{R}^+$ continues en temps et à valeurs dans $H^2(\mathbb{R}^{+*}) \times H^2(\mathbb{R}^{+*})$.
Enfin, suivant [1], nous terminons par une preuve de la persistance de régularité finie pour les solutions au problème de Cauchy ; ce résultat est démontré sur $\mathbb{R}$ et ne semble pas pouvoir se généraliser à $\mathbb{R}^+$ en raison de l'apparition de termes de bords gênants ;

Théorème 1.2.5. *Soient $\bar{\rho}$ et $\bar{u}$ deux constantes données et soient $(\rho_0 - \bar{\rho}, u_0 - \bar{u}) \in H^1(\mathbb{R}) \times H^2(\mathbb{R})$ avec support compact, et $(\rho_0, u_0 - \bar{u}) \in \Lambda_{\sigma_0} \times H^1_0$, vérifiant $1 + \rho_0 > 0$; soit $T > 0$.*
Alors il existe une unique solution (ρ, u) au système de Boussinesq (1.13) dans $L^\infty(0, T, H^1(\mathbb{R}) \times H^2(\mathbb{R}))$ avec donnée initiale (ρ_0, u_0).

1.2.2 Un problème aux limites pour le système de Saint Venant linéarisé

Ce chapitre porte sur l'étude d'un problème aux limites pour les équations de Saint Venant bidimensionnelles linéarisées. Le système de Saint Venant linéarisé autour d'un état constant (u_0, v_0, h_0) s'écrit :

$$\begin{cases} \dfrac{\partial u}{\partial t} + u_0 \dfrac{\partial u}{\partial x} + v_0 \dfrac{\partial u}{\partial y} + \dfrac{\partial \Phi}{\partial x} - fv = F_1, \\ \dfrac{\partial v}{\partial t} + u_0 \dfrac{\partial v}{\partial x} + v_0 \dfrac{\partial v}{\partial y} + \dfrac{\partial \Phi}{\partial y} + fu = F_2, \\ \dfrac{\partial \Phi}{\partial t} + u_0 \dfrac{\partial \Phi}{\partial x} + v_0 \dfrac{\partial \Phi}{\partial y} + \Phi_0 (\dfrac{\partial u}{\partial x} + \dfrac{\partial v}{\partial y}) = F_3, \end{cases} \tag{1.29}$$

où $\Phi_0 = gh_0$ et où $F = (F_1, F_2, F_3)$ désigne un terme source introduit ici par souci de généralité mathématique.
Ici u et v désignent les composantes horizontales de la vitesse du fluide, $\Phi = g\eta$ si η représente la déviation de la surface libre, et nous avons introduit ici un terme prenant en compte l'action de la force de Coriolis de magnitude notée f. Sous cette forme ce système est utilisé pour modéliser des phénomènes météorologiques (voir [22], [23]).

Le domaine sur lequel nous nous plaçons est un rectangle $\mathcal{M} = [0, L_1] \times [0, L_2]$; nous considérons des conditions aux limites périodiques dans la direction y et nous déterminons des conditions de Dirichlet dans la direction x qui rendent le problème bien posé. Nous traitons principalement le cas d'un régime sous critique (tel que $u_0^2 + v_0^2 < gh_0$) où il existe des ondes se propageant dans les deux directions selon x en précisant là où elles ont lieu les différences avec le cas surcritique (tel que $u_0^2 + v_0^2 > gh_0$).

Un changement de variables adéquat permet de symétriser le système et de le diagonaliser dans la direction x : on pose

$$\begin{pmatrix} \xi \\ \zeta \\ \eta \end{pmatrix} = \begin{pmatrix} 1 & 0 & \frac{1}{\sqrt{\Phi_0}} \\ 0 & \frac{1}{\sqrt{2}} & 0 \\ 1 & 0 & -\frac{1}{\sqrt{\Phi_0}} \end{pmatrix} \begin{pmatrix} u \\ v \\ \Phi \end{pmatrix}$$

Avec les nouvelles variables $k = v_0\xi + \sqrt{\frac{\Phi_0}{2}}\zeta$, $\ell = v_0\xi + \sqrt{\frac{\Phi_0}{2}}(\xi - \eta)$, $m = v_0\xi - \sqrt{\frac{\Phi_0}{2}}\zeta$, et en introduisant les notations suivantes :

$$\begin{cases} A_\xi U = \overline{u_0}\xi_x + k_y, \\ A_\zeta U = u_0\zeta_x + \ell_y, \\ A_\eta U = \underline{u_0}\eta_x + m_y, \end{cases} \quad \text{et} \quad \begin{cases} \gamma_\xi U = \overline{u_0}\xi n_x + k n_y, \\ \gamma_\zeta U = u_0\zeta n_x + \ell n_y, \\ \gamma_\eta U = \underline{u_0}\eta n_x + m n_y. \end{cases}$$

où $\overline{u_0} = u_0 + \sqrt{\Phi_0}$ et $\underline{u_0} = u_0 - \sqrt{\Phi_0}$, nous pouvons définir l'espace

$$\begin{aligned} D(A) = \{ U = (\xi, \zeta, \eta) \in L^2(\mathcal{M})^3 \,/ & A_\xi U,\, A_\zeta U,\, A_\eta U \in L^2(\mathcal{M}) \text{ et} \\ & \gamma_\xi U(0,y) = \gamma_\zeta U(0,y) = \gamma_\eta U(L_1,y) = 0 \text{ pour p.t. y dans } (0,L_2), \\ & \gamma_\xi U(x,0) = -\gamma_\xi U(x,L_2),\ \gamma_\zeta U(x,0) = -\gamma_\zeta U(x,L_2), \\ & \gamma_\eta U(x,0) = -\gamma_\eta U(x,L_2) \text{ pour p.t. x dans } (0,L_1)\}. \end{aligned}$$

Nous utilisons ensuite la théorie des semi-groupes pour démontrer que le problème est bien posé dans cet espace :

Theorem 1.2.1. *Soit $U_0 \in D(A)$ et $T > 0$; soit $F \in L^1([0,T]; L^2(\mathcal{M})^3)$. Alors il existe une unique solution U du système (1.29) avec la donnée initiale U_0 et $U \in L^\infty(0,T; D(A)) \cap C([0,T]; L^2(\mathcal{M})^3)$.*

Une étude du cas périodique dans les deux directions est également présentée.

1.2.3 Une méthode multi-niveaux pour la résolution numérique du système de Saint Venant

Le but de ce chapitre est d'étudier l'efficacité d'une méthode multi-niveaux basée sur un schéma volumes finis pour la résolution des équations de Saint Venant (1.1) en dimension deux. Les méthodes multi-niveaux permettent de modéliser des phénomènes complexes faisant intervenir plusieurs échelles de grandeur (comme la turbulence par exemple) en traitant différement les petites et les grandes échelles ; le but est de fournir une description correcte du problème, ceci avec un temps de calcul réduit. Les méthodes auxquelles nous nous intéressons font intervenir le concept d'inconnues incrémentales, introduit dans [28] dans le cadre des différences finies. Le principe est de décomposer les inconnues du problème en plusieurs composantes (une composante y représentant les grandes échelles et une composante z représentant les petites échelles pour un calcul à deux niveaux) que l'on désigne par inconnues incrémentales. Des discrétisations spécifiques sont ensuite appliquées à ces différentes composantes dans le but d'améliorer la performance du schéma (temps de calcul, stabilité ou autre). Ces méthodes ont été largement développées pour la discrétisation d'équations ou de systèmes paraboliques ou elliptiques, mais aucune étude de ce type pour des systèmes purement hyperboliques ne semble encore avoir été réalisée. Pour un aperçu de l'étude de ces méthodes pour des problèmes elliptiques ou paraboliques dans le contexte de discrétisations par différences finies, éléments finis, méthodes spectrales ou ondelettes, voir les nombreuses références [6]-[13]. Dans [13], est étudiée la performance de divers schémas multi-niveaux (basés sur une discrétisation par méthodes

spectrales) sur le système de Saint Venant auquel est ajouté un opérateur hyperdissipatif, pour la simulation de phénomènes de turbulence dans des écoulements atmosphériques ou océaniques. Dans [14] les auteurs s'intéressent à l'implantation d'une méthode multi-niveaux par volumes finis pour la simulation des équations de Burgers visqueuses. Lorsque la discrétisation spatiale est faite à l'aide de méthodes spectrales ou d'ondelettes les inconnues incrémentales ont une signification physique dans la mesure où elles représentent réellement les petites ou grande échelles des inconnues. Dans notre travail comme dans [14], les inconnues incrémentales y et z que nous considérons résultent d'une décomposition purement algébrique des inconnues basée sur les propriétés du développement de Taylor ; nous montrons cependant que z est d'ordre h^2 où h est le pas d'espace de la discrétisation et que y a le même ordre de grandeur que l'inconnue de départ ; de plus la décomposition proposée aura l'avantage important de préserver la conservativité du schéma.

La discrétisation spatiale par volumes finis est particulièrement adaptée au caractère système de lois de conservation hyperboliques du système de Saint Venant. Nous basons ici notre méthode multi-niveaux sur des schémas upwind-centrés qui ont été développés pour ce type de systèmes. Le caractère upwind de ces schémas les rend robustes, de plus ils ne nécessitent pas la résolution de problèmes de Riemann ce qui les rend relativement simples à utiliser et permettent de travailler sur des grilles non décalées. La construction et les propriétés de ces schémas sont détaillées dans [17]-[20].

Dans les simulations numériques, le domaine de calcul est un carré de taille $L_x \times L_y$ et nous considérons le cas de conditions aux limites périodiques. Dans un premier temps nous nous sommes attachés à tester notre méthode multi-niveaux à deux niveaux sur la résolution d'un problème analytique en ajoutant un terme source aux équations : nous partons d'une donnée initiale périodique et comparons la solution calculée par le code multi-niveaux avec la solution exacte qui est connue. La méthode multi-niveaux permet de minimiser le temps de calcul tout en conservant une erreur petite. Elle présente donc le grand intérêt de permettre d'effectuer des simulations rapides sur des grilles comportant un grand nombre de points (grâce au gain en temps de calcul) tout en rendant des solutions correctes. Plus le nombre d'itérations passées au niveau grossier est important, plus la résolution est rapide ; cependant passer un trop grand nombre d'iterations au niveau grossier fait perdre en précision. Il faut donc traiter avec ces deux aspects et passer suffisament de temps au niveau fin pour garantir une meilleure résolution qu'au niveau grossier.
Dans un deuxième temps nous testons la méthode sur des données intiales tirées de [13] et qui modélisent un écoulement turbulent. Dans ce cas physique la méthode se révèle également performante, nous comparons ici les solutions obtenues avec des solutions de référence qui sont calculées préalablement par une résolution à un niveau avec un très grand nombre de volumes de discrétisation. Nous vérifions également la conservation de la norme L^1 de la hauteur d'eau (qui est ici positive).
Dans un troisième temps nous présentons les résultats obtenus avec une résolution sur trois niveaux de grille. La méthode révèle dans ce cas sa plus grande efficacité : en effet on obtient une résolution précise du problème avec un gain de temps de calcul assez important par rapport au calcul à un niveau sur la grille fine. La récursivité de la méthode permet également d'utiliser

si besoin plus de trois niveaux de discrétisations.

Bibliographie

[1] C. J. Amick, Regularity and uniqueness of solutions to the boussinesq system of equations, *J. Diff. Eq., 54*, 1984.

[2] E. Audusse, M. O. Bristeau, Transport of pollutant in shallow water, a two time steps kinetic method, *M2AN Math. Model. Num. Anal., 37, no. 2*, 2003.

[3] J. Bona, M. Chen, J. C. Saut, Boussinesq Equations and Other Systems for Small-amplitude Long Waves in Nonlinear Dispersive Media I : Derivation and Linear Theory, *J. Nonlinear Sci. 12, no. 4*, 2002.

[4] J. Bona, M. Chen, J. C. Saut, Boussinesq Equations and Other Systems for Small-amplitude Long Waves in Nonlinear Dispersive Media II : The nonlinear theory, *Nonlinearity 17,*, 2004.

[5] J. V. Boussinesq, Théorie générale des mouvements qui sont propagés dans un canal rectangulaire horizontal, *C. R. Acad. Sci. Paris 73*, 1871.

[6] C. Calgaro, J. Laminie, R. Temam, Dynamical multilevel schemes for the solution of evolution equations by hierarchical finite element discretization *Appl. Numer. Math. 23(4)*, 1997.

[7] J. P. Chehab, Incremental unknowns method and compact schemes *RAIRO Model. Math. Anal. Num. 32(1)*, 1998.

[8] M. Chen, R. Temam, Incremental unknowns for solving partial differential equations *Numer. Math. 59*, 1991.

[9] M. Chen, R. Temam, Incremental unknowns in finite differences : condition number of the matrix *SIAM J. Matrix Anal. Appl. 14(2)*, 1993.

[10] A. Debussche, J. Laminie, E. Zahrouni, A dynamical multi-level scheme for the Burgers equation : wavelet and hierarchical finite element *J. Sci. Comput. 25(3)*, 2005.

[11] T. Dubois, F. Jauberteau, R. Temam, Dynamic multilevel methods and the numerical simulation of turbulence *Cambridge University Press, Cambridge*, 1999.

[12] T. Dubois, F. Jauberteau, R. Temam, Incremental unknowns, multilevel methods and the numerical simulation of turbulence *Comput. Methods Appl. Mech. Engrg. 159(1-2)*, 1998.

[13] T. Dubois, F. Jauberteau, R. Temam, J. Tribbia, Multilevel schemes for the shallow water equations *J. Comput. Phys. 207*, 2005.

[14] S. Faure, J. Laminie, R. Temam, Finite volume discretization and multilevel methods in flow problems, *J. Sci. Comput., 25(1-2)* , 2005.

[15] S. Faure, Méthodes de volumes finis et multiniveaux pour les équations de Navier-Stokes, de Burgers et de la chaleur, *Thèse de Doctorat.*

[16] A. S. Fokas, B. Pelloni, Boundary Value Problems for Boussinesq Type Systems, *Math. Phys., Anal. Geom. 8*, 2005.

[17] A. Kurganov, E. Tadmor, New high-resolution central schemes for nonlinear conservation laws and convection-diffusion equations, *J. Comput. Phys. 160*, 2000.

[18] A. Kurganov, G. Petrova, A third-order semi-discrete genuinely multidimensionnal central scheme for hyperbolic conservation laws and related problems *Numer. Math. 88*, 2001.

[19] A. Kurganov, S. Noelle, G. Petrova, Semidiscrete central upwind schemes for hyperbolic conservation laws and Hamilton-Jacobi equations, *SIAM J. Sci. Comput. 23, no3*, 2001.

[20] A. Kurganov, D. Levy, Central-upwind schemes for the Saint-Venant system,*M2AN, Vol.36, no3*, 2002.

[21] D. Lannes, Modélisation des ondes de surface et justification mathématique, *Ecole d'été Théorie mathématique des ondes non linéaires dispersives*, 2005.

[22] A. McDonald. A step toward transparent boundary conditions for meteorological models. *Monthly Weather Review*, 130 :140–151, 2001.

[23] A. McDonald. Transparent boundary conditions for the shallow-water equations : testing in a nested environment. *Monthly Weather Review*, 131 :698–705, 2002.

[24] A. J. C. de Saint Venant, Théorie du mouvement non permanent des eaux, avec application aux crues des rivières et à l'introduction des marées dans leur lit, *C. R. Acad. Sci. Paris, 73*, 1871.

[25] M. E. Schonbek, Existence of solutions for the Boussinesq system of equations, *J. Differential Equations*, 42, 1981, no. 3, 325–352.

[26] D. Serre, Systèmes hyperboliques de lois de conservation, I et II,*Diderot, Paris*, 1996.

[27] J. J. Stoker, Water waves, the mathematical theory with applications, *Wiley*, 1985.

[28] R. Temam, Inertial manifolds and multigrid methods *SIAM J. Math. Anal., 21(1)*, 1990.

[29] R. Temam, Multilevel methods for the simulation of turbulence. A simple model *J. Comput. Phys., 127(2)*, 1996.

[30] G. B. Whitham, Linear and non linear waves, *Wiley and Sons Inc., New York*, 1999.

Chapitre 2

Existence de solutions pour un système de Boussinesq sur la demi droite et sur un intervalle fini

Soumis pour publication.

K. ADAMY*
*Laboratoire de Mathématiques, Université Paris-Sud
CNRS UMR 8628, 91405, Orsay, France.

Abstract : The initial boundary-value problem for a Boussinesq system is studied on the half line and on a finite interval. Global existence of weak solutions satisfying the boundary conditions is proven and uniqueness for solutions in a suitable class is studied. A proof of the persistence of finite regularity for solutions in the whole space is also presented.

2.1 Introduction

We are concerned with the study of Boussinesq systems of the form :

$$\begin{aligned}&\rho_t + u_x + (\rho u)_x + a u_{xxx} - b\rho_{xxt} = 0,\\ &u_t + \rho_x + uu_x + c\rho_{xxx} - du_{xxt} = 0.\end{aligned}$$

These systems are a first order approximation to the Euler equations in the case where the non linear and dispersive effects are of the same order, ([2], [3], [5], [15]). The classical Boussinesq system corresponds to $a = 0$, $b = 0$, $c = 0$, $d = 1/3$. It was proposed by Boussinesq to model the two way propagation of surface waves in a channel of constant depth which are of small amplitude and of long wavelength.
We will study in particular the system :

$$\begin{aligned}&\rho_t + u_x + (\rho u)_x = 0,\\ &u_t + \rho_x + uu_x - u_{xxt} = 0.\end{aligned} \tag{2.1}$$

Here $u(t,x)$ represents the horizontal velocity and $w(t,x) = 1 + \rho(t,x)$ the height of the free surface of the fluid above the bottom.
In [14], the well-posedness for the 1D-Cauchy problem for this system is proven, using a parabolic regularization. Here, we adapt the method used in [14] to show the existence of a solution for the initial boundary value problem on the semi-infinite space with the following initial and boundary conditions :

$$\begin{cases} \rho(0,x) = \rho_0(x) \ \ \forall x \in \mathbb{R}^+, \\ u(0,x) = u_0(x) \ \ \forall x \in \mathbb{R}^+, \\ u(t,0) = 0 \ \ \forall t \geq 0. \end{cases} \tag{2.2}$$

We then examine the case of a non homogeneous boundary condition $u(t,0) = g(t)$, and present the most important aspects of the proof on a finite interval.. A study of the appropriate boundary conditions that give a well-posed problem for the linearised system and for smooth data, either on the half line, or on a finite interval was made in [9]. Here we restrict ourselves to boundary conditions that involve u.

In Section 2.2, we show that the regularized system has a unique smooth solution satisfying the two boundary conditions $\rho(t,0) = 0$, $u(t,0) = 0$ with smooth initial data. Then in Section 2.3 we derive an a priori estimate from an entropy inequality, using the hyperbolic part of the system. We obtain an ϵ-independent bound on u in H^1 thanks to the presence of the dispersive term and on ρ in an Orlicz space ([12]) ; we also obtain global existence. In Section 2.4, following the method used in [14], we make use of the a priori estimates to find a subsequence of solutions $(\rho_\epsilon, u_\epsilon)$ of the regularized problem which converges weakly to a solution to the boundary value problem (2.1). In Section 2.5, by smoothing the data, we obtain the existence of a solution to the boundary value problem (2.1) with data $(\rho_0, u_0) \in \Lambda \times H_0^1$, where Λ is an Orlicz space based on the convex function $\rho \log \rho$. In Section 2.6, we present a result for the non homogeneous boundary value problem, we describe the main aspects of the proof, which follows the main steps as before. In Section 2.7 we outline the most important parts of the study of the problem on a finite interval ($[0,1]$ to simplify notations), following the same method. Then in Section

2.8, we show a result concerning uniqueness of solutions to the boundary-value problem on $\mathbb{R}^+$; we finally present in an Appendix a proof for the persistence of finite regularity for the solutions of the Boussinesq system on $\mathbb{R}$.

2.2 Local existence for the regularized system

In this section we prove local existence by applying the contraction mapping principle to the following regularized system :

$$\begin{cases} \rho_t + u_x + (u\rho)_x = \epsilon\rho_{xx}, \\ u_t + \rho_x + uu_x = u_{xxt}. \end{cases} \tag{2.3}$$

with the boundary conditions :

$$\begin{cases} u(t,0) = 0 \ \ \forall t \geq 0, \\ \rho(t,0) = 0 \ \ \forall t \geq 0. \end{cases} \tag{2.4}$$

We use the following notations :

$$C_c^k = \{g; g \in C^k(\mathbb{R}^{+*}), \text{with compact support}\},$$

$$C_0^k = \{g; g \in C^k(\mathbb{R}^{+*}), \lim_{x\to+\infty} g(x) = 0, \text{ and } g(0) = 0\}.$$

For any $t_0 > 0$, let $E = C([0,t_0], C_0^2 \times C_0^2)$. We introduce on E the following norm :

$$||u(t)|| = \sup_x |u(t,x)|$$

More precisely, we show :

Theorem 2.2.1. *For any initial data $(\rho_0, u_0) \in C_0^2 \times C_0^2$, there exists a constant $t_0 > 0$ depending only on $||\rho_0||, ||u_0||$ and ϵ such that the initial boundary value problem (2.3)-(2.4) has a unique solution $(\rho, u) \in C([0,t_0]; C_0^2 \times C_0^2)$.*

Proof. We invert the linear part of the first equation of (2.3) (see [7]) and because of the boundary conditions and since the functions tend to zero at infinity, we obtain after a formal integration by parts :

$$\rho(t,x) = \int_{\mathbb{R}^+} [G^\epsilon(t,x-y) - G^\epsilon(t,x+y)]\rho_0(y)dy$$
$$- \int_0^t \int_{\mathbb{R}^+} [G_x^\epsilon(t-s,x-y) + G_x^\epsilon(t-s,x+y)](u(s,y) + \rho(s,y)u(s,y))dyds.$$

Here, G^ϵ is the heat kernel : $G^\epsilon(x,t) = \dfrac{1}{\sqrt{4\pi\epsilon t}} \exp\left(\dfrac{-x^2}{4t\epsilon}\right)$.
We can also invert the second equation of (2.3), using the solution of the differential equation $u - u_{xx} = f$ with $u(0) = 0$ and $\lim_{x\to\infty} u(x) = 0$ and find :

$$u(t,x) = u_0(x) + \int_0^t \int_{\mathbb{R}^+} [K(x+y) + K(x-y)](\rho(s,y) + \frac{u^2}{2}(s,y))dyds.$$

where $K(x) = \text{sgn(x)}\frac{1}{2}\exp(-|x|)$.
We define the map Γ from E into itself, $\Gamma(\rho,u) = (\Gamma_1(\rho,u),\Gamma_2(\rho,u))$ where :

$$\begin{aligned}\Gamma_1(\rho,u) &= \int_{\mathbb{R}^+}[G^\epsilon(t,x-y) - G^\epsilon(t,x+y)]\rho_0(y)dy \\ &\quad - \int_0^t\int_{\mathbb{R}^+}[G^\epsilon_x(t-s,x-y) + G^\epsilon_x(t-s,x+y)](u(s,y)+\rho(s,y)u(s,y))dyds \\ \Gamma_2(\rho,u) &= u_0(x) + \int_0^t\int_{\mathbb{R}^+}[K(x+y)+K(x-y)](\rho(s,y)+\frac{u^2}{2}(s,y))dyds\end{aligned}$$

Finding a solution (ρ,u) of (2.3) in E is equivalent to solving the fixed point problem : $\Gamma(\rho,u) = (\rho,u)$.

If we denote by $\Omega_{t_0} = \{(\rho,u)\in E; ||\rho(t)|| + ||u(t)|| \leq r \ \ \forall t\in[0,t_0]\}$, with r sufficiently big and depending on $||\rho_0||, ||u_0||$, then Γ is a contraction map from Ω_{t_0} into itself for $t_0 > 0$ sufficiently small and depending on $||u_0||$, $||\rho_0||$, ϵ. By the contraction mapping principle, system (2.3) has a unique solution in Ω_{t_0}, which also satisfies the boundary conditions (2.4).

The uniqueness of the solution in E follows from the integral formulations by using a Gronwall inequality. □

2.3 A priori estimates and consequences

In this section we establish a priori estimates which are independent of ϵ for the solutions obtained in Theorem 2.2.1 ; we also prove global existence of solutions to the regularized problem (2.3).
The energy estimates are obtained using the same method as in [14] : we construct a positive convex entropy for the associated hyperbolic system :

$$\begin{cases}\rho_t + (u+u\rho)_x = 0, \\ u_t + (\rho + u^2/2)_x = 0.\end{cases} \tag{2.5}$$

Thanks to this entropy, we obtain an estimate for u in H^1 and for ρ in an Orlicz space based on the function $(1+\rho)\log(1+\rho)$. We note $w = 1+\rho$, then system (2.5) becomes :

$$\begin{cases}w_t + (uw)_x = 0, \\ u_t + (w + u^2/2)_x = 0.\end{cases} \tag{2.6}$$

with initial data $w_0(x) = 1+\rho_0(x)$ and $u_0(x)$.
A pair of functions (η,q) is an entropy-entropy flux pair if all smooth solutions of (2.6) satisfy :

$$\eta(u)_t + q(u)_x = 0 \Longleftrightarrow \nabla\eta.\nabla f = \nabla q \tag{2.7}$$

where f : $\mathbb{R}^2 \to \mathbb{R}^2$ is the mapping :

$$f(w,u) = (wu, w+u^2/2).$$

We now need the following lemma, which is a consequence of the maximum principle for the heat equation, see [7], [10], [14] :

Lemma 2.3.1. *Let $(\rho, u) \in C([0,t_0], C_0^2 \times C_0^2)$ be a solution of (2.3) with initial data (ρ_0, u_0). If $1+\rho_0(x) > 0$, then*

$$1+\rho(t,x) \geq 0 \ \forall\, x \in \mathbb{R}^+,\ t \geq 0.$$

Considering Lemma (2.3.1), if $1+\rho_0 > 0$, following Schonbek (see [14]), we can introduce the positive convex function :

$$\sigma_0(w) = w\log w + 1 - w.$$

It is important to notice that for ρ sufficiently large, σ_0 behaves like $\rho\log(\rho)$; that is there exists $M > 0$ and $C_1, C_2 > 0$ such that

$$C_1 \leq \frac{\sigma_0(w)}{\rho\log\rho} \leq C_2, \ \text{if} \rho \geq M$$

We then introduce the Orlicz space Λ_{σ_0} :

$$\Lambda_{\sigma_0} = \{\rho;\ \int_{\mathbb{R}^+} \sigma_0(1+\rho)(x)dx < \infty\}$$

Theorem 2.3.1. *Let $(\rho_0, u_0) \in C_0^2 \times C_0^2 \cap \Lambda_{\sigma_0} \times H_0^1$ satisfying $1+\rho_0 > 0$ and (ρ, u) be a solution of (2.3) with initial data (ρ_0, u_0). Then there exists a constant c_0 depending only on ρ_0 and u_0 such that*

$$\int_{\mathbb{R}^+} \frac{u^2}{2}dx + \int_{\mathbb{R}^+} \frac{u_x^2}{2}dx + \int_{\mathbb{R}^+} \sigma_0(w)dx \leq c_0 \tag{2.8}$$

Proof. System (2.3) writes :

$$\begin{cases} w_t + (uw)_x = \epsilon w_{xx}, \\ u_t + (w + u^2/2)_x = u_{xxt}. \end{cases} \tag{2.9}$$

Let $\eta(w,u)$, $q(w,u)$ be a pair of functions which satisfy (2.7). Then all smooth solutions of (2.9) satisfy :

$$\eta(w,u)_t + q(w,u)_x = \epsilon\frac{\partial\eta}{\partial w}w_{xx} + \frac{\partial\eta}{\partial u}u_{xxt}.$$

We choose $\eta(w,u) = \dfrac{u^2}{2} + \sigma(w)$.

The compatibility condition (2.7) gives :

$$\begin{aligned} \eta(w,u)_t + q(w,u)_x &= \epsilon\sigma^{'}(w)w_{xx} + uu_{xxt} \\ &= \epsilon\sigma(w)_{xx} - \epsilon\sigma^{''}(w)w_x^2 + (uu_{xt})_x - (\frac{u_x^2}{2})_t. \end{aligned} \tag{2.10}$$

As we want a positive convex entropy $\tilde{\eta}$ we substract from η its linear part at the point $(\bar{w} = 1, \bar{u} = 0)$ and obtain :

$$\begin{aligned} \tilde{\eta}(w,u) &= \eta(w,u) - \eta(1,0) - \nabla\eta(1,0).[(w-1,u)^T] \\ &= \frac{u^2}{2} + w\log w - \rho \\ &= \frac{u^2}{2} + \sigma_0(w) \end{aligned}$$

If q was an entropy flux associated with η then a simple computation shows that

$$\tilde{q}(w,u) = q(w,u) - q(\bar{w},\bar{u}) - \nabla\eta(\bar{w},\bar{u})[f(w,u) - f(\bar{w},\bar{u})]$$

satisfies $\nabla\tilde{\eta}.\nabla f = \nabla\tilde{q}$.
The functions $\tilde{\eta}$ and $\tilde{q}$ satisfy (2.7) and thus (2.10), we integrate (2.10) over the space $F := \{(s,x); \delta \leq x \leq N, 0 \leq s \leq t\}$.

$$\begin{aligned}
\int_F \tilde{\eta}_t + \tilde{q}_x &= \int_\delta^N (\tilde{\eta}(t,x) - \tilde{\eta}(0,x))dx + \int_0^t (\tilde{q}(s,N) - \tilde{q}(s,\delta))ds \\
&= \epsilon \int_0^t (\sigma_0(w)_x(s,N) - \sigma_0(w)_x(s,\delta))ds - \epsilon \int_F \sigma_0''(w)w_x^2 \\
&+ \int_0^t (uu_{xt}(s,N) - uu_{xt}(s,\delta))ds - \int_\delta^N \big(\frac{u_x^2}{2}(t,x) - \frac{u_{0,x}^2}{2}(x)\big)dx \\
&\leq \int_0^t (uu_{xt}(s,N) - uu_{xt}(s,\delta))ds - \int_\delta^N \big(\frac{u_x^2}{2}(t,x) - \frac{u_{0,x}^2}{2}(x)\big)dx + \\
&\epsilon \int_0^t (\sigma_0(w)_x(s,N) - \sigma_0(w)_x(s,\delta))ds,
\end{aligned}$$

because the function σ_0 is convex, which implies $\sigma_0'' \geq 0$.
Since $(\rho,u) \in C([0,\infty); C_0^2 \times C_0^2)$, and thanks to the boundary conditions $\rho(t,0) = 0$, $u(t,0) = 0$, we have that :

$$\lim_{\delta\to 0, N\to+\infty} \tilde{q}(s,N) - \tilde{q}(s,\delta) = \tilde{q}(\bar{w},\bar{u}) - \tilde{q}(w(s,0),u(s,0)) = 0$$

$$\lim_{\delta\to 0, N\to+\infty} uu_{xt}(s,N) - uu_{xt}(s,\delta) = 0$$

and

$$\begin{aligned}
\lim_{\delta\to 0, N\to+\infty} \sigma_0(w)_x(s,N) - \sigma_0(w)_x(s,\delta) &= \sigma_0'(\bar{w}) \lim_{N\to+\infty} w_x(s,N) - \sigma_0'(w(s,0))w_x(s,0) \\
&= 0
\end{aligned}$$

since $\sigma_0'(1) = \log(1) = 0$.
If we let tend δ to 0 and N to $+\infty$, using the Lebesgue dominated convergence theorem, we obtain

$$\int_{\mathbb{R}^+} \tilde{\eta}(t,x)dx + \int_{\mathbb{R}^+} \frac{u_x^2}{2}dx \leq \int_{\mathbb{R}^+} \tilde{\eta}(w_0,u_0)dx + \int_{\mathbb{R}^+} \frac{u_{0,x}^2}{2}dx,$$

By hypothesis, (ρ_0,u_0) belong to $\Lambda_{\sigma_0} \times H_0^1$ so we can denote by c_0 the finite quantity $\int_{\mathbb{R}^+} \tilde{\eta}(w_0,u_0)dx + \int_{\mathbb{R}^+} \frac{u_{0,x}^2}{2}dx$ and obtain

$$\int_{\mathbb{R}^+} \frac{u^2(t,x)}{2} + \int_{\mathbb{R}^+} \sigma_0(w(t,x))dx + \int_{\mathbb{R}^+} \frac{u_x^2}{2}dx \leq c_0.$$

where c_0 is a constant independent of ϵ. □

Because of the Sobolev embedding of $H^1(\mathbb{R}^+)$ into $L^\infty(\mathbb{R}^+)$ and due to the estimate (2.8) on w, we can deduce the following estimates :

Corollary 2.3.1. *Let $(\rho_0, u_0) \in C_0^2 \times C_0^2 \cap \Lambda_{\sigma_0} \times H_0^1$ satisfying $1 + \rho_0 >)$ and (ρ, u) be a solution of (2.3) with initial data (ρ_0, u_0). Then*

$$\sup_x |u(t,x)| \leq c_0 \tag{2.11}$$

and

$$\text{for all set } A \text{ of finite mesure, } \int_A |\rho| dx \leq c_A \tag{2.12}$$

where c_A depends only on ρ_0, u_0, A.

Theorem 2.3.2. *Let $(\rho_0, u_0) \in C_0^2 \times C_0^2 \cap \Lambda_{\sigma_0} \times H_0^1$. Let (ρ, u) be a solution of 2.3) with initial data (ρ_0, u_0), then*

$$||\rho(t,.)||_\infty \leq c_0\sqrt{t/\epsilon} + ||\rho_0||_\infty) \exp(c_0\sqrt{t/\epsilon}).$$

Proof. We use the integral formulation of ρ :

$$\begin{aligned}\rho(t,x) = &\int_{\mathbb{R}^+} [G^\epsilon(t, x-y) - G^\epsilon(t, x+y)]\rho_0(y)dy \\ &- \int_0^t \int_{\mathbb{R}^+} [G_x^\epsilon(t-s, x-y) + G_x^\epsilon(t-s, x+y)](u(s,y) + \rho(,y)u(s,y))dyds\end{aligned}$$

This implies

$$\begin{aligned}||\rho(t,.)||_\infty &\leq ||\rho_0||_\infty c_0\sqrt{\frac{t}{\epsilon}} + c_0 \int_0^t ||\rho(s,.)||_\infty \int_0^\infty |G\epsilon_x(t-s, x-y| + |G_x^\epsilon(t-s, x+y)|dyds \\ &\leq ||\rho_0||_\infty c_0\sqrt{\frac{t}{\epsilon}} + c_0 \int_0^t ||\rho(s,.)||_\infty \frac{1}{\sqrt{\epsilon(t-s)}}ds\end{aligned}$$

Then Gronwall's inequality allows to conclude. □

These a priori estimates are determinant for the following theorems; moreover, thanks to the estimates of Theorem (2.3.1) and Corollary (2.3.1), we can extend the local solution to a global one.

Theorem 2.3.3. *Let $(\rho_0, u_0) \in C_0^2 \times C_0^2 \cap \Lambda_{\sigma_0} \times H_0^1$ satisfying $1 + \rho_0 > 0$. Then there exists a unique solution $(\rho, u) \in C([0, \infty[; C_0^2 \times C_0^2)$ to the boundary value problem (2.3) with initial data (ρ_0, u_0) and it satisfies*

$$1 + \rho(t,x) \geq 0, \text{ for all } t > 0, \ x \in \mathbb{R}^+$$

The lower bound on ρ comes from the local one.

2.4 Existence of Solutions for the Boussinesq System with Smooth Data

In this section, following the method used in [14], we make use of the ϵ-independant estimates to obtain a subsequence of solutions $(\rho_\epsilon, u_\epsilon)$ with smooth data (ρ_0, u_0) which converges weakly to a solution (ρ, u) of (2.1).
We obtain a $L^2(\mathbb{R}^+)$-convergence on compact sets for u_ϵ for all t and a weak $L^1(\mathbb{R}^+ \times \mathbb{R}^+)$-convergence on compact sets for ρ_ϵ, thanks to a Dunford's theorem on weakly sequentially compact sets of L^1, see [8].

We first prove this convergence theorem.

Theorem 2.4.1. *Let (ρ_0, u_0) be in $C_0^2 \times C_0^2 \cap \Lambda_{\sigma_0} \times H_0^1$ satisfying $1 + \rho_0 > 0$. For each $\epsilon > 0$ let $(\rho_\epsilon, u_\epsilon) \in C([0,\infty), C_0^2 \times C_0^2)$ be the solution to the boundary-value problem (2.3) with initial data (ρ_0, u_0).*
Then there exists a subsequence $(\rho_\epsilon, u_\epsilon)$ and (ρ, u) such that :

(i) For any $\Phi \in L^\infty(\mathbb{R}^+ \times \mathbb{R}^+)$ with compact support

$$\lim_{\epsilon \to 0} \int_0^\infty \int_0^\infty (\rho_\epsilon(t,x) - \rho(t,x))\Phi(t,x)dxdt = 0.$$

(ii) For any $T > 0$, for any $\Psi \in \mathcal{D}(\mathbb{R}^{+*})$

$$\lim_{\epsilon \to 0} \int_0^\infty |u_\epsilon(t,x) - u(t,x)|^2 |\Psi(t,x)|^2 dx = 0 \text{ for all } t \in [0,T].$$

Proof. Let S be any compact set of $\mathbb{R}^+ \times \mathbb{R}^+$. Let us show that there exists a subsequence still denoted ρ_ϵ such that ρ_ϵ converges weakly. We need the following compactness result :

Lemma 2.4.1. *If a set K in $L^1(S, \Sigma, \mu)$ is weakly sequentially compact, then*

$$\lim_{\mu(E) \to 0} \int_E f(s)\mu(s)ds = 0 \text{ uniformly for } f \in K$$

If $\mu(S) < \infty$ then this condition is sufficient for a bounded set K to be sequentially compact.

We use here the second part of the lemma with μ the Lebesgue measure on $\mathbb{R}^+ \times \mathbb{R}^+$, and $K = \{\rho_\epsilon|_S\}$; thanks to the estimate (2.12) of Corrolary 2.3.1, K is bounded since S is compact. Let $E \subset S$ and let $E_r = \{(t,x); \rho_\epsilon(t,x) \leq r\}$.

$$\begin{aligned} \int_E \rho_\epsilon(t,x)dxdt &= \int_{E \cap E_r} \rho_\epsilon(t,x)dxdt + \int_{E \cap E_r^c} \rho_\epsilon(t,x)dxdt \\ &\leq r\mu(E) + \int_{E \cap E_r^c} \frac{1}{\log r} \rho_\epsilon \log \rho_\epsilon dxdt \end{aligned}$$

Then, if we take r sufficiently large, we can use the a priori estimate (2.8), and obtain :

$$\int_E \rho_\epsilon(t,x)dxdt \leq r\mu(E) + \frac{1}{C_1 \log r} c_0 |P_t E|$$

where P_t is the projection of E in the t-direction.
Consequently

$$\lim_{\mu(E)\to 0}\int_E \rho_\epsilon = 0, \text{ uniformly for any } \rho_\epsilon|_S$$

Applying the lemma, for any compact set S of $\mathbb{R}^+ \times \mathbb{R}^+$, there is a subsequence $\rho_\epsilon(S)$ which is weakly convergent in $L^1(S)$.
Now let $S_n = [0,n] \times [0,n]$ and let ρ_ϵ^n be the corresponding subsequence converging weakly in $L^1(S_n)$. By a diagonalization process, we can find a subsequence $\rho_{\epsilon_k}^k$ of ρ_ϵ which is weakly convergent in $L^1(S_n)$ for all n to a function ρ.
Let $\Phi \in L^\infty(\mathbb{R}^+ \times \mathbb{R}^+)$ with compact support S; there exists n such that $S \subset S_n$ and if we let $\rho_\epsilon = \rho_{\epsilon_k}^k$, we have, since $\Phi \in L^\infty(S_n)$,

$$\lim_{\epsilon\to 0}\int\int_S (\rho_\epsilon - \rho)\Phi dxdt = 0.$$

which concludes the proof of the first point of the theorem.

For the second part, we use the compact injection of H^1 in L^2 on bounded sets of $\mathbb{R}^+$.
By the a priori bound (2.8), for all $t > 0$, $u_\epsilon(t,.)$ is bounded in $H^1(\mathbb{R}^+)$ thus for all $\Phi \in \mathcal{D}(\mathbb{R}^{+*})$, $(u_\epsilon\Phi)$ is bounded in $H^1(\text{supp }\Phi)$. Therefore for each t, there exists a subsequence $u_{\epsilon(t)}$ and a function $u \in L^2(\text{supp }\Phi)$ such that

$$\lim_{\epsilon(t)\to 0}\int_0^{+\infty} |u_{\epsilon(t)}(t,x) - u(t,x)|^2|\Phi(t,x)|^2 dx = 0.$$

By a diagonalization process, for all $T > 0$, we can find a subsequence still denoted u_ϵ such that :

$$\lim_{\epsilon(t)\to 0}\int_0^{+\infty} |u_\epsilon(t,x) - u(t,x)|^2|\Phi(t,x)|^2 dx = 0 \ \ \forall\, t \in \mathbb{Q} \cap [0,T].$$

To prove the strong convergence in $L^2(\mathbb{R}^+)$ for each $t \in [0,T]$, it is sufficient to show that for all $\Phi \in \mathcal{D}(\mathbb{R}^{+*})$:

$$\lim_{\epsilon\to 0}\int_{\mathbb{R}^+} |u_\epsilon(t,x) - u(t,x)||\Phi(t,x)| dx = 0. \tag{2.13}$$

Let a and b be two finite constants in $\mathbb{R}^+$; to show (2.13), we need to show the following inequality :

$$\Big|\int_a^b u_\epsilon(t_2,x) - u_\epsilon(t_1,x)dx\Big| \le c\,|t_2 - t_1|, \text{for all } t_1,\, t_2 \ge 0. \tag{2.14}$$

where $c = c(a,b,\rho_0,u_0)$.
We use the integral representation of u_ϵ :

$$u_\epsilon(t,x) = u_0(x) + \int_0^t\int_{\mathbb{R}^+} [K(x+y) + K(x-y)](\rho_\epsilon(s,y) + \frac{u_\epsilon^2}{2}(s,y)dyds$$

Integrating $u_\epsilon(t_2,x)-u_\epsilon(t_1,x)$ over $[a,b]$, we obtain :

$$\begin{aligned}\int_a^b u_\epsilon(t_2,x)-u_\epsilon(t_1,x)dx &= \int_a^b\int_{t_1}^{t_2}\int_{\mathbb{R}^+}[K(x+y)+K(x-y)](\rho_\epsilon(s,y)+\frac{u_\epsilon^2}{2}(s,y))dydsdx\\
&= \int_a^b\int_{t_1}^{t_2}\int_{-\infty}^{x} K(z)(\rho_\epsilon(s,x-z)+\frac{u_\epsilon^2}{2}(s,x-z))dzdsdx\\
&+ \int_a^b\int_{t_1}^{t_2}\int_{x}^{+\infty} K(z)(\rho_\epsilon(s,z-x)+\frac{u_\epsilon^2}{2}(s,z-x)dzdsdx\\
&= -\int_a^b\int_{t_1}^{t_2}\int_{-x}^{+\infty} K(\nu)(\rho_\epsilon(s,x+\nu)+\frac{u_\epsilon^2}{2}(s,x+\nu))d\nu dsdx\\
&+ \int_a^b\int_{t_1}^{t_2}\int_{x}^{+\infty} K(z)(\rho_\epsilon(s,z-x)+\frac{u_\epsilon^2}{2}(s,z-x)dzdsdx\end{aligned}$$

where we performed successively the change of variables $z=x-y$, $z=x+y$, and $\nu=-z$.
Thanks to estimate (2.8), we have

$$\begin{aligned}\Big|\int_a^b\int_{t_1}^{t_2}\int_{-x}^{+\infty} K(\nu)\frac{u_\epsilon^2}{2}(s,x+\nu)d\nu dsdx\Big| &\le \int_a^b\int_{t_1}^{t_2} c_0\int_{\mathbb{R}} K(\nu)d\nu dsdx\\
&\le c_0|b-a||t_2-t_1|\end{aligned}$$

and similarly for the other term involving u_ϵ.
Then by Fubini's theorem,

$$\begin{aligned}\Big|\int_a^b\int_{t_1}^{t_2}\int_{-x}^{+\infty} K(\nu)\rho_\epsilon(s,x+\nu)d\nu dsdx\Big| &\le \int_{t_1}^{t_2}\int_{-\infty}^{+\infty}|K(\nu)|\int_a^b|\rho_\epsilon(s,x+\nu)|dxd\nu ds\\
&\le c_0c|t_2-t_1|(1+|b-a|)\end{aligned}$$

The last inequality follows from an auxiliary estimate, indeed we have :

$$\begin{aligned}\int_a^b|\rho_\epsilon(s,x+\nu)|dx &= \int_{\nu+a}^{\nu+b}|\rho_\epsilon(s,r)|dr\\
&= \int_{[\nu+a,\nu+b]\cap\{r;|\rho_\epsilon(s,r)|\le k\}}|\rho_\epsilon(s,r)|dr\\
&+ \int_{[\nu+a,\nu+b]\cap\{r;|\rho_\epsilon(s,r)|> k\}}|\rho_\epsilon(s,r)|dr\\
&\le k|b-a|+\frac{1}{\log k}\int_{\nu+a}^{\nu+b}|\rho_\epsilon\log\rho_\epsilon(s,r)|dr\\
&\le cc_0(1+|b-a|)\end{aligned}$$

if we take k sufficiently large so that $\int_{\{r;|\rho_\epsilon|>k\}}\rho_\epsilon\log\rho_\epsilon dx\le c_0$, using estimate (2.8).
We can then deduce estimate (2.14) with c depending on a, b, ρ_0, and u_0.

Considering this result of regularity in t for the u_ϵ, we obtain :

$$\begin{aligned}\int_a^b |u_\epsilon(t,x)-u_{\bar\epsilon}(t,x)|dx &\leq \int_a^b |u_\epsilon(t,x)-u_\epsilon(\bar t,x)|dx+\int_a^b |u_\epsilon(\bar t,x)-u_{\bar\epsilon}(\bar t,x)|dx\\ &+ \int_a^b |u_{\bar\epsilon}(\bar t,x)-u_{\bar\epsilon}(t,x)|dx\\ &\leq c|t-\bar t|+|b-a|\Big(\int_a^b |u_\epsilon(\bar t,x)-u_{\bar\epsilon}(\bar t,x)|^2\Big)^{1/2}+c|t-\bar t|\end{aligned}$$

For any $t\in[0,T]$, let $\bar t$ be a rationnal number sufficiently close to t; as $u_\epsilon(\bar t,.)$ converges in $L^2([a,b])$, then $u_\epsilon(t,.)$ is a Cauchy sequence in $L^1([a,b])$ and thus converges towards a limit that is u, which proves (2.13).
Now we can write, for all $t\in[0,T]$:

$$\int_{\mathbb{R}^+}|(u_\epsilon(t,x)-u(t,x))\Phi(t,x)|^2dx\leq 2||\Phi(t,.)||^2_{L^\infty(\mathbb{R}^+)}c_0\int_{\mathbb{R}^+}|u_\epsilon(t,x)-u(t,x)||\Phi(t,x)|dx$$

thanks to estimation (2.11).
Finally, with (2.13), we have the announced convergence result. □

Now we show that the limit functions (ρ,u) obtained in the preceding theorem are solutions of the Boussinesq system, and satisfy the boundary conditions (2.4).

Theorem 2.4.2. *Let $(\rho_0,u_0)\in C_0^2\times C_0^2\cap\Lambda_{\sigma_0}\times H_0^1$ satisfying $1+\rho_0>0$. Let ρ and u be the limit functions obtained in Theorem (2.4.1), then (ρ,u) is a weak solution of the initial value problem for the Boussinesq system with data (ρ_0,u_0).*

Proof. The proof follows the scheme of the one in ([14]). Let $(\rho_\epsilon,u_\epsilon)$ be the converging subsequences of Theorem (2.4.1).
For any $\Phi\in\mathcal{D}(\mathbb{R}^{+*}\times\mathbb{R}^{+*})$ we have :

$$\begin{aligned}\int_0^{+\infty}\int_0^{+\infty}\rho_\epsilon\Phi_t dxdt+\int_0^{+\infty}\int_0^{+\infty}(u_\epsilon+u_\epsilon\rho_\epsilon)\Phi_x dxdt=\\ \epsilon\int_0^{+\infty}\int_0^{+\infty}\rho_\epsilon\Phi_{xx}dxdt,\\ \int_0^{+\infty}\int_0^{+\infty}u_\epsilon\Phi_t dxdt+\int_0^{+\infty}\int_0^{+\infty}\Big(\frac{u_\epsilon^2}{2}+\rho_\epsilon\Big)\Phi_x dxdt=\\ \int_0^{+\infty}\int_0^{+\infty}u_\epsilon\Phi_{xxt}dxdt.\end{aligned}$$

First, thanks to estimation (2.12) of Corrolary (2.3.1),

$$\lim_{\epsilon\to0}\epsilon\int_0^{+\infty}\int_0^{+\infty}\rho_\epsilon\Phi_{xx}dxdt=0$$

since the integrals work on supp Φ which is of finite measure.
We need to show that (ρ, u) satisfy the equations in the distributionnal sense, that is :

$$\int_0^{+\infty}\int_0^{+\infty} \rho\Phi_t dxdt + \int_0^{+\infty}\int_0^{+\infty} (u+\rho u)\Phi_x dxdt = 0,$$
$$\int_0^{+\infty}\int_0^{+\infty} u\Phi_t dxdt + \int_0^{+\infty}\int_0^{+\infty} \big(\frac{u^2}{2}+\rho\big)\Phi_x dxdt = \int_0^{+\infty}\int_0^{+\infty} u\Phi_{xxt} dxdt.$$

Therefore let us prove that :

$$\lim_{\epsilon\to 0}\Big[\int_0^{+\infty}\int_0^{+\infty} (\rho_\epsilon-\rho)\Phi_t dxdt + \int_0^{+\infty}\int_0^{+\infty} (u_\epsilon+\rho_\epsilon u_\epsilon - u - \rho u)\Phi_x dxdt\Big] = 0, \tag{2.15}$$

$$\begin{aligned}\lim_{\epsilon\to 0}\Big[&\int_0^{+\infty}\int_0^{+\infty} (u_\epsilon-u)\Phi_t dxdt + \int_0^{+\infty}\int_0^{+\infty} \big(\frac{u_\epsilon^2}{2}+\rho_\epsilon-\frac{u^2}{2}-\rho\big)\Phi_x dxdt \\ &+\int_0^{+\infty}\int_0^{+\infty} (u_\epsilon-u)\Phi_{xxt} dxdt\Big] = 0.\end{aligned} \tag{2.16}$$

By the weak convergence of ρ_ϵ and the strong convergence of u_ϵ, the linear terms are easy to treat.
For the first non linear term, we write

$$\int_0^{+\infty}\int_0^{+\infty} (\rho_\epsilon u_\epsilon - \rho u)\Phi_x = \int\int_S \rho_\epsilon(u_\epsilon-u)\Phi_x + \int\int_S (\rho_\epsilon-\rho)u\Phi_x \tag{2.17}$$

where $S = \text{supp } \Phi$.
Up to the extraction of a new subsequence of u_ϵ, we know that $u_\epsilon(t,.)$ converges towards $u(t,.)$ almost everywhere in $\mathbb{R}^+$ for all $t \in [0,T]$.
Moreover $u_\epsilon(t,.)$ and $u(t,.)$ belong to L^∞, Φ_x is bounded and $\int_S |\rho_\epsilon| \leq c_S$ by (2.12). Thus by the dominated convergence theorem, the first term of (2.17) converges towards 0.

For the second term of (2.17), we note that since $u \in L^\infty$, $u\Phi_x \in L^\infty$ and has a compact support, therefore by Theorem (2.4.1),

$$\lim_{\epsilon\to 0}\int_0^{+\infty}\int_0^{+\infty} (\rho_\epsilon-\rho)u\Phi_x dxdt = 0.$$

Hence the left hand side of (2.17) tends to zero as ϵ approaches zero.

There is one remaining term to study in (2.16); by using the L^2 strong convergence of u_ϵ, and the dominated convergence theorem, we can see that :

$$\lim_{\epsilon\to 0}\int_0^{+\infty}\int_0^{+\infty} (u_\epsilon^2-u^2)\Phi dxdt = 0.$$

The proof of (2.15) and (2.16) is now complete.

We have to verify that u satisfies the boundary condition. We know that for all $t > 0$, $u_\epsilon(t,.) \in H_0^1(\mathbb{R}^+)$, and is bounded in the H^1-norm, therefore there exists a subsequence still denoted u_ϵ which converges weakly in H_0^1 towards u. Since $H_0^1(\mathbb{R}^+)$ is closed for the weak convergence, $u \in H_0^1$, and thus $u(t,0) = 0$, for all $t \geq 0$.

Now we show that

$$\lim_{t\to 0} u(t,x) = u_0(x) \text{ almost everywhere,} \tag{2.18}$$

and

$$\lim_{t\to 0} \int_{\mathbb{R}^+} (\rho(t,x) - \rho_0(x))\Phi(x)dx = 0 \ \ \forall\, \Phi \in \mathcal{D}(\mathbb{R}^+). \tag{2.19}$$

For u, we write :

$$|u(t,x) - u_0(t,x)| \leq |u(t,x) - u_\epsilon(t,x)| + |u_\epsilon(t,x) - u_0(x)|. \tag{2.20}$$

For the second term of (2.20), we use the integral representation of u_ϵ.

$$\begin{aligned}
|u_\epsilon(t,x) - u_0(x)| &\leq \int_0^t \int_{\mathbb{R}^+} |K(x+y) + K(x-y)|\big(\frac{u_\epsilon^2(s,y)}{2} + \rho_\epsilon(s,y)\big)dyds \\
&\leq \int_0^t \int_{\mathbb{R}^+} u_\epsilon^2(s,y)dyds + \int_0^t \int_{E_k} k|K(x+y) + K(x-y)|dyds \\
&+ \int_0^t \int_{E_k^c} \frac{2}{\log k}\rho_\epsilon \log \rho_\epsilon dyds
\end{aligned}$$

where E_k is the projection on the second variable of the space $\{(s,r); \rho_\epsilon(s,r) \leq k\}$. Using the same means as above with k sufficiently large and estimation (2.8), we obtain :

$$|u_\epsilon(t,x) - u_0(x)| \leq ct \text{ with c a constant.}$$

Using this and making ϵ tend to zero in (2.20), we find (2.18), which shows that the function u takes on the good initial data u_0.

Now let us establish that $\rho(t,.)$ converges towards ρ_0 in $\mathcal{D}'(\mathbb{R}^{+*})$.
Here is a first lemma :

Lemma 2.4.2. *Let $\Phi \in \mathcal{D}(\mathbb{R}^{+*})$, supp $\Phi \subset S$. Let $T > 0$ and (t_n) be a sequence of $[0,T]$. Then there exists a subsequence ρ_ϵ of solutions of (2.3) such that*

$$\lim_{\epsilon\to 0} \int_0^{+\infty} (\rho_\epsilon(t_n,x) - \rho(t_n,x))\Phi(x)dx = 0.$$

Proof. The proof of this Lemma uses the same tools as the proof of (2.4.1)(i) : we apply Lemma (2.4.1) with $\mu = dx$ and $K = \{\rho_{\epsilon|S}\}$, thus we obtain for each $t \in [0,T]$ a subsequence $\rho_{\epsilon(t)}$ which converges weakly in $L^1(\mathbb{R}^+)$ and then by a diagonalization process, the dependance on t in ϵ disappears for a sequence t_n and Lemma (2.4.2) follows. □

We then need this other Lemma :

Lemma 2.4.3. *Let S be a compact set in $\mathbb{R}^+$, and $N(S)$ be a neighbourhood of finite measure of S. Let t_n be any sequence in $[0,T]$ such that $\lim_{n\to+\infty} t_n = 0$. Then there exists a subsequence still denoted t_n such that*

$$\lim_{t_n\to 0}\int_a^b \rho_\epsilon(t_n,x) - \rho_0(x)dx = 0$$

for almost every a, b in $N(S)$.

Proof. We use the integral representation of ρ_ϵ to show that

$$\lim_{t_n\to 0}\int_{N(S)}\int_{N(S)} \Big|\int_a^b \rho_\epsilon(t_n,x) - \rho_0(x)dx\Big|dadb = 0. \tag{2.21}$$

The convergence for a subsequence of t_n for a and b almost everywhere in $N(S)\times N(S)$ will then follow.

$$\begin{aligned}
&\int_{N(S)}\int_{N(S)} \Big|\int_a^b \rho_\epsilon(t_n,x) - \rho_0(x)dx\Big|dadb\\
&\quad\le \int_{N(S)}\int_{N(S)} \Big|\int_a^b\int_{\mathbb{R}^+} (G^\epsilon(t,x-y) - G^\epsilon(t,x+y))(\rho_0(y)-\rho_0(x))dydx\Big|dadb\\
&\quad+ \int_{N(S)}\int_{N(S)} \Big|\int_a^b\int_0^{t_n}\int_{\mathbb{R}^+} (G^\epsilon_x(t-s,x-y) + G^\epsilon_x(t-s,x+y))\\
&\quad\times(\rho_\epsilon(s,y)u_\epsilon(s,y) + u_\epsilon(s,y))dydsdx\Big|dadb.
\end{aligned}$$

We study each term of the right hand side. First of all,

$$\lim_{t_n\to 0}\Big|\int_a^b\int_{\mathbb{R}^+} (G^\epsilon(t_n,x-y) - G^\epsilon(t_n,x+y))(\rho_0(y)-\rho_0(x))dydx\Big| = 0$$

since $G^\epsilon(t_n,x)$ tends to zero as t_n tends to zero almost everywhere.

For the second term we have

$$\begin{aligned}
&\int_{N(S)}\int_{N(S)}\Big|\int_a^b\int_0^{t_n}\int_{\mathbb{R}^+} [G^\epsilon_x(t-s,x-y) + G^\epsilon_x(t-s,x+y)]\\
&\quad\times[\rho_\epsilon(s,y)u_\epsilon(s,y) + u_\epsilon(s,y)]dsdydx\Big|dadb\\
&\quad= \int_{N(S)}\int_{N(S)}\Big|\int_0^{t_n}\int_{\mathbb{R}^+} [\rho_\epsilon(s,y)u_\epsilon(s,y) + u_\epsilon(s,y)][G^\epsilon(t_n-s,b-y)\\
&\quad- G^\epsilon(t_n-s,a-y) + G^\epsilon(t_n-s,b+y) - G^\epsilon(t_n-s,a+y)]dyds\Big|dadb\\
&\quad\le c_0\int_{N(S)}\int_{N(S)}\int_0^{t_n}\int_{\mathbb{R}^+} \Big|1+\rho_\epsilon(s,y)\Big|\Big|G^\epsilon(t_n-s,b-y) - G^\epsilon(t_n-s,a-y)\\
&\quad+ G^\epsilon(t_n-s,b+y) - G^\epsilon(t_n-s,a+y)\Big|dydsdadb
\end{aligned}$$

After performing several change of variables, this last term is bounded by

$$c_0 \int_{N(S)} \int_{N(S)} \int_0^{t_n} \int_{\mathbb{R}^+} G^\epsilon(t_n - s, z) \Big[|\rho_\epsilon(s, b - z)| + |\rho_\epsilon(s, a - z)| + |\rho_\epsilon(s, z - b)| + \rho_\epsilon(s, z - a)| \Big] dz ds da db + 2c_0 |N(S)|^2 t_n$$

Then, after an interversion of the integral signs by Fubini Theorem, we use the a priori estimate (2.12) and obtain for example for the first term

$$\begin{aligned} & c_0 \int_{N(S)} \int_{N(S)} \int_0^{t_n} \int_{\mathbb{R}^+} G^\epsilon(t_n - s, z) |\rho_\epsilon(s, b - z)| dz ds da db \\ & \leq c_0 |N(S)| \int_0^{t_n} \int_{\mathbb{R}^+} |G^\epsilon(t - s, z)| \int_{N(S)} |\rho_\epsilon(s, z - b)| db dz ds \\ & \leq \frac{c_0}{2} |N(S)| c_{N(S)} t_n \end{aligned}$$

and similarly for the other terms. Finally (2.21) is proven. □

Now let $\Phi \in \mathcal{D}(\mathbb{R}^{+*})$. To conclude the proof of (2.19), we introduce a sequence s_m of step functions with support in a neighourhood $N(S)$ of $S =$ supp Φ :

$$s_m(x) = \sum_{i \geq 0} \alpha_i \chi_i$$

where the χ_i are characteristic functions of intervals $[a_i, b_i]$, where the a_i and b_i are chosen so that Lemma (2.4.3) works. Then

$$\begin{aligned} \Big| \int_{\mathbb{R}^+} (\rho(t_n, x) - \rho_0(x)) \Phi(x) dx \Big| & \leq \Big| \int_{\mathbb{R}+} (\rho(t_n, x) - \rho_\epsilon(t_n, x)) \Phi(x) dx \Big| \\ & + \Big| \int_{N(S)} \rho_\epsilon(t_n, x)(\Phi(x) - s_m(x)) dx \Big| + \Big| \sum_{i \geq 0} \alpha_i \int_{a_i}^{b_i} \rho_\epsilon(t_n, x) - \rho_0(x) dx \Big| \\ & + \Big| \int_{N(S)} \rho_0(x)(s_m(x) - \Phi(x)) dx \Big| \end{aligned}$$

where ρ_ϵ is the subsequence given by Lemma (2.4.2).
Let $\beta > 0$. With Lemma (2.4.2), we can choose ϵ such that the first integral is less than $\beta/4$. Then as $\int_{N(S)} |\rho_\epsilon| dx \leq c$ and as $\rho_0 \in C_c^2$, we can choose m so that the two integrals involving s_m are less than $\beta/4$. To bound the last integral, we use Lemma (2.4.3) and choose n large enough, finally :

$$\Big| \int_{\mathbb{R}^+} (\rho(t_n, x) - \rho_0(x)) \Phi(x) dx \Big| \leq \beta.$$

and (2.19) is proven, which achieves the proof of Theorem (2.4.2). □

2.5 Existence of Solutions to the Boussinesq System

We recall that $\sigma_0(1+\rho)(x) = (1+\rho(x))\log(1+\rho(x)) - \rho(x)$ is the positive convex function introduced in Section 2.2.
In this section we show the existence of solutions in $L^\infty(\mathbb{R}^+; \Lambda_{\sigma_0} \times H^1)$ of the boundary value problem (2.1) with initial data in $\Lambda_{\sigma_0} \times H_0^1$, where

$$\Lambda_{\sigma_0} = \Big\{\rho; \int_{\mathbb{R}^+} \sigma_0(1+\rho)(x)dx < \infty\Big\}.$$

We will say that (ρ_0, u_0) satisfy (C) if :
- $\inf_{x\in\mathbb{R}^+}(1+\rho_0(x)) > 0$,
- there exists $L > 0$ such that $\rho_0(x) = 0$ for almost every $x \geq L$.

Theorem 2.5.1. *Let $(\rho_0, u_0) \in \Lambda_{\sigma_0} \times H_0^1(\mathbb{R}^{+*})$ satisfying (C). Then there exists a weak solution of the system (2.1) with data (ρ_0, u_0) satisfying the boundary condition $u(t,0) = 0$ for almost every $t > 0$.*
Moreover (ρ, u) belongs to $L^\infty(\mathbb{R}^+; \Lambda_{\sigma_0} \times H_0^1)$.

Proof. We first extend the initial data to $\mathbb{R}$ and then use a regularisation process.
Let $\tilde{u}_0$ be the extension of u_0 by zero :

$$\tilde{u}_0(x) = \begin{cases} u_0(x), & x \geq 0 \\ 0, & x < 0 \end{cases}$$

and let $\tilde{\rho}_0$ be the even extension of ρ_0 to $\mathbb{R}$.
Let $\Psi \in \mathcal{D}(\mathbb{R})$ be such that

$$\int_{\mathbb{R}} \Psi(x)dx = 1,\ \Psi \geq 0,\ \text{supp}\ \Psi \subset B(0,1),\ \Psi \text{ even}\ .$$

and define

$$\Psi_\epsilon(x) = \frac{1}{\epsilon}\Psi(\frac{x}{\epsilon}),$$

Let ν be a $C^\infty(\mathbb{R})$ function such that

$$\nu(x) = \begin{cases} 1, & x \geq 1, \\ 0, & x \leq 1/2 \end{cases},$$

let $\nu_\epsilon(x) = \nu(x/\epsilon)$ and consider

$$\tilde{\rho}_0^\epsilon = \nu_\epsilon(\tilde{\rho}_0 * \Psi_\epsilon),\ \tilde{u}_0^{\epsilon,h} = (\phi_h(\tilde{u}_0) * \Psi_\epsilon).$$

where $\nu_\epsilon(x) = \nu(x/\epsilon)$ and where for $h > 0$, ϕ_h represents a translation operator, namely $\forall y \in \mathbb{R},\ \phi_h(\tilde{u}_0)(y) = \tilde{u}_0(y-h)$.
The sequence functions $\tilde{\rho}_0^\epsilon$ and $\tilde{u}_0^{\epsilon,h}$ belong in particular to $C_0^2(\mathbb{R}^+)$ for ϵ sufficiently small and

$$\tilde{\rho}_0^\epsilon \underset{\epsilon\to 0}{\longrightarrow} \rho_0 \text{ in } L^1(\mathbb{R}^+)$$

$$\tilde{u}_0^{\epsilon,h} \xrightarrow[\epsilon\to 0,\ h\to 0]{} u_0 \text{ in } H^1(\mathbb{R}^+)$$

Now let $(\rho_\epsilon, u_\epsilon)$ be the global solution of system (2.3) of Theorem (2.2.1) with initial data $(\tilde{\rho}_0^\epsilon, \tilde{u}_0^{\epsilon,h})$ (we omit the dependence in h in the notations for the sake of simplicity).
Let us show an estimate of this type :

$$\int_{\mathbb{R}^+} \eta(w_\epsilon, u_\epsilon)dx + \int_{\mathbb{R}^+} \frac{u_{\epsilon,x}^2}{2}dx \le C\int_{\mathbb{R}^+} \eta(w_0, u_0)dx + C\int_{\mathbb{R}^+} \frac{u_{0,x}^2}{2}dx + C', \tag{2.22}$$

with the same notations as before that is

$$w_\epsilon = 1+\rho_\epsilon,\ \ w_0 = 1+\rho_0,\ \ \eta(w,u) = \frac{u^2}{2} + \sigma_0(\rho).$$

After that, we can repeat the proofs of Theorems (2.4.1) and (2.4.2) and find a subsequence $(\rho_\epsilon, u_\epsilon)$ which converges weakly to a solution of system (2.1).
With the a priori estimate (2.8), we have

$$\int_{\mathbb{R}^+} \eta(w_\epsilon, u_\epsilon)dx + \int_{\mathbb{R}^+} \frac{u_{\epsilon,x}^2}{2}dx \le \int_{\mathbb{R}^+} \eta(\tilde{w}_0^\epsilon, \tilde{u}_0^{\epsilon,h})dx + \int_{\mathbb{R}^+} \frac{(\tilde{u}_{0,x}^{\epsilon,h})^2}{2}dx.$$

Let $\gamma(u) = \dfrac{u^2}{2}$; we use Jensen's inequality with the two positive convex functions γ and σ_0 and with the probability measure :

$$d\epsilon(x) = \Psi_\epsilon(x-y)dy = \frac{1}{\epsilon}\Psi(\frac{x-y}{\epsilon})dy$$

With these notations we can write

$$\eta((\tilde{w}_0^\epsilon), (\tilde{u}_0^{\epsilon,h})) + \frac{(\tilde{u}_{0,x}^{\epsilon,h})^2}{2} = \gamma\Big(\int_{\mathbb{R}} \phi_h(\tilde{u}_0)(y)d\epsilon(x)\Big)$$
$$+\gamma\Big(\int_{\mathbb{R}} \tilde{u}_{0,x}(y-h)d\epsilon(x)\Big) + \sigma_0\Big(\int_{\mathbb{R}} \tilde{w}_0(y)\nu_\epsilon(x)d\epsilon(x)\Big).$$

Using Jensen's inequality, we obtain

$$\eta(\tilde{w}_0^\epsilon, \tilde{u}_0^{\epsilon,h}) + \frac{(\tilde{u}_{0,x}^{\epsilon,h})^2}{2} \le \int_{\mathbb{R}} \gamma(\tilde{u}_0(y-h))d\epsilon(x) + \int_{\mathbb{R}} \gamma(\tilde{u}_{0,x}(y-h))d\epsilon(x)$$
$$+\int_{\mathbb{R}} \sigma_0(\tilde{w}_0(y)\nu_\epsilon(x))d\epsilon(x).$$

We integrate on $\mathbb{R}^+$,

$$\int_{\mathbb{R}^+} \eta(\tilde{w}_0^\epsilon, \tilde{u}_0^{\epsilon,h}) + \frac{(\tilde{u}_{0,x}^{\epsilon,h})^2}{2}dx \le \int_{\mathbb{R}^+}\int_{\mathbb{R}} \gamma(\tilde{u}_0(y-h))d\epsilon(x)dx$$
$$+\int_{\mathbb{R}^+}\int_{\mathbb{R}} \gamma(\tilde{u}_{0,x}(y-h))d\epsilon(x)dx + \int_{\mathbb{R}^+}\int_{\mathbb{R}} \sigma_0(\tilde{w}_0(y)\nu_\epsilon(x))d\epsilon(x)dx$$

and using Fubini's theorem, we find

$$\begin{aligned}\int_{\mathbb{R}^+} \eta(\tilde{w}_0^\epsilon, \tilde{u}_0^{\epsilon,h}) + \frac{(\tilde{u}_{0,x}^{\epsilon,h})^2}{2} dx \leq & \int_{\mathbb{R}} \frac{\tilde{u}_0^2(y-h)}{2} \frac{1}{\epsilon} \int_{\mathbb{R}^+} \Psi\big(\frac{x-y}{\epsilon}\big) dxdy \\ & + \int_{\mathbb{R}} \frac{\tilde{u}_{0,x}^2(y-h)}{2} \frac{1}{\epsilon} \int_{\mathbb{R}^+} \Psi\big(\frac{x-y}{\epsilon}\big) dxdy \\ & + \int_{\mathbb{R}} \sigma_0(\tilde{w}_0(y)\nu_\epsilon(x)) \frac{1}{\epsilon} \int_{\mathbb{R}^+} \Psi\big(\frac{x-y}{\epsilon}\big) dxdy \\ & + \int_{\mathbb{R}} |\tilde{\rho}_0(y)| \frac{1}{\epsilon} \int_{\mathbb{R}^+} \Psi\big(\frac{x-y}{\epsilon}\big) dxdy \\ & \leq \int_{\mathbb{R}} \frac{\tilde{u}_0^2(y)}{2} dy + \int_{\mathbb{R}} \frac{\tilde{u}_{0,x}^2(y)}{2} dy \\ & + \int_{\mathbb{R}} \sigma_0(\tilde{w}_0(y)) dy + \int_{\mathbb{R}} |\tilde{\rho}_0(y)| dy.\end{aligned}$$

Since σ_0 and $\tilde{w}_0$ are even, we finally obtain

$$\int_{\mathbb{R}^+} \eta(\tilde{w}_0^\epsilon, \tilde{u}_0^{\epsilon,h}) + \frac{(\tilde{u}_{0,x}^{\epsilon,h})^2}{2} dx \leq 2 \int_{\mathbb{R}^+} \eta(w_0, u_0) + \frac{u_{0,x}^2}{2} dy + \int_{\mathbb{R}} |\tilde{\rho}_0(y)| dy$$

The right hand side is finite, since $(\rho_0, u_0) \in \Lambda_{\sigma_0} \times H_0^1$ and satisfy (C); in particular ρ_0 being in Λ_{σ_0} and satisfying (C) implies that $\rho_0 \in L^1$. And (2.22) is proven.

It remains to check that the solution (ρ, u) takes on the inital data (ρ_0, u_0).; for any $\Phi \in \mathcal{D}(\mathbb{R}^{+*})$, we can write

$$\begin{aligned}\Big| \int_{\mathbb{R}^+} (\rho(t,x) - \rho_0(t,x))\Phi(x)dx \Big| \leq & \Big| \int_{\mathbb{R}^+} (\rho(t,x) - \rho_\epsilon(t,x))\Phi(x)dx \Big| \\ & + \Big| \int_{\mathbb{R}^+} (\rho_\epsilon(t,x) - \tilde{\rho}_0^\epsilon(t,x))\Phi(x)dx \Big| \\ & + \int_{\mathbb{R}^+} (\tilde{\rho}_0^\epsilon(t,x) - \rho_0(t,x))\Phi(x)dx \Big|\end{aligned}$$

and similarly for u, and it is clear, using the regularisation of the data and what has been done before that

$$\lim_{t \to 0} \int_{\mathbb{R}^+} (\rho(t,x) - \rho_0(t,x))\Phi(x)dx = 0$$

and

$$\lim_{t \to 0} \int_{\mathbb{R}^+} (u(t,x) - u_0(t,x))\Phi(x)dx = 0$$

Now thanks to the H^1 bound of u_ϵ, for each t there exists a subsequence $u_{\epsilon(t)}$ such that $u_{\epsilon(t)}$ converges weakly in H^1 towards u and as before, since H_0^1 is closed for the weak convergence, $u \in L^\infty([0, \infty[; H_0^1(\mathbb{R}^{+*}))$.

To conclude the proof and show that $\rho \in L^\infty([0,\infty[;\Lambda_{\sigma_0})$, let us introduce :

$$\Omega_n = [0,n], \quad E_{c_0} = \{\rho; \int_{\Omega_n} \sigma_0(1+\rho) \leq c_0\}.$$

Thanks to the a priori bound (2.8), the subsequence $(\rho_\epsilon, u_\epsilon)$ which converges weakly to (ρ, u) and which is solution of system (2.3) satisfies $\rho_\epsilon|_{\Omega_n} \in E_{c_0}$.
For each fixed t, let $\rho_{\epsilon(t)}$ be a subsequence of ρ_ϵ which converges weakly in $L^1(\Omega_n)$ to $\rho(t,.)$. Since E_{c_0} is a convex subset of $L^1(\Omega_n)$, its weak closure is equal to its strong closure (see [13]), therefore there exixts a subsequence $p_k \in E_{c_0}$ which converges strongly in $L^1(\Omega_n)$ and thus (up to the extraction of a subsequence) almost everywhere in Ω_n to $\rho|_{\Omega_n}$. So,

$$\lim_{k\to\infty} \sigma_0(1+p_k(x)) = \sigma_0(1+\rho|_{\Omega_n}(t,x)) \text{ almost everywhere in } \Omega_n.$$

Now using Fatou's Lemma (σ_0 is positive),

$$\int_{-n}^{n} \sigma_0(1+\rho(t,x))dx \leq \text{liminf} \int_{-n}^{n} \sigma_0(1+p_k(x))dx \leq c_0$$

Thus $\rho(t,.) \in E_{c_0}$.
Let n tend to infinity, we can conclude that $\rho \in L^\infty([0,\infty[;\Lambda_{\sigma_0})$. □

Since the Orlicz space Λ_{σ_0} is contained in $L^1_{loc}(\mathbb{R}^+)$ (see [12]), we have

Corollary 2.5.1. *Let $(u_0,\rho_0) \in \Lambda_{\sigma_0} \times H^1_0(\mathbb{R}^{+*})$ satisfying (C). Then the solution (ρ,u) of system (2.1) belongs to $L^\infty([0,\infty[;L^1_{loc} \times H^1_0)$.*

Remark 2.5.1. *Here we studied the non linear system on the half line with the boundary condition $u(t,0) = 0$; in [9] are presented two other possible boundary conditions that yield a linearly well posed problem on the half line with smooth data : either $\eta(t,0) = 0$, or $u_x(t,0) = 0$. They also show in [9] that the appropriate boundary conditions that should be given on a finite intervall $[0,L]$ are either $\eta(t,x)$ or any one of the functions $u(t,x)$ or $u_x(t,x)$ for both $x = 0$ and $x = L$.*
In the last section, we explain the case of the initial boundary value problem on $[0,1]$, with boundary conditions on u.

2.6 The Boundary Value Problem with a non homogeneous boundary condition

We present here briefly the case where the boundary condition on $x = 0$ is non zero; we study the Boussinesq system with the following initial and boundary conditions :

$$\begin{cases} \rho(0,x) = \rho_0(x) \ \ \forall x \in \mathbb{R}^+, \\ u(0,x) = u_0(x) \ \ \forall x \in \mathbb{R}^+, \\ u(t,0) = g(t) \quad \forall t \geq 0, \end{cases} \tag{2.23}$$

where $g \in C^1(\mathbb{R}^+)$.
The method used above can be adapted to obtain the following result :

Theorem 2.6.1. *Let $g \in C^1(\mathbb{R}^+)$ and let $T > 0$; let $(\rho_0, u_0) \in \Lambda_{\sigma_0} \times H^1(\mathbb{R}^+)$ satisfy (C) and $u_0(0) = g(0)$;*
Then there exists a weak solution to the system (2.1) with initial data (ρ_0, u_0) satisfying the boundary condition $u(t,0) = g(t)$ for almost every $t \in [0,T]$.
Moreover (ρ, u) belongs to $L^\infty([0,T]; L^1_{loc} \times H^1)$.

Proof. We present the most important aspects of the proof.
First we solve the corresponding regularized problem with the contraction mapping principle; the integral formulations of the solutions are here :

$$\begin{aligned}\rho(t,x) &= \int_{\mathbb{R}^+} [G^\epsilon(t,x-y) - G^\epsilon(t,x+y)]\rho_0(y)dy \\ &\quad - \int_0^t \int_{\mathbb{R}^+} [G^\epsilon_x(t-s,x-y) + G^\epsilon_x(t-s,x+y)](u(s,y) + \rho(s,y)u(s,y))dyds \\ u(t,x) &= u_0(x) + \int_0^t \int_{\mathbb{R}^+} [K(x+y) + K(x-y)](\rho(s,y) + \frac{u^2}{2}(s,y))dyds + e^{-x}g(t)\end{aligned}$$

As before we can find a unique solution $(\rho, u) \in C([0,t_0]; C^2_0 \times C^2_0)$ to the initial boundary-value problem (2.3)-(2.4) with initial data $(\rho_0, u_0) \in C^2_0 \times C^2_0$.
For the a priori estimates, we first introduce a function $h(t,x) = g(t)\Phi(x)$, where $\Phi \in \mathcal{D}(\mathbb{R})$, $\Phi(0) = 1$, the important fact is that $h(t,0) = g(t)$.
Now let $v(t,x) = u(t,x) - h(t,x)$ where u is the first component of the solution to the regularized problem. Then (ρ, v) satisfies :

$$\begin{cases} w_t + (wv)_x - \epsilon w_{xx} = -(hw)_x, \\ v_t + w_x + vv_x - v_{xxt} = h_{xxt} - h_t - hh_x - (hv)_x. \end{cases} \tag{2.24}$$

where $w = 1 + \rho$, and $v(t,0) = 0$, $\rho(t,0) = 0$.

We can apply the same method as above using the entropy of the associated hyperbolic system $\eta(w,v) = \dfrac{v^2}{2} + \sigma_0(w)$.
We find

$$\eta(w,v)_t + q(w,v)_x = \epsilon w_{xx}\sigma_0'(w) - (hw)_x\sigma_0'(w) + vv_{xxt} + (h_{xxt} - h_t - hh_x)v - (hv)_x v,$$

which we integrate over $F = \{(s,x); \delta \le x \le N, 0 \le s \le t\}$. After letting δ tend to zero and N tend to infinity, and after simplifications it remains :

$$\begin{aligned}\int_{\mathbb{R}^+} \eta(w,v) + \frac{v_x^2}{2}dx \le \int_{\mathbb{R}^+} \eta(w_0,v_0) + \frac{v_{0,x}^2}{2}dx - \int_0^t \int_{\mathbb{R}^+} (hw)_x\sigma_0'(w)dxds \\ - \int_0^t \int_{\mathbb{R}^+} v(hv)_x dxds + \int_0^t \int_{\mathbb{R}^+} (h_{xxt} - h_t - hh_x)vdxds\end{aligned}$$

But now using the expression of $\sigma_0(w) = w\log w + 1 - w$, and the boundary conditions,

$$\begin{aligned}
-\int_0^t\int_{\mathbb{R}^+}(hw)_x\sigma_0'(w)dxds &= -\int_0^t\int_{\mathbb{R}^+}hw_x\sigma_0'(w) - \int_0^t\int_{\mathbb{R}^+}h_x w\log w \\
&= -\int_0^t\int_{\mathbb{R}^+}(\sigma_0(w))_x h - \int_0^t\int_{\mathbb{R}^+}\sigma_0(w)h_x + \int_0^t\int_{\mathbb{R}^+}(w-1)h_x \\
&= \int_0^t\int_{\mathbb{R}^+}\rho h_x \leq \int_0^t ||h_x(s,.)||_{L^\infty}||\rho||_{L^1(supp(\Phi))} \\
&\leq c_0\int_0^t ||h_x(s,.)||_{L^\infty}
\end{aligned}$$

And,

$$\begin{aligned}
-\int_0^t\int_{\mathbb{R}^+}v(hv)_x dxds &= \int_0^t\int_{\mathbb{R}^+}v_x hv = \int_0^t\int_{\mathbb{R}^+}\frac{v^2}{2}h_x \\
&\leq \int_0^t ||h_x(s,.)||_{L^\infty}\int_{\mathbb{R}^+}\frac{v^2}{2}dxds
\end{aligned}$$

And

$$\int_0^t\int_{\mathbb{R}^+}(h_{xxt} - h_t - hh_x)vdxds \leq \int_0^t \frac{1}{2}||(h_{xxt} - h_t - hh_x)(s,.)||_{L^2}^2 + \frac{1}{2}||v(s,.)||_{L^2}^2 ds$$

Finally, since $\sigma_0(w) \geq 0$, we obtain for $t \in [0,T]$,

$$\begin{aligned}
\int_{\mathbb{R}^+}\frac{v^2(t,x)}{2} + \sigma_0(w(t,x)) + \frac{v_x^2(t,x)}{2}dx &\leq \int_{\mathbb{R}^+}\frac{v_0^2}{2} + \sigma_0(w_0) + \frac{v_{0,x}^2}{2} + C_{h,T} \\
&+ C_{h,T}\int_0^t\int_{\mathbb{R}^+}\frac{v^2(s,x)}{2} + \sigma_0(w(s,x)) + \frac{v_x^2(s,x)}{2}dxds
\end{aligned}$$

where $C_{h,T}$ is a constant depending on h and on T.
Then using a Gronwall lemma, we can obtain, for all $t \in [0,T]$:

$$\int_{\mathbb{R}^+}\frac{v^2}{2} + \sigma_0(w) + \frac{v_x^2}{2} \leq (\int_{\mathbb{R}^+}\frac{v_0^2}{2} + \sigma_0(w_0) + \frac{v_{0,x}^2}{2} + C_{h,T})e^{C_{h,T}T}$$

Since $u(t,x) = v(t,x) + h(t,x)$, the triangular inequality yields :

$$\begin{aligned}
\int_{\mathbb{R}^+}\frac{u^2}{2} + \sigma_0(w) + \frac{u_x^2}{2} &\leq (\int_{\mathbb{R}^+}\frac{u_0^2}{2} + \sigma_0(w_0) + \frac{u_{0,x}^2}{2} + C_{h,T})e^{C_{h,T}T} \\
&+ \sup_{0\leq t\leq T}||h(t,.)||_{H^1}^2(1 + e^{C_{h,T}T}) \\
&\leq (\int_{\mathbb{R}^+}\frac{u_0^2}{2} + \sigma_0(w_0) + \frac{u_{0,x}^2}{2} + C_{h,T})e^{C_{h,T}T} \\
&+ C\sup_{0\leq t\leq T}|g(t)|(1 + e^{C_{h,T}T})
\end{aligned}$$

The estimates of Corollary (2.3.1) and Theorem (2.3.2) remain unchanged and we can extend on $[0,T]$ the solution $(\rho_\epsilon, u_\epsilon)$ of the regularized problem. The next steps of the proof apply, since the existence of a solution (ρ, u) of (2.1) satisfying (2.23) with $u \in L^\infty([0,T]; H^1)$ is equivalent to the existence of a solution (ρ, v) of (2.24) with $v \in L^\infty([0,T]; H_0^1)$. □

2.7 The Boundary Value Problem on [0,1].

We are here interested with the study of the Boussinesq system on $[0,1]$ supplemented with the following initial and boundary conditions :

$$\begin{cases} \rho(0,x) = \rho_0(x) \ \ \forall x \in \mathbb{R}^+, \\ u(0,x) = u_0(x) \ \ \forall x \in \mathbb{R}^+, \\ u(t,0) = u(t,1) = 0 \ \ \forall t \geq 0. \end{cases} \tag{2.25}$$

We first solve by the same means as before the regularized problem with the following boundary conditions :

$$\begin{cases} u(t,0) = u(t,1) = 0 \ \ \forall t \geq 0, \\ \rho(t,0) = \rho(t,1) = 0. \end{cases} \tag{2.26}$$

In all this section, we denote by $C_0^2 = \{u \in C^2(0,1); u(0) = u(1) = 0\}$.
For initial data $(\rho_0, u_0) \in C_0^2(0,1) \times C_0^2(0,1)$, there exists $t_0 > 0$ and a unique solution $(\rho_\epsilon, u_\epsilon) \in C([0,t_0]; C_0^2 \times C_0^2)$, which satisfies :

$$\begin{aligned} \rho_\epsilon(t,x) &= \int_0^1 [\theta^\epsilon(t,x-y) - \theta^\epsilon(t,x+y)]\rho_0(y)dy \\ &\quad - \int_0^t \int_0^1 [\theta_x^\epsilon(t-s,x-y) + \theta_x^\epsilon(t-s,x+y)](u_\epsilon(s,y) + \rho_\epsilon(s,y)u_\epsilon(s,y))dyds \\ u_\epsilon(t,x) &= u_0(x) - \frac{1}{2}\int_0^t \int_0^x (e^{x-y} + e^{y-x})(\rho_\epsilon(s,y) + \frac{u_\epsilon^2}{2}(s,y))dyds \\ &\quad + \frac{\mathrm{sh}(x)}{(e^{-1}-e)} \int_0^t \int_0^1 (e^{y-1} + e^{1-y})(\rho_\epsilon(s,y) + \frac{u_\epsilon^2}{2}(s,y))dyds \end{aligned}$$

where $\theta^\epsilon(t,x) = \sum_{m \in \mathbf{Z}} G^\epsilon(t, x+2m)$.

If we suppose $1 + \rho_0(x) > 0$, we then obtain the a priori estimate (2.8) similarly as before. We thus get the estimate (2.11), and the estimate (2.12) can be improved, since we work on $[0,1]$, which is of finite measure : here for all $t > 0$, ρ_ϵ is uniformly bounded in $L^1(0,1)$.
The solution can be extended to $\mathbb{R}^+$ and the convergence Theorem obtained in Section 2.4 becomes :

Theorem 2.7.1. *Let (ρ_0, u_0) be in $C_0^2 \times C_0^2$ such that $1 + \rho_0 > 0$. For each $\epsilon > 0$ let $(\rho_\epsilon, u_\epsilon) \in C([0,\infty[, C_0^2 \times C_0^2)$ be the solution to the boundary-value problem (2.3)-(2.26) with initial data (ρ_0, u_0).*
There exists a subsequence $(\rho_\epsilon, u_\epsilon)$ and (ρ, u) such that :

(i) For any $T > 0$, for any $\Phi \in L^\infty((0,T) \times (0,1))$

$$\lim_{\epsilon \to 0} \int_0^T \int_0^1 (\rho_\epsilon(t,x) - \rho(t,x))\Phi(t,x)dxdt = 0.$$

(ii) For any $T > 0$,

$$\lim_{\epsilon \to 0} \int_0^1 |u_\epsilon(t,x) - u(t,x)|^2 dx = 0 \text{ for all } t \in [0,T].$$

The proof, which follows exactly the same method, is quite simplified on $[0,1]$. To show that the limit functions obtained are solutions of the Boussinesq system, and satisfy the boundary conditions, we repeat the proof of Theorem (2.4.2), which is easier here.
We finally obtain the following result :

Theorem 2.7.2. *Let $(\rho_0, u_0) \in \Lambda_{\sigma_0} \times H_0^1(0,1)$ such that $\inf_{x\in[0,1]}(1+\rho_0(x)) > 0$.*
Then there exists a weak solution of the system (2.1) with initial data (ρ_0, u_0), satisfying the boundary conditions $u(t,0) = u(t,1) = 0$ for almost every $t > 0$.
Moreover (ρ, u) belongs to $L^\infty(\mathbb{R}^+; \Lambda_{\sigma_0} \times H_0^1(0,1)) \subset L^\infty(\mathbb{R}^+; L^1(0,1) \times H_0^1(0,1))$.

To prove this Theorem, we procede as in Section 2.5 : we extend the initial data to $\mathbb{R}$ and use a regularization and truncature proceed. We extend u_0 by zero as it lies in H_0^1 and ρ_0 by parity and then periodicity. The method is then exactly the same, we show an estimate similar to (2.22) and are able to find a subsequence $(\rho_\epsilon, u_\epsilon)$ which converges weakly to a solution of the initial-boundary value problem (2.1)-(2.25), which lies in $L^\infty([0,\infty[; \Lambda_{\sigma_0} \times H_0^1(0,1))$.

2.8 Uniqueness of smooth solutions

We now prove the following result concerning uniqueness of solutions to the initial boundary-value problem (2.1)-(2.2).

Theorem 2.8.1. *Let $T > 0$ and assume that (ρ, u) and $(\tilde\rho, \tilde u)$ satisfy (2.1)-(2.2) with (ρ, u) and $(\tilde\rho, \tilde u) \in L^\infty([0,T]; H^1(\mathbb{R}^+) \times H^2(\mathbb{R}^+))$. Then $(\rho, u) = (\tilde\rho, \tilde u)$ on $[0,T] \times \mathbb{R}^+$.*

Proof. Let $\gamma = \rho - \tilde\rho$ and $v = u - \tilde u$; they satisfy $v(t,0) = 0$ and :

$$\begin{aligned} &\gamma_t + v_x + uu_x - \tilde u\tilde u_x - v_{xxt} = 0, \\ &v_t + \gamma_x + u\rho_x + u_x\rho - \tilde u\tilde\rho_x - \tilde u_x\tilde\rho = 0. \end{aligned}$$

Multiplying the first line by v and the second by γ and integrating on $\mathbb{R}^+$, we find :

$$\int_{\mathbb{R}^+} vv_t - \int_{\mathbb{R}^+} v_{xxt}v = -\int_{\mathbb{R}^+} (\gamma_x v + v^2u_x + \tilde u v v_x)$$

and

$$\int_{\mathbb{R}^+} \gamma\gamma_t = -\int_{\mathbb{R}^+} \gamma v_x - \int_{\mathbb{R}^+} \gamma(u\rho_x + u_x\rho - \tilde u\tilde\rho_x - \tilde u_x\rho)$$

After some integration by parts, considering the fact that v takes its values in H^2 and that $v(t,0) = 0$ we obtain

$$\begin{aligned} \frac{1}{2}\frac{d}{dt}\int_{\mathbb{R}^+} v^2 + v_x^2 + \gamma^2 = &-\int_{\mathbb{R}^+} (\gamma_x v + v^2u_x + \tilde u v v_x) \\ &- \int_{\mathbb{R}^+} \gamma v_x - \int_{\mathbb{R}^+} \gamma(u\gamma_x + v\tilde\rho_x + v_x\rho + \gamma\tilde u_x) \end{aligned}$$

Thanks to the regularity of v and γ, we have

$$\Big|\int_{\mathbb{R}^+} v^2u_x + \tilde u v v_x\Big| \le ||v||_\infty ||v||_{H^1}^2$$

and since $\int_{\mathbb{R}^+} \gamma\gamma_x u = \frac{1}{2}\int_{\mathbb{R}^+} \gamma^2 u_x$

$$\Big|\int_{\mathbb{R}^+} \gamma(u\gamma_x + v\tilde{\rho}_x + v_x\rho + \gamma\tilde{u}_x)\Big| \leq \frac{||u_x||_\infty + ||\tilde{u}_x||_\infty}{2}\int_{\mathbb{R}^+}\gamma^2 + (||v_x||_\infty||\rho||_{L^2} + ||\tilde{\rho}_x||_{L^2}||v||_\infty)||\gamma||_{L^2} \leq C\int_{\mathbb{R}^+}(\gamma^2 + v^2 + v_x^2)$$

since for the last term,

$$||\gamma||_{L^2}||\tilde{\rho}_x||_{L^2}||v||_\infty \leq C||\gamma||_{L^2}(||v||_{L^2}^{1/2} + ||v_x||_{L^2}^{1/2}) \leq C'\int_{\mathbb{R}^+}\gamma^2 + v^2 + v_x^2.$$

Finally we have

$$\frac{1}{2}\frac{d}{dt}\int_{\mathbb{R}^+}\gamma^2 + v^2 + v_x^2 \leq C\int_{\mathbb{R}^+}\gamma^2 + v^2 + v_x^2$$

and since $v(0,x) = v_x(0,x) = \gamma(0,x) = 0\ \forall x \in \mathbb{R}^+$, it follows the expected result. □

2.9 Appendix : regularity of solutions to the Boussinesq system on the infinite space

In this section we consider solutions to the Boussinesq system and study their regularity. In [1], Amick shows that given two constants $\bar{\rho}$ and $\bar{u}$, and given an initial data $(\rho - \bar{\rho}, u - \bar{u}) \in C_0^\infty(\mathbb{R})$ with $\rho(x) > 1$, $x \in \mathbb{R}$, then the corresponding solution to the Boussinesq system (ρ, u) is infinitely differentiable on $\mathbb{R}^+ \times \mathbb{R}$, and is unique.
Following [1], the aim of this appendix is to furnish a proof of the persistence of a finite regularity for the solutions to the Boussinesq system, namely :

Theorem 2.9.1. *Let $\bar{\rho}$ and $\bar{u}$ be given constants and let $(\rho_0 - \bar{\rho}, u_0 - \bar{u}) \in H^1(\mathbb{R}) \times H^2(\mathbb{R})$ be with compact support, and $(\rho_0, u_0 - \bar{u}) \in \Lambda_{\sigma_0} \times H_0^1$, such that $1 + \rho_0 > 0$. Let $T > 0$, then the solutions $(\rho^\epsilon, u^\epsilon)$ to the regularized system with inital data (ρ_0, u_0) satisfy for all $t \in [0,T]$,*

$$||D^j u^\epsilon(t,.)||_{L^2(\mathbb{R})} \leq C_{T,j},\ ||D^k\rho^\epsilon(t,.)||_{L^2(\mathbb{R})} \leq C_{T,k},\ \ 0 \leq j \leq 2,\ \ 0 \leq k \leq 1,$$

where $C_{T,j}$, $C_{T,k}$ are constants depending only on T, j and k.
The solutions (ρ, u) to the Boussinesq system belong to $L^\infty(0,T,H^1(\mathbb{R}) \times H^2(\mathbb{R}))$.

Corollary 2.9.1. *Let $\bar{\rho}$ and $\bar{u}$ be given constants and let $(\rho_0 - \bar{\rho}, u_0 - \bar{u}) \in H^1(\mathbb{R}) \times H^2(\mathbb{R})$ be with compact support, with $(\rho_0, u_0 - \bar{u}) \in \Lambda_{\sigma_0} \times H_0^1$ and $1 + \rho_0 > 0$. For all $T > 0$, there exists a unique solution (ρ, u) to the Boussinesq system in $L^\infty(0,T,H^1(\mathbb{R}) \times H^2(\mathbb{R}))$.*

This regularity result does not seem to extend to solutions on $\mathbb{R}^+$; indeed in the proof of 2.9.1, a bad boundary term appears which cannot be easily dealt with.
The proof of Corollary 2.9.1 follows from Theorem 2.9.1 using Section 8.

2.9.1 Proof of the estimates

From now and then, we will denote by c_0 any constant depending on $||\tilde{\rho}_0||_{H^1}$, $||\tilde{u}_0||_{H^2}$, or T, and independant of ϵ.
Let $T > 0$, let $\bar{\rho}$ and $\bar{u}$ be given constants, and let $(\rho_0 - \bar{\rho}, u_0 - \bar{u}) \in C_0^\infty(\mathbb{R}) \times C_0^\infty(\mathbb{R})$. Then (see [14]) there exists a unique solution $(\rho^\epsilon, u^\epsilon) \in C([0,T]; C_0^\infty(\mathbb{R}) \times C_0^\infty(\mathbb{R}))$ to the regularized system which satisfies :

$$\int_{\mathbb{R}^+} \frac{(u^\epsilon - \bar{u})^2}{2} dx + \int_{\mathbb{R}^+} \frac{(u_x^\epsilon)^2}{2} dx + \int_{\mathbb{R}^+} \sigma_0(w^\epsilon) dx \leq c_0. \tag{2.27}$$

After denoting $(\tilde{\rho}^\epsilon, \tilde{u}^\epsilon) = (\rho^\epsilon - \bar{\rho}, u^\epsilon - \bar{u})$ and $(\tilde{\rho}_0, \tilde{u}_0) = (\rho_0 - \bar{\rho}, u_0 - \bar{u})$, the solution satisfies the following regularized system :

$$\tilde{\rho}_t + \tilde{u}_x + [(\tilde{\rho} + \bar{\rho})(\tilde{u} + \bar{u})]_x = \epsilon \tilde{\rho}_{xx}, \tag{2.28}$$

$$\tilde{u}_t + \tilde{\rho}_x + (\tilde{u} + \bar{u})\tilde{u}_x = \tilde{u}_{xxt}, \tag{2.29}$$

and can be written :

$$\begin{aligned} \tilde{\rho}^\epsilon(t,x) = &\int_{\mathbb{R}} G^\epsilon(t, x-y)\tilde{\rho}_0(y)dy \\ &- \int_0^t \int_{\mathbb{R}} G_x^\epsilon(t-s, x-y)(\tilde{u}^\epsilon(s,y) + (\tilde{\rho}^\epsilon(s,y) + \bar{\rho})(\tilde{u}^\epsilon(s,y) + \bar{u}))dyds \end{aligned} \tag{2.30}$$

$$\tilde{u}^\epsilon(t,x) = \tilde{u}_0(x) + \int_0^t \int_{\mathbb{R}} K(x-y)(\tilde{\rho}^\epsilon(s,y) + \frac{(\tilde{u}^\epsilon)^2}{2}(s,y) + \bar{u}\tilde{u}^\epsilon)dyds \tag{2.31}$$

By (2.27), there exists a constant c_0 such that

$$||\tilde{u}^\epsilon(t,.)||_{L^2} \leq c_0, \ ||D_x\tilde{u}^\epsilon(t,.)||_{L^2} \leq c_0, \text{ and } ||\tilde{u}^\epsilon(t,.)||_\infty \leq c_0.$$

Then we write

$$D_x\tilde{u}^\epsilon(t,x) = \int_0^t \tilde{\rho}^\epsilon(s,x)ds + F^\epsilon(t,x) \tag{2.32}$$

where

$$\begin{aligned} F^\epsilon(t,x) = (u_0)_x(x) &+ \int_0^t \Big[\frac{(\tilde{u}^\epsilon)^2(s,x)}{2} + \bar{u}\tilde{u}^\epsilon(s,x)\Big]ds \\ &- \frac{1}{2}\int_0^t \int_{\mathbb{R}} e^{-|y-x|}\Big[\tilde{\rho}^\epsilon(s,y) + \frac{(\tilde{u}^\epsilon)^2(s,y)}{2} + \bar{u}\tilde{u}^\epsilon(s,y)\Big]dyds \end{aligned}$$

Thanks to the estimates on $\tilde{u}^\epsilon$ obtained previously and since $\tilde{u}_0 \in H^2(\mathbb{R})$, we have

$$||F^\epsilon(t,.)||_{L^2}, \ ||F^\epsilon(t,.)||_\infty, \ ||F_x^\epsilon(t,.)||_{L^2} \leq c_0$$

Thus obtaining an ϵ-independant estimate of $||D_x\tilde{\rho}^\epsilon||_{L^2}$ will give automatically an estimate of $||D_{xx}\tilde{u}^\epsilon||_{L^2}$.
To reach this estimate we first show the following Lemma :

Lemma 2.9.1. *For all $t \in [0,T]$,*

$$||\tilde{\rho}^\epsilon(t,.)||_{L^\infty} \leq c_0, \text{ and } ||D_x\tilde{u}^\epsilon(t,.)||_{L^\infty} \leq c_0.$$

Proof. Using (2.32), the first estimate gives the second one easily. For the first part, let $M \geq 1$ be an odd integer and let us multiply (2.28) by $(\tilde{\rho}^\epsilon)^M$ and integrate on $\mathbb{R}$, then

$$\begin{aligned}\frac{1}{M+1}\frac{d}{dt}\int_{\mathbb{R}}(\tilde{\rho}^\epsilon)^{M+1} &= -(1+\bar{\rho})\int_{\mathbb{R}}(\tilde{\rho}^\epsilon)^M(\tilde{u}^\epsilon)_x - \frac{M}{M+1}\int_{\mathbb{R}}(\tilde{\rho}^\epsilon)^{M+1}(\tilde{u}^\epsilon)_x \\ &\quad - \epsilon M\int_{\mathbb{R}}(\tilde{\rho}^\epsilon_x)^2(\tilde{\rho}^\epsilon)^{M-1}\end{aligned}$$

Since M is odd we can write, using (2.32),

$$\begin{aligned}\frac{1}{M+1}\frac{d}{dt}\int_{\mathbb{R}}(\tilde{\rho}^\epsilon)^{M+1} + \epsilon M\int_{\mathbb{R}}(\tilde{\rho}^\epsilon_x)^2(\tilde{\rho}^\epsilon)^{M-1} &= -(1+\bar{\rho})\int_{\mathbb{R}}(\tilde{\rho}^\epsilon)^M(t,x)\int_0^t\tilde{\rho}^\epsilon(s,x)dsdx \\ &\quad -(1+\bar{\rho})\int_{\mathbb{R}}(\tilde{\rho}^\epsilon)^M(t,x)F^\epsilon(t,x)dx \\ &\quad -\frac{M}{M+1}\int_{\mathbb{R}}(\tilde{\rho}^\epsilon)^{M+1}(t,x)\int_0^t\tilde{\rho}^\epsilon(s,x)dsdx \\ &\quad -\frac{M}{M+1}\int_{\mathbb{R}}(\tilde{\rho}^\epsilon)^{M+1}(t,x)F^\epsilon(t,x)dx \\ &= I_1+I_2+I_3+I_4\end{aligned}$$

Since $-\tilde{\rho}^\epsilon \leq 1+\bar{\rho}$ and using (2.32), we have

$$I_3 \leq \frac{M}{M+1}(1+\bar{\rho})T\int_{\mathbb{R}}(\tilde{\rho}^\epsilon)^{M+1} \text{ and } |I_4| \leq c_0\int_{\mathbb{R}}(\tilde{\rho}^\epsilon)^{M+1}.$$

Moreover, for $M \geq 1$, $|\tilde{\rho}^\epsilon|^M \leq (\tilde{\rho}^\epsilon)^{M+1} + |\tilde{\rho}^\epsilon|$ and

$$|I_2| \leq (1+\bar{\rho})\int_{\mathbb{R}}|F^\epsilon|(\tilde{\rho}^\epsilon)^{M+1} + (1+\bar{\rho})\int_{\mathbb{R}}|F^\epsilon||\tilde{\rho}^\epsilon| \leq c_0(1+\int_{\mathbb{R}}(\tilde{\rho}^\epsilon)^{M+1})$$

where we used the same arguments as above for the estimation of $||\tilde{\rho}^\epsilon(t,.)||_{L^1}$.
Finally,

$$\begin{aligned}\frac{1}{M+1}\int_{\mathbb{R}}(\tilde{\rho}^\epsilon)^{M+1}(t,x)dx &\leq \frac{1}{M+1}\int_{\mathbb{R}}\tilde{\rho}_0(x)^{M+1}dx \\ &\quad + c_0\int_{\mathbb{R}}\Big[1+\int_0^t\int_{\mathbb{R}}(\tilde{\rho}^\epsilon)^{M+1}(s,x)dxds\Big] \\ &\quad + (1+\bar{\rho})\int_{\mathbb{R}}\int_0^t(\tilde{\rho}^\epsilon(s,x))^M\int_0^s\tilde{\rho}^\epsilon(z,x)dzdsdx \\ &\leq \frac{1}{M+1}\int_{\mathbb{R}}\tilde{\rho}_0(x)^{M+1}dx \\ &\quad + c_0(1+\int_0^t\int_{\mathbb{R}}(\tilde{\rho}^\epsilon(s,x))^{M+1}dxds),\end{aligned}$$

where we used Holder's inequality for the last term.
Now thanks to a Gronwall's lemma, we obtain :

$$\Big(\int_{\mathbb{R}}(\tilde{\rho}^{\epsilon}(t,x))^{M+1}dx\Big)^{\frac{1}{M+1}} \leq \Big[\int_{\mathbb{R}}\tilde{\rho}_0(x)^{M+1}dx + c_0\Big]^{\frac{1}{M+1}} e^{c_0 T} \leq c_0.$$

If we let tend M to $+\infty$, we obtain the desired estimate :

$$||\tilde{\rho}^{\epsilon}(t,.)||_{L^{\infty}} \leq c_0.$$

□

We finish by the following Lemma :

Lemma 2.9.2. *For all $t \in [0,T]$,*

$$||D_x\tilde{\rho}^{\epsilon}(t,.)||_{L^2} \leq c_0, \text{ and } ||D_{xx}\tilde{u}^{\epsilon}(t,.)||_{L^2} \leq c_0$$

Proof. We multiply (2.28) by $(\tilde{\rho}^{\epsilon})_{xx}$ and integrate on $\mathbb{R}$,

$$\begin{aligned}\frac{1}{2}\frac{d}{dt}\int_{\mathbb{R}}(\tilde{\rho}^{\epsilon}_x)^2 + \epsilon\int_{\mathbb{R}}\tilde{\rho}^{\epsilon}_{xx} &= -\frac{3}{2}\int_{\mathbb{R}}(\tilde{\rho}^{\epsilon}_x)^2\tilde{u}^{\epsilon}_x - \int_{\mathbb{R}}\tilde{\rho}^{\epsilon}\tilde{\rho}^{\epsilon}_x\tilde{u}^{\epsilon}_{xx} - (1+\bar{\rho})\int_{\mathbb{R}}\tilde{\rho}^{\epsilon}_x\tilde{u}^{\epsilon}_{xx} \\ &= I_1(t) + I_2(t) + I_3(t).\end{aligned}$$

By Lemma 2.9.1,

$$|I_1(t)| \leq c_0\int_{\mathbb{R}}(\tilde{\rho}^{\epsilon}_x(t,x))^2dx.$$

Then

$$\int_{\mathbb{R}}(\tilde{\rho}^{\epsilon}_x(t,x))^2dx \leq \int_{\mathbb{R}}(\tilde{\rho}_{0\,x}(x))^2dx + \int_0^t |I_2(s)| + |I_3(s)|ds + c_0\int_{\mathbb{R}}\int_0^t |\tilde{\rho}^{\epsilon}_x(s,x)|^2dsdx$$

Using (2.32) and Lemma 2.9.1, we find

$$\begin{aligned}\int_0^t |I_2(s)|ds &\leq c_0\int_0^t\Big(\int_{\mathbb{R}}|\tilde{\rho}^{\epsilon}_x(s,x)|\int_0^s|\tilde{\rho}^{\epsilon}_x(z,x)|dz + c_0\int_{\mathbb{R}}|\tilde{\rho}^{\epsilon}_x(s,x)||F^{\epsilon}_x(s,x)|dx\Big)ds \\ &\leq c_0\int_{\mathbb{R}}\int_0^t|\tilde{\rho}^{\epsilon}_x(s,x)|^2dsdx.\end{aligned}$$

and similarly for the third term I_3, which gives the desired estimate after applying a Gronwall inequality.
The second estimate of the Lemma is a consequence of (2.32). □

2.9.2 Regularity of the solutions

Now let $(\rho_0 - \bar{\rho}, u_0 - \bar{u}) \in H^1(\mathbb{R}) \times H^2(\mathbb{R})$ be with compact support and satisfy $(\rho_0, u_0 - \bar{u}) \in \Lambda_{\sigma_0} \times H^1_0$ and $1 + \rho_0(x) > 0$, and let $T > 0$.
We start by smoothing the data by using a regularizing sequence as in Section 5 : let $(\rho_0^\epsilon, u_0^\epsilon) \in C_c^\infty \times C_c^\infty$ be such that

$$\rho_0^\epsilon \to \rho_0 \text{ in } H^1(\mathbb{R}) \text{ and } u_0^\epsilon \to u_0 \text{ in } H^2(\mathbb{R}). \tag{2.33}$$

If $(\rho^\epsilon, u^\epsilon)$ is the solution of the regularized problem (2.28)-(2.29), thanks to Section 9.1, since $||\rho_0^\epsilon||_{H^1} \leq ||\rho_0||_{H^1}$ and $||u_0^\epsilon||_{H^2} \leq ||u_0||_{H^2}$, we have

$$||D_x^j \tilde{u}^\epsilon(t,.)||_{L^2} \leq c_0 \text{ and } ||D_x^j \tilde{\rho}^\epsilon(t,.)||_{L^2} \leq c_0, \;\; 0 \leq j \leq 2, \;\; 0 \leq k \leq 1.$$

Moreover this solution satisfies (2.27), and there exists a subsequence still denoted $(\rho^\epsilon, u^\epsilon)$ which converges weakly towards a weak solution (ρ, u) to the Boussinesq system (see [14]) ; and $(\rho, u - \bar{u}) \in L^\infty([0,\infty]; \Lambda_{\sigma_0} \times H^1)$.

This subsequence satisfies (2.33) therefore for all j, k ($j \in \{0,2\}$, $k \in \{0,1\}$), $D_x^k \rho^\epsilon$ and $D_x^j u^\epsilon$ are bounded in $L^\infty(0,T;L^2(\mathbb{R}))$ and we can extract another subsequence still denoted $(\rho^\epsilon, u^\epsilon)$ such that

$$D_x^k \rho^\epsilon \overset{*}{\rightharpoonup} f^k \text{ in } L^\infty(0,T;L^2(\mathbb{R}))$$
$$D_x^j u^\epsilon \overset{*}{\rightharpoonup} g^j \text{ in } L^\infty(0,T;L^2(\mathbb{R}))$$

Now $||f^k||_{L^\infty(0,T;L^2)} \leq \liminf ||D_x^k \rho^\epsilon||_{L^\infty(0,T;L^2)} \leq c_0$ therefore $f^k \in L^\infty(0,T;L^2(\mathbb{R}))$ and similarly $g^j \in L^\infty(0,T;L^2(\mathbb{R}))$.

Invoquing the uniqueness of the limit in $\mathcal{D}'((0,T) \times \mathbb{R})$, we conclude that $f^k = D_x^k \rho$ and $g^j = D_x^j u$; thus $\rho \in L^\infty(0,T;H^1(\mathbb{R}))$ and $u \in L^\infty(0,T;H^2(\mathbb{R}))$.

Bibliographie

[1] C. J. Amick, Regularity and uniqueness of solutions to the boussinesq system of equations, *J. Diff. Eq., 54*, 1984.

[2] T. B. Benjamin, Lectures on nonlinear wave motion, *Lectures in Applied Mathematics, Vol.15, Amer. Math. Soc., Providence, R.I.*, 1974.

[3] J. Bona, R. Smith, A model for the two-way propagation of water waves in a channel, *Math. Proc.Cambridge Philos., Soc. 79*, 1976.

[4] J. Bona, V. Dougalis, An initial and boundary-value problem for a model equation for propagation of long waves, *J. Math. Anal Appl., 75*, 1980.

[5] J. Bona, M. Chen, J. C. Saut, Boussinesq Equations and Other Systems for Small-amplitude Long Waves in Nonlinear Dispersive Media I : Derivation and Linear Theory, *J. Nonlinear Sci. 12, no. 4*, 2002.

[6] J. Bona, M. Chen, J. C. Saut, Boussinesq Equations and Other Systems for Small-amplitude Long Waves in Nonlinear Dispersive Media II : The nonlinear theory, *Nonlinearity 17*, 2004.

[7] J. R. Cannon, The One-dimensional Heat Equation, *Encyclopedia of Mathematics and its Applications*, 23, 1984.

[8] N. Dunford, J. Schwartz, Linear Operators. Part 1. *Pure and Applied Mathematics, Vol.VII, Interscience Publishers, New York*

[9] A. S. Fokas, B. Pelloni, Boundary Value Problems for Boussinesq Type Systems, *Math. Phys., Anal. Geom. 8*, 2005.

[10] A. Friedman, Partial Differential Equations of Parabolic Type, *Prentice Hall, Englewood Cliffs, N.J.*, 1964.

[11] P. D. Lax, Shock Waves and Entropy Contributions to Non-Linear Functionnal Analysis, *Academic Press, New York*, 1971.

[12] M. M. Rao, Z. D. Ren, Theory of Orlicz Spaces, *Monographs and Textbooks in Pure and Applied Mathematics, 146, Marcel Dekker Inc., New York*, 1991.

[13] W. Rudin, Functionnal Analysis, *McGraw-Hill, New York*, 1973.

[14] M. E. Schonbek, Existence of solutions for the Boussinesq system of equations, *J. Differential Equations*, 42, 1981, no. 3, 325–352.

[15] G. B. Whitham, Linear and Nonlinear Waves, *Pure and Applied Mathematics, Wiley-Interscience, New-York-London-Sydney*, 1974.

Chapitre 3

Sur les équations de Saint Venant avec périodicité dans une direction

Article paru dans Applicable Analysis, Volume 86, no 5, (2007), pages 537 - 553.

K. ADAMY*
*Laboratoire de Mathématiques, Université Paris-Sud
CNRS UMR 8628, 91405, Orsay, France.

Abstract : The linearized two-dimensionnal Shallow Water equations, supplemented with suitable boundary conditions in one direction and periodicity in the other direction are considered. The well-posedness of this mixed boundary value problem is proven, using the linear semi-group theory. The well-posedness of the totally periodic problem is also proven.

3.1 Introduction

In this article we are concerned with the linearized two-dimensionnal Shallow Water equations (see [5]). This system is a hyperbolic system which describes wave motion in a shallow homogeneous fluid when the horizontal wave length is much longer than the vertical scale of motion and than the depth of the fluid. These equations are often employed in models for oceanic or atmospheric flows and correspond to a level of physical complexity intermediate between the quasi-geostrophic equations and the full primitive equations (see [8], [5]).
The full Shallow Water equations are linearized around a constant flow (u_0, v_0, Φ_0). In most relevant geophysical problems the flow is subcritical, that is $u_0^2 + v_0^2 < \Phi_0$; we will here mainly consider this case, which is the most interesting and difficult, but all what is done works similarly in the supercritical case.
The fluid fills a two-dimensionnal domain and we will restrict ourselves to the case of functions which are periodic in the y-direction. We will describe appropriate boundary conditions (in both the subcritical and supercritical cases) that should be imposed in the x-direction in order to have a well-posed problem.
The well-posedness of the problem will be established using a semi-group approach; all the difficulties reside in showing the positiveness of the operator on its domain and of its adjoint : we will use a method of regularisation to obtain it.
The article is organized as follows : first, we present in Section 3.2 the model and the notations we use, then, in Section 3.3, we recall some results of the semi-groups theory. In Section 3.4.1, we prove the positiveness of the operator A and of its adjoint $A^\star$, and we obtain the well-posedness of our problem in Section 3.5. Finally, in Section 3.6, we prove the well-posedness of the space-periodic problem, that is when functions are periodic in the two directions.

3.2 Functionnal framework and notations

We are interested in the 2D-shallow water equations, linearized around a constant flow (u_0, v_0, Φ_0) :

$$\begin{cases} \dfrac{\partial u}{\partial t} + u_0 \dfrac{\partial u}{\partial x} + v_0 \dfrac{\partial u}{\partial y} + \dfrac{\partial \Phi}{\partial x} - fv = 0, \\ \dfrac{\partial v}{\partial t} + u_0 \dfrac{\partial v}{\partial x} + v_0 \dfrac{\partial v}{\partial y} + \dfrac{\partial \Phi}{\partial y} + fu = 0, \\ \dfrac{\partial \Phi}{\partial t} + u_0 \dfrac{\partial \Phi}{\partial x} + v_0 \dfrac{\partial \Phi}{\partial y} + \Phi_0 (\dfrac{\partial u}{\partial x} + \dfrac{\partial v}{\partial y}) = 0, \end{cases} \tag{3.1}$$

with

$$\begin{cases} u(x,y,0) = u^0(x,y), \\ v(x,y,0) = v^0(x,y), \\ \Phi(x,y,0) = \Phi^0(x,y). \end{cases}$$

Here u and v are the x and y components of the velocity, $\Phi = gz$ is the geopotential height (where g is the gravity, and z is the depth variation of the free surface) ; and the terms u_0, v_0, Φ_0 and f are respectively the advecting velocities, the mean geopotential height, and the Coriolis parameter, and are all positive constants. The domain under consideration is $\mathcal{M}_\infty = (0, L_1) \times \mathbb{R}$ and we set $\mathcal{M} = (0, L_1) \times (0, L_2)$, where L_2 is the period in the y-direction. This system can

also be written :

$$\begin{pmatrix} u_t \\ v_t \\ \Phi_t \end{pmatrix} + B_1 \begin{pmatrix} u_x \\ v_x \\ \Phi_x \end{pmatrix} + B_2 \begin{pmatrix} u_y \\ v_y \\ \Phi_y \end{pmatrix} + \begin{pmatrix} 0 & -f & 0 \\ f & 0 & 0 \\ 0 & 0 & 0 \end{pmatrix} \begin{pmatrix} u \\ v \\ \Phi \end{pmatrix} = 0,$$

where $B_1 = \begin{pmatrix} u_0 & 0 & 1 \\ 0 & u_0 & 0 \\ \Phi_0 & 0 & u_0 \end{pmatrix}$ and $B_2 = \begin{pmatrix} v_0 & 0 & 0 \\ 0 & v_0 & 1 \\ 0 & \Phi_0 & v_0 \end{pmatrix}$;

B_1 has three eigenvalues, u_0 and $u_0 \pm \sqrt{\Phi_0}$; we diagonalize the system along the x-direction by introducing the new variables :

$$\xi = u + \frac{1}{\sqrt{\Phi_0}}\Phi,\ \eta = u - \frac{1}{\sqrt{\Phi_0}}\Phi,\ \zeta = \sqrt{2}v.$$

We then obtain the following system in (ξ, ζ, η) :

$$\begin{cases} \xi_t + (u_0 + \sqrt{\Phi_0})\xi_x + v_0\xi_y + \sqrt{\frac{\Phi_0}{2}}\zeta_y - \frac{f}{\sqrt{2}}\zeta = 0, \\ \zeta_t + u_0\zeta_x + v_0\zeta_y + \sqrt{\frac{\Phi_0}{2}}(\xi - \eta)_y + \frac{f}{\sqrt{2}}(\xi + \eta) = 0, \\ \eta_t + (u_0 - \sqrt{\Phi_0})\eta_x + v_0\eta_y - \sqrt{\frac{\Phi_0}{2}}\zeta_y - \frac{f}{\sqrt{2}}\zeta = 0, \end{cases} \tag{3.2}$$

with $\xi(x, y, 0) = \xi^0(x, y),\ \zeta(x, y, 0) = \zeta^0(x, y),\ \eta(x, y, 0) = \eta^0(x, y)$.

This system is equivalent to :

$$\begin{pmatrix} \xi_t \\ \zeta_t \\ \eta_t \end{pmatrix} + A \begin{pmatrix} \xi_x \\ \zeta_x \\ \eta_x \end{pmatrix} + B \begin{pmatrix} \xi_y \\ \zeta_y \\ \eta_y \end{pmatrix} + C \begin{pmatrix} \xi \\ \zeta \\ \eta \end{pmatrix} = 0,$$

where A is diagonal, B is self-adjoint, C is skew-symmetric, and

$$A = \begin{pmatrix} u_0 + \sqrt{\Phi_0} & 0 & 0 \\ 0 & u_0 & 0 \\ 0 & 0 & u_0 - \sqrt{\Phi_0} \end{pmatrix},\ B = \begin{pmatrix} v_0 & \sqrt{\frac{\Phi_0}{2}} & 0 \\ \sqrt{\frac{\Phi_0}{2}} & v_0 & -\sqrt{\frac{\Phi_0}{2}} \\ 0 & -\sqrt{\frac{\Phi_0}{2}} & v_0 \end{pmatrix},$$

$$C = \begin{pmatrix} 0 & \frac{-f}{\sqrt{2}} & 0 \\ \frac{f}{\sqrt{2}} & 0 & \frac{f}{\sqrt{2}} \\ 0 & \frac{-f}{\sqrt{2}} & 0 \end{pmatrix}.$$

We will also write $\overline{u_0} = u_0 + \sqrt{\Phi_0}$, $\underline{u_0} = u_0 - \sqrt{\Phi_0}$, $\bar{f} = f/\sqrt{2}$, and $\Phi_1 = \sqrt{\Phi_0}/\sqrt{2}$. As we said before, we will mainly consider the subcritical case where $0 < u_0^2 + v_0^2 < \Phi_0 = 2\Phi_1^2$, so in this case, the three eigenvalues of A have different signs, u_0 and $\overline{u_0}$ are strictly positive, and $\underline{u_0}$ is strictly negative.

We will denote by H the space $L^2(\mathcal{M})^3$; we endow it with the scalar product of $L_2(\mathcal{M})^3$: $(U,V) = \int_{\mathcal{M}}(U_1V_1 + U_2V_2 + U_3V_3)dxdy$, which makes H a Hilbert space. Let also :

$$\begin{aligned} D &= \{U = (\xi,\zeta,\eta) \in C^\infty(\overline{\mathcal{M}}),\ \xi,\zeta,\eta \text{ are periodic of period } L_2 \\ &\quad \text{in the y-direction}\}. \end{aligned} \tag{3.3}$$

Let us also introduce the following new variables which will be useful : $k = v_0\xi + \Phi_1\zeta$, $\ell = v_0\zeta + \Phi_1(\xi - \eta)$, and $m = v_0\eta - \Phi_1\zeta$.

With all these new notations, our problem becomes :

$$\begin{cases} \xi_t + \overline{u_0}\xi_x + k_y - \bar{f}\zeta = 0, \\ \zeta_t + u_0\zeta_x + \ell_y + \bar{f}(\xi + \eta) = 0, \\ \eta_t + \underline{u_0}\eta_x + m_y - \bar{f}\zeta = 0. \end{cases} \tag{3.4}$$

with $U(x,y,0) = U^0(x,y)$. And let us finally note :

$$\begin{cases} A_\xi U = \overline{u_0}\xi_x + k_y, \\ A_\zeta U = u_0\zeta_x + \ell_y, \\ A_\eta U = \underline{u_0}\eta_x + m_y. \end{cases}$$

and

$$\begin{cases} \gamma_\xi U = \overline{u_0}\xi n_x + kn_y, \\ \gamma_\zeta U = u_0\zeta n_x + \ell n_y, \\ \gamma_\eta U = \underline{u_0}\eta n_x + mn_y. \end{cases}$$

where $\mathbf{n}= (n_x, x_y)$ is the unit outward vector to $\partial\mathcal{M}$.

If we suppose that $U \in H$ and that $A_\xi U, A_\zeta U$ and $A_\eta U$ are in $L^2(\mathcal{M})$, we can define the traces of ξ,ζ,η and k,ℓ,m on the edges of $\mathcal{M}$ (see [3]). Indeed, ξ (and similarly ζ,η) belongs to $L^2(\mathcal{M})$ and thus ξ_x belongs to $L^2_x(0,L_1;H_y^{-1}(0,L_2))$. Therefore ξ is almost everywhere equal to a continuous function from $[0,L_1]$ into $H_y^{-1}(0,L_2)$ and its traces at $x = 0$ and L_1 belong to $H_y^{-1}(0,L_2)$. Furthermore, all the linear preceding mappings being continuous, the mapping $\xi \mapsto$ trace of ξ on $\{0\}\times(0,L_2)$ or $\{L_1\}\times(0,L_2)$ is continuous from $X = \{U \in L^2(\mathcal{M})^3,\ A_\xi U,\ A_\zeta U,\ A_\eta U \in L^2(\mathcal{M})\}$, endowed with the norm

$$|U|_X = \{\,|U|^2_{L^2(\mathcal{M})^3} + |A_\xi U|^2_{L^2(\mathcal{M})} + |A_\zeta U|^2_{L^2(\mathcal{M})} + |A_\eta U|^2_{L^2(\mathcal{M})}\}^{1/2},$$

into $H_y^{-1}(0,L_2)$. In fact, by interpolation (see [4]), they belong to $(L^2,H^{-1})_{1/2}$
$= ((H_0^1,L^2)_{1/2})' = (H_{00}^{1/2}(0,L_2))'$ but we will not make use of this improvement. Similarly, the traces of ζ,η at $x = 0$ and $x = L_1$ are defined and belong to $H_y^{-1}(0,L_2)$ and the corresponding traces operators are continuous from X into $H_y^{-1}(0,L_2)$.

Since the linear matrix transforming ξ,ζ,η into k,ℓ,m is invertible, we conclude that similarly, k,ℓ,m are almost everywhere equal to continuous functions from $[0,L_1]$ into $H_y^{-1}(0,L_2)$ and

therefore their traces at $x = 0$ and L_1 exist, belong to $H_y^{-1}(0, L_2)$, and depend continuously on U. To obtain the traces on $y = 0$ and L_2, we invert the roles of ξ, ζ, η and k, ℓ, m. For example $k_y = A_\xi U - \overline{u_0}\,\xi_x$ belongs to $L_y^2(0, L_2, H_x^{-1}(0, L_1))$ so that k is almost everywhere equal to a function continuous from $[0, L_2]$ into $H_x^{-1}(0, L_1)$ and its traces at $y = 0$ and L_2 are defined, belong to $H_x^{-1}(0, L_1))$, and depend continuously on $U \in X$. Similarly, ℓ and m are almost everywhere equal to functions continuous from $[0, L_2]$ into $H_x^{-1}(0, L_1)$. Inverting the linear matrix transforming ξ, ζ, η into k, ℓ, m, we find that ξ, ζ, η are also continuous from $[0, L_2]$ into $H_x^{-1}(0, L_1)$ and their traces at $y = 0, L_2$ are defined too, belong to $H_x^{-1}(0, L_1)$ and depend continuously of $U \in X$.

Let us now define our functionnal framework. Problem (1) can be written in the functional form :

$$\frac{dU}{dt} + AU = F \ , \ U(0) = U^0, \tag{3.5}$$

where here $F = 0$, $U^0 = (\xi^0, \zeta^0, \eta^0)^T \in D(A)$, $U(t) = (\xi(t), \zeta(t), \eta(t))^T$, and $AU(t) = (A_\xi U(t), A_\zeta U(t), A_\eta U(t))^T$.

Remark 3.2.1. *In the physical problem, $F = 0$, but for mathematical generality, we will consider F as non zero.*

The domain of the operator A will be :

$$\begin{aligned} D(A) = \{ U = (\xi, \zeta, \eta) \in H \,/ & A_\xi U,\ A_\zeta U,\ A_\eta U \in L^2(\mathcal{M}) \text{ and} \\ & \gamma_\xi U(0, y) = \gamma_\zeta U(0, y) = \gamma_\eta U(L_1, y) = 0 \text{ for a.e. y in } (0, L_2), \\ & \gamma_\xi U(x, 0) = -\gamma_\xi U(x, L_2),\ \gamma_\zeta U(x, 0) = -\gamma_\zeta U(x, L_2), \\ & \gamma_\eta U(x, 0) = -\gamma_\eta U(x, L_2) \text{ for a.e. x in } (0, L_1)\}. \end{aligned}$$

The boundary conditions above are proposed in order to achieve the positivity of the operator A and will be explained in the following sections.
Our goal is to apply the Hille-Yosida theorem to the operator A with domain $D(A)$ in order to show that problem (4.2) is well posed for $U_0 \in D(A)$.

Remark 3.2.2. *In the supercritical case where $\underline{u_0} > 0$, $D(A)$ will be :*

$$\begin{aligned} D(A) = \{ U = (\xi, \zeta, \eta) \in H \,/ & A_\xi U,\ A_\zeta U,\ A_\eta U \in L^2(\mathcal{M}) \textit{ and} \\ & \gamma_\xi U(0, y) = \gamma_\zeta U(0, y) = \gamma_\eta U(0, y) = 0 \textit{ for a.e. } y \textit{ in } (0, L_2), \\ & \gamma_\xi U(x, 0) = -\gamma_\xi U(x, L_2),\ \gamma_\zeta U(x, 0) = -\gamma_\zeta U(x, L_2), \\ & \gamma_\eta U(x, 0) = -\gamma_\eta U(x, L_2), \textit{ for a.e. } x \textit{ in } (0, L_1)\}. \end{aligned}$$

3.3 Reminders

We briefly recall some results that we will use to show that our problem is well posed. First is the Hille-Yosida theorem, stated in the following form (see [7], [2]).

Theorem 3.3.1 (Hille-Yosida). *Let H be a Hilbert space, and let $A : D(A) \subset H \to H$ be a linear unbounded operator with domain $D(A)$. Let us assume :*

- *A is closed,*
- *$(AU, U) \geq 0$, $\forall U \in D(A)$,*
- *$\exists \mu > 0$ such that $A + \mu I$ is onto .*

Then, $\forall\, U_0 \in H$, $\forall\, F \in L^1(0,T;H)$, there exists a unique solution $U \in C([0,T],H)$ of (3.5) such that $U(0) = U_0$ and

$$\forall t \in [0,T],\ U(t) = e^{-tA}U_0 + \int_0^t e^{-(t-s)}AF(s)ds.$$

If furthermore $U_0 \in D(A)$ and $F' = dF/dt \in L^1(0,T,H)$ then $U \in L^\infty(0,T;D(A))$, and $U' \in L^\infty(0,T;H)$.

We will also use the following elementary lemma :

Lemma 3.3.1. *Let $A : D(A) \subset H \to H$ be a closed operator with domain $D(A)$ dense in H and let $A^* : D(A^*) \subset H \to H$ be its adjoint. Suppose that A and A^* are both positive. Then for all $\mu > 0$, $A + \mu I$ and $A^* + \mu I$ are onto.*

Proof. Let $\mu > 0$ and let $F \in H$ be fixed. For $\epsilon > 0$, we consider the variationnal problem : *To find $U_\epsilon \in D(A)$ such that :*

$$\epsilon(AU_\epsilon, A\widetilde{U}) + (AU_\epsilon, \widetilde{U}) + \mu(U_\epsilon, \widetilde{U}) = (F, \widetilde{U}),\ \forall \widetilde{U} \in D(A) \tag{3.6}$$

Existence and uniqueness of U_ϵ follow easily from the Lax-Milgram lemma; then we consider the operator :

$$\widetilde{U} \longrightarrow (AU_\epsilon, A\widetilde{U}) = \frac{1}{\epsilon}(F - \mu U_\epsilon - AU_\epsilon, \widetilde{U})$$

It is continuous on $D(A)$ for the topology of H; thus, $AU_\epsilon \in D(A^*)$ and by definition of A^* (see ([9])

$$\epsilon A^* AU_\epsilon + AU_\epsilon + \mu U_\epsilon = F. \tag{3.7}$$

We then take the scalar product in H of (3.6) with AU_ϵ. We obtain :

$$\epsilon(A^*AU_\epsilon, AU_\epsilon) + \|AU_\epsilon\|^2 + \mu(U_\epsilon, AU_\epsilon) = (F, AU_\epsilon)$$

Since A and $A^\star$ are positive, we find $\|AU_\epsilon\|_H \leq \|F\|_H$. Thus U_ϵ is bounded in $D(A)$ and there exists $U \in D(A)$ and a subsequence still denoted U_ϵ such that U_ϵ converges weakly towards U in $D(A)$, that is

$$\begin{cases} U_\epsilon \rightharpoonup U \text{ in } H, \\ AU_\epsilon \rightharpoonup AU \text{ in } H. \end{cases}$$

Letting ϵ tend to 0 in (3.6) we obtain :

$$(AU, \widetilde{U}) + \mu(U, \widetilde{U}) = (F, \widetilde{U}),\ \forall \widetilde{U} \in D(A).$$

Since $D(A)$ is dense in H, this implies that $AU + \mu U = F$ with U in $D(A)$. The proof for $A^* + \mu I$ is the same. □

Thus to use this lemma we will show that A and $A^\star$ are positive and closed.

3.4 Proof of the main results

3.4.1 Positiveness of A

Let us first justify the boundary conditions; in the case where $\underline{u_0} < 0$, we have to impose two fields at the inflow and one field at the outflow, whereas when $\underline{u_0} > 0$ three boundary conditions must be imposed at the inflow.
Let us compute the scalar product (AU, U) in $L^2(\mathcal{M})$ for $U \in D$ (defined in (3.3)).

$$\begin{aligned}
(AU,U) &= \int_{\mathcal{M}} [\overline{u_0}\xi_x\xi + v_0\xi_y\xi + \Phi_1\zeta_y\xi + u_0\zeta_x\zeta + v_0\zeta_y\zeta + \Phi_1\zeta\xi_y \\
&\quad + \underline{u_0}\eta_x\eta + v_0\eta_y\eta - \Phi_1(\zeta\eta_y + \eta\zeta_y)]dxdy \\
&= \int_{\mathcal{M}} \frac{1}{2}[\overline{u_0}(\xi^2)_x + u_0(\zeta^2)_x + \underline{u_0}(\eta^2)_x] \\
&\quad + \int_{\mathcal{M}} \frac{v_0}{2}[(\xi^2)_y + (\zeta^2)_y + (\eta^2)_y] + \int_{\mathcal{M}} \Phi_1((\zeta\xi)_y - (\zeta\eta)_y) \\
&= \int_{\partial\mathcal{M}} \frac{1}{2}[\overline{u_0}\xi^2 + u_0\zeta^2 + \underline{u_0}\eta^2]n_x \\
&\quad + \frac{v_0}{2}\int_{\partial\mathcal{M}} (\xi^2 + \zeta^2 + \eta^2)n_y + \Phi_1 \int_{\partial\mathcal{M}} \zeta(\xi - \eta)n_y
\end{aligned}$$

Thanks to the periodicity in the y-direction, we obtain :

$$\begin{aligned}
(AU,U) &= \int_0^{L_2} \frac{\overline{u_0}}{2}(\xi^2(L_1,y) - \xi^2(0,y))dy + \int_0^{L_2} \frac{u_0}{2}(\zeta^2(L_1,y) - \zeta^2(0,y))dy \\
&\quad + \int_0^{L_2} \frac{\underline{u_0}}{2}(\eta^2(L_1,y) - \eta^2(0,y))dy
\end{aligned}$$

So, in the subcritical case where $\underline{u_0} < 0$, we can insure the positiveness of A, $(AU, U) \geq 0, \forall U \in D(A)$ by imposing $\xi(0,y) = \zeta(0,y) = \eta(L_1,y) = 0$. In the supercritical case we must impose the three components to be zero at $x = 0$. In the subcritical case, the operator A is therefore positive for $U \in D$ and verifying the above boundary conditions, i.e. for $U \in D_{BC}$,

$$D_{BC} = D \cap \{U \text{ s.t. } \xi(0,y) = \zeta(0,y) = \eta(L_1,y) = 0\} \tag{3.8}$$

We now have to show the positiveness for $U \in D(A)$; we will proceed by regularisation.

Let us start by extending U to the slab $[0, L_1] \times \mathbb{R}$ by periodicity in y.
We will denote by $\mathcal{M}^\sharp$ the symmetric of $\mathcal{M}$ with respect to the line $y = L_2$, and by $\widetilde{\mathcal{M}}$ the set $\mathcal{M} \cup \mathcal{M}^\sharp$.
Let $U \in D(A)$. We call $\widetilde{U}$ the extension of U to $\widetilde{\mathcal{M}}$ by symmetry :

$$\widetilde{U}(x,y) = \begin{cases} U(x,y), & \text{for } (x,y) \in \mathcal{M}, \\ U(x, y - L_2), & \text{for } (x,y) \in \mathcal{M}^\sharp. \end{cases}$$

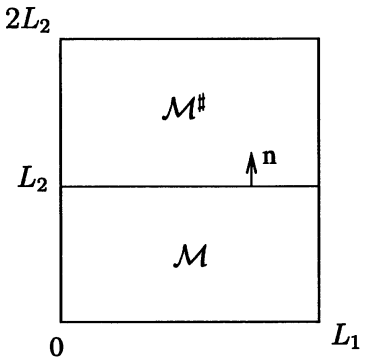

Remark 3.4.1. *The functional operator A is defined on $D(A)$ and acts on functions of H ; we will call $\mathcal{A}$ the differential operator which acts on functions defined on $[0, L_1] \times \mathbb{R}$.*

We have that $\widetilde{U} \in L^2(\widetilde{\mathcal{M}})$; let us check that $\mathcal{A}_\xi \widetilde{U} = \widetilde{A_\xi U}$, we will thus also have $\mathcal{A}_\xi \widetilde{U} \in L^2(\widetilde{\mathcal{M}})$ and the same for $\mathcal{A}_\varsigma \widetilde{U}$ and $\mathcal{A}_\eta \widetilde{U}$.
Let $\Phi \in \mathcal{D}(\widetilde{\mathcal{M}})$[1].

$$\begin{aligned}
\int_{\widetilde{\mathcal{M}}} \mathcal{A}_\xi \widetilde{U} \cdot \Phi &= \int_{\mathcal{M}} (\overline{u_0}\xi_x + k_y)\Phi + \int_{\mathcal{M}^\sharp} (\overline{u_0}\widetilde{\xi}_x + \widetilde{k}_y)\Phi \\
&= \int_{\mathcal{M}} A_\xi^* \Phi \cdot U + \int_{\partial\mathcal{M}} \gamma_\xi U \cdot \Phi + \int_{\mathcal{M}} \Phi(x,y)\overline{u_0}\xi_x(x, y - L_2) \\
&+ \int_{\mathcal{M}} \Phi(x,y) k_y(x, y - L_2) \\
&= \int_{\mathcal{M}} A_\xi^* \Phi(x,y) \cdot U(x,y) dxdy + \int_0^{L_1} \gamma_\xi U(x, L_2)\Phi(x, L_2) dx \\
&+ \int_{\mathcal{M}} A_\xi^* \Phi(x,y) \cdot U(x, y - L_2) dxdy + \int_0^{L_1} \gamma_\xi U(x, 0)\Phi(x, L_2) dx
\end{aligned}$$

Thanks to periodicity, we obtain :

$$\int_{\widetilde{\mathcal{M}}} \mathcal{A}_\xi \widetilde{U} \cdot \Phi = \int_{\widetilde{\mathcal{M}}} A_\xi^* \Phi \cdot \widetilde{U}$$

and $\mathcal{A}_\xi \widetilde{U} \in L^2(\widetilde{\mathcal{M}})$.

We then extend U to the slab $[0, L_1] \times \mathbb{R}$ by periodicity and obtain a function $\widetilde{U}$ defined on $[0, L_1] \times \mathbb{R}$, and we have $\mathcal{A}_\xi \widetilde{U} \in L^2_x(0, L_1, L^2_{y\,loc}(\mathbb{R}))$.
Since $\widetilde{\xi}$ is periodic in y, we can truncate the y-Fourier series for a.e. x, and we obtain functions $\xi_n = P_n \widetilde{\xi}$, which are smooth in y, for a.e. $x \in (0, L_1)$. Furthermore,

$$|\xi_n(x,.)|_{L^2(0,L_2)} = |P_n \widetilde{\xi}(x,.)|_{L^2(0,L_2)} \leq |\xi(x,.)|_{L^2(0,L_2)}, \tag{3.9}$$

$$|P_n \mathcal{A}_\xi \widetilde{U}(x,.)|_{L^2(0,L_2)} = |P_n \widetilde{A_\xi U}(x,.)|_{L^2(0,L_2)} \leq |\widetilde{A_\xi U}(x,.)|_{L^2(0,L_2)} \tag{3.10}$$

[1]Here $\mathcal{D}(\mathcal{M})$ denotes the Schwartz space of C^∞ functions with compact support in $\mathcal{M}$

and, as $n \to \infty$,

$$\xi_n \xrightarrow[n\to\infty]{} \xi,\ (\widetilde{A_\xi U})_n \xrightarrow[n\to\infty]{} A_\xi U \text{ in } L^2(0,L_1;L^2(0,L_2)). \tag{3.11}$$

Proceeding similarly with ζ and η, we obtain a sequence of functions U_n smooth in y for a.e. $x \in (0,L_1)$, with properties similar to (3.9)-(3.11) ; in particular

$$|U_n(x,.)|_{(L^2(0,L_2))^3} \leq |U(x,.)|_{(L^2(0,L_2))^3}, \tag{3.12}$$

$$|AU_n(x,.)|_{(L^2(0,L_2))^3} \leq |AU(x,.)|_{(L^2(0,L_2))^3}. \tag{3.13}$$

and $U_n \xrightarrow[n\to\infty]{} U$ in $D(A)$. Since the P_n truncation operates only in the y-direction, the U_n satisfy the same boundary conditions as U on $x = 0$ and L_1, namely $\xi_n(0,y) = \zeta_n(0,y) = \eta_n(L_1,y) = 0$, for a.e. $y \in (0,L_2)$.

Finally the $U_n \in D(A)$ and $(AU_n, U_n) \geq 0$ is easy to prove for such functions. Since $AU_n \xrightarrow[n\to\infty]{} AU$ and $U_n \xrightarrow[n\to\infty]{} U$ strongly in $L^2(0,L_1;L^2(0,L_2))$, we finally obtain $(AU,U) \geq 0$, $\forall U \in D(A)$.

Remark 3.4.2. *In [3] Lax and Phillips obtain similar results by regularisation in the tangential direction y.*

3.4.2 Positiveness of the adjoint of A

In this section, we first compute the adjoint $A^\star$ of A, and then show that it is positive on its domain $D(A^\star)$.

Let $U = (\xi,\zeta,\eta)$ be in D_{BC}, defined in (3.8) and $U' = (\xi',\zeta',\eta')$ be in D (defined in (3.3)). With the same notations as before, we have

$$(AU,U') = \int_{\mathcal{M}} \overline{u_0}\xi_x\xi' + k_y\xi' + \int_{\mathcal{M}} u_0\zeta_x\zeta' + \ell_y\zeta' + \int_{\mathcal{M}} \underline{u_0}\eta_x\eta' + m_y\eta'.$$

We can perform integrations by parts and find :

$$\begin{aligned}
(AU,U') &= -\int_{\mathcal{M}} \overline{u_0}\,\xi_x'\xi + \xi_y'k + \int_{\partial\mathcal{M}} \overline{u_0}\,\xi\xi' n_x + k\xi' n_y \\
&- \int_{\mathcal{M}} u_0\,\zeta_x'\zeta + \ell\zeta_y' + \int_{\partial\mathcal{M}} u_0\,\zeta\zeta' n_x + \ell\zeta' n_y \\
&- \int_{\mathcal{M}} \underline{u_0}\,\eta\eta_x' + m\eta_y' + \int_{\partial\mathcal{M}} \underline{u_0}\,\eta\eta' n_x + m\eta' n_y \\
&= -\int_{\mathcal{M}} (\overline{u_0}\xi_x' + v_0\xi_y')\xi + \Phi_1\xi_y'\zeta - \int_{\mathcal{M}} (u_0\zeta_x' + v_0\zeta_y')\zeta + \Phi_1(\xi-\eta)\zeta_y' \\
&- \int_{\mathcal{M}} (\underline{u_0}\eta_x' + v_0\eta_y')\eta - \Phi_1\eta_y'\zeta + \int_{\partial\mathcal{M}} (\overline{u_0}\xi\xi' n_x + u_0\zeta\zeta' n_x + \underline{u_0}\eta\eta' n_x)
\end{aligned}$$

$$
\begin{aligned}
(AU, U') &= -\int_{\mathcal{M}} (\overline{u_0}\xi' + k_y')\xi - \int_{\mathcal{M}} (u_0\zeta_x' + \ell_y')\zeta - \int_{\mathcal{M}} (\underline{u_0}\eta_x' + m_y')\eta \\
&+ \int_0^{L_2} [\overline{u_0}\xi(L_1, y)\xi'(L_1, y) + u_0\zeta(L_1, y)\zeta'(L_1, y) + \underline{u_0}\eta(0, y)\eta'(0, y)]dy.
\end{aligned}
$$

Hence by definition of A^*, see [9], we find $(AU, U') = (U, A^*U')$, $\forall\ U \in D_{BC}$, $\forall\ U' \in D_{BC^*}$, where D_{BC} is defined in (3.8) and :

$$
\begin{aligned}
D_{BC^*} = \{&U = (\xi, \zeta, \eta) \in C^\infty(\overline{\mathcal{M}}),\ \xi, \zeta, \eta \text{ are periodic of period } L_2 \\
&\text{in the y-direction and } \xi(L_1, y) = \zeta(L_1, y) = \eta(0, y) = 0\}.
\end{aligned} \tag{3.14}
$$

and $A^*U = -AU,\ \forall U \in D_{BC^*}$.

The domain $D(A^*)$ of A^* is :

$$
\begin{aligned}
D(A^*) = \{\ &U = (\xi, \zeta, \eta) \in H\ /A_\xi U,\ A_\zeta U,\ A_\eta U \in L^2(\mathcal{M}) \text{ and },\\
&\gamma_\xi U(L_1, y) = \gamma_\zeta U(L_1, y) = \gamma_\eta U(0, y) = 0 \text{ for a.e. y in } (0, L_2),\\
&\gamma_\xi U(x, 0) = -\gamma_\xi U(x, L_2),\ \gamma_\zeta U(x, 0) = -\gamma_\zeta U(x, L_2),\\
&\gamma_\eta U(x, 0) = -\gamma_\eta U(x, L_2) \text{ for a.e. x in } (0, L_1)\}.
\end{aligned}
$$

Remark 3.4.3. *In the supercritical case where $\underline{u_0} > 0$, the adjoint boundary conditions would be : $\gamma_\xi U(L_1, y) = \gamma_\zeta U(L_1, y) = \gamma_\eta U(L_1, y) = 0$.*
All what follows in the section works similarly.

Using again the same approximation of y-Fourier series as before, and thanks to the computation above which can be applied for the truncation of the y-Fourier series of the corresponding functions, we find that $(AU, V) = (U, A^*V)$, $\forall U \in D(A)$, $\forall V \in D(A^*)$, where $A^* = -A$. Now it remains to check that A^* is positive on its domain. Let $V = (\xi, \zeta, \eta)$ be in D_{BC^*}, thanks to the computations which have already been done for A,

$$
\begin{aligned}
(A^*V, V) &= -(AV, V) \\
&= -\int_{\partial\mathcal{M}} \frac{1}{2}[\overline{u_0}\xi^2 + u_0\zeta^2 + \underline{u_0}\eta^2]n_x - \frac{v_0}{2}\int_{\partial\mathcal{M}} (\xi^2 + \zeta^2 + \eta^2)n_y \\
&- \Phi_1 \int_{\partial\mathcal{M}} \zeta(\xi - \eta)n_y \\
&= \frac{1}{2}\int_0^{L_2} [\overline{u_0}\xi^2(0, y) + u_0\zeta^2(0, y) + \underline{u_0}\eta^2(L_1, y)]dy
\end{aligned}
$$

Because of the adjoint boundary conditions, we thus find $(A^*V, V) \geq 0$, $\forall V \in D_{BC^*}$; then, by approximation we obtain as before $(A^*V, V) \geq 0$ for all $V \in D(A^*)$.

3.5 Well-posedness of the problem

We now have to check first that A is closed, and then that $D(A)$ is dense in H. For the closure of A, let us take a sequence $U_n = (\xi_n, \zeta_n, \eta_n)$ of elements of $D(A)$ such that :

$$\begin{cases} U_n \xrightarrow[n\to\infty]{} U \text{ in } H, \\ A_\xi U_n \xrightarrow[n\to\infty]{} F_\xi, \\ A_\zeta U_n \xrightarrow[n\to\infty]{} F_\zeta \text{ in } H, \\ A_\eta U_n \xrightarrow[n\to\infty]{} F_\eta. \end{cases}$$

with $(F_\xi, F_\zeta, F_\eta) \in H$; then all the above sequences converge in the distribution sense in $\mathcal{M}$ and thus :

$$\begin{cases} A_\xi U = F_\xi + \dfrac{f}{\sqrt{2}}\zeta, \\ A_\zeta U = F_\zeta - \dfrac{f}{\sqrt{2}}(\xi + \eta) \quad \text{in } \mathcal{D}'(\mathcal{M}), \\ A_\eta U = F_\eta + \dfrac{f}{\sqrt{2}}\zeta. \end{cases}$$

So $(A_\xi U, A_\zeta U, A_\eta U) \in H$. Moreover, U is periodic in the y-direction, and the boundary conditions are satisfied, by continuity of the trace operators. Therefore $U \in D(A)$ and $AU = F$, which means that A is closed.

For the density of $D(A)$ in H, we note that $D(A)$ contains the space of C^∞ functions on $[0, L_1] \times [0, L_2]$ with compact support in x and periodic in y, this space being dense into H.

We now have all the conditions to conclude : A and A^* are positive, A is closed with domain $D(A)$ dense in H. Thus applying Lemma 3.3.1, $A + \mu I$ is onto for all $\mu > 0$, and the theorem of Hille-Yosida applies :

Theorem 3.5.1. *For every $U_0 \in D(A)$ defined in Section 3.2 and for every $F \in L^1(0,T;H)$, there exists a unique $U \in L^\infty(0,T;D(A)) \cap C([0,T],H)$, with $U' \in L^\infty(0,T;H)$ which satisfies (3.1).*

3.6 The periodic case

In this section, we show that the problem (3.1) is well-posed, in the case of functions which are periodic of period L_1 in the x-direction and of period L_2 in the y-direction. In this case we apply the Hille-Yosida theorem and show the positivity of the operator A, and the surjectivity of $A + \mu I$, for some $\mu > 0$.

We use the same notations as in the former sections, but here the domain of the operator A is :

$$\begin{aligned} D(A) = \{ U = (\xi, \zeta, \eta) \in H \,/ & A_\xi U,\ A_\zeta U,\ A_\eta U \in L^2(\mathcal{M}) \text{ and} \\ & \gamma_\xi U(0,y) = -\gamma_\xi U(L_1,y),\ \gamma_\zeta U(0,y) = -\gamma_\zeta U(L_1,y), \\ & \gamma_\eta U(0,y) = 0 = \gamma_\eta U(L_1,y), \text{ for a.e. y in } (0,L_2), \\ & \gamma_\xi U(x,0) = -\gamma_\xi U(x,L_2),\ \gamma_\zeta U(x,0) = -\gamma_\zeta U(x,L_2), \\ & \gamma_\eta U(x,0) = -\gamma_\eta U(x,L_2) \text{ for a.e. x in } (0,L_1)\}. \end{aligned}$$

The operator A is closed on $D(A)$.

3.6.1 Positiveness

First by the same computations as before and thanks to the periodicity, we have that $(AU,U) = 0,\ \forall U \in C^\infty_{per}(\mathbb{R}^2)$. The positiveness of A is shown by Fourier approximation similarly as in Section 3.4.1.
Let $U \in D(A)$. We can extend U by periodicity in the two directions to $\mathbb{R}$ and we call $\widetilde{U}$ this extension. By the same means as before, if we call $\mathcal{A}$ the differential operator which corresponds to A and which acts on functions defined on $\mathbb{R}$, we have that $\mathcal{A}_\xi \widetilde{U} = \widetilde{A_\xi U}$ so that $\mathcal{A}_\xi \widetilde{U} \in L^2_{loc}(\mathbb{R}^2)$ and similarly for $\mathcal{A}_\zeta \widetilde{U}$ and $\mathcal{A}_\eta \widetilde{U}$.

Now, since $\widetilde{U}$ is periodic in the two directions, we can truncate the Fourier series of $\widetilde{\xi}$, $\widetilde{\zeta}$ and $\widetilde{\eta}$ and obtain a sequence of functions U_n which is smooth in x and y on $\mathcal{M}$ with the following properties :

$$|U_n|_H \le |U|_H, \tag{3.15}$$
$$|AU_n|_H \le |AU|_H. \tag{3.16}$$

and $U_n \xrightarrow[n\to\infty]{} U$ in $D(A)$. Then similarly as in Section 3.4.1, we can compute the scalar product (AU,U) in $L^2(\mathcal{M})$ for functions U which are smooth and find zero due to the periodicity in x and y. Finally, $U_n \in D(A)$ and $(AU_n, U_n) = 0$, and letting $n \to \infty$, we obtain that $(AU,U) = 0\ \forall\, U \in D(A)$.

3.6.2 Surjectivity

We must finally prove that there exists $\mu > 0$ such that $A + \mu I$ is surjective from $D(A)$ into H. Instead of defining A^* and showing its positivity, we give here a direct proof.
Let $(F_\xi, F_\zeta, F_\eta) \in H$, we have to find $(\xi, \zeta, \eta) \in D(A)$ such that

$$\begin{cases} \overline{u_0}\xi_x + v_0\eta_y + \Phi_1\zeta_y - \bar{f}\zeta + \mu\xi = F_\xi, \\ u_0\zeta_x + v_0\zeta_y + \Phi_1(\xi_y - \eta_y) + \bar{f}(\xi + \eta) + \mu\zeta = F_\zeta, \\ \underline{u_0}\eta_x + v_0\eta_y - \Phi_1\eta_y - \bar{f}\zeta + \mu\eta = F_\eta. \end{cases}$$

Since the functions considered are periodic, we can use Fourier series; we will note for k and ℓ in $\mathbb{Z}$, $\hat{\xi}(k,\ell) = \int_{\mathcal{M}} e^{-i(xk+y\ell)}\xi(x,y)dxdy$, (and similarly for ζ and η), we then have : $\hat{\xi_x} = ik\hat{\xi}$ and $\hat{\xi_y} = i\ell\hat{\xi}$. The equations satisfied by the Fourier coefficients are the following :

$$\begin{cases} [i(k\overline{u_0}+\ell v_0)+\mu]\hat{\xi}+(i\ell\Phi_1-\bar{f})\hat{\zeta}=\hat{F}_\xi, \\ (i\ell\Phi_1+\bar{f})\hat{\xi}+[i(u_0k+v_0\ell)+\mu]\hat{\zeta}+(\bar{f}-i\Phi_1\ell)\hat{\eta}=\hat{F}_\zeta, \\ -(i\ell\Phi_1+\bar{f})\hat{\zeta}+[i(k\underline{u_0}+v_0\ell)+\mu]\hat{\eta}=\hat{F}_\eta. \end{cases}$$

This can be written as $M\begin{pmatrix}\hat{\xi}\\ \hat{\zeta}\\ \hat{\eta}\end{pmatrix}=\begin{pmatrix}\hat{F}_\xi\\ \hat{F}_\zeta\\ \hat{F}_\eta\end{pmatrix}$, where

$$M=\begin{pmatrix} i[k\overline{u_0}+\ell v_0]+\mu & i\ell\Phi_1-\bar{f} & 0 \\ i\ell\Phi_1+\bar{f} & i(ku_0+\ell v_0)+\mu & -i\ell\Phi_1+\bar{f} \\ 0 & -i\ell\Phi_1+\bar{f} & i(k(u_0-\Phi_1)+\ell v_0)+\mu \end{pmatrix}$$

We introduce $\nu=i(u_0k+v_0\ell)+\mu$ and $\sigma=\bar{f}+i\ell\Phi_1)$. The matrix M then becomes

$$M=\begin{pmatrix} \nu+i\sqrt{\Phi_0}k & -\bar{\sigma} & 0 \\ \sigma & \nu & \bar{\sigma} \\ 0 & -\sigma & \nu-i\sqrt{\Phi_0}k \end{pmatrix}$$

We then compute its determinant :

$$\begin{aligned} \det M &= \nu(\nu^2+\Phi_0k^2+2|\sigma|^2) \\ &= \nu[\nu^2+\Phi_0k^2+2(\bar{f}^2+\Phi_1^2\ell^2)] \\ &= \nu[\nu^2+\Phi_0(k^2+\ell^2)+f^2] \end{aligned}$$

Since $\nu=i(u_0k+v_0\ell)+\mu$ then $\forall\mu\geq\mu_0>0$ one has $\nu\neq 0$. If the expression between brackets is non zero (see below) then $\det M\neq 0$ and one can invert the matrix M which gives :

$$M^{-1}=\frac{1}{\det \mathrm{M}}\begin{pmatrix} \nu(\nu-i\sqrt{\Phi_0}k)+\mid\sigma\mid^2 & \bar{\sigma}(\nu-i\sqrt{\Phi_0}k) & -\bar{\sigma}^2 \\ -\sigma(\nu-i\sqrt{\Phi_0}k) & \nu^2+\Phi_0k^2 & -\bar{\sigma}(\nu+i\sqrt{\Phi_0}k) \\ -\sigma^2 & \sigma(\nu+i\sqrt{\Phi_0}k) & \nu(\nu+i\sqrt{\Phi_0}k)+\mid\sigma\mid^2 \end{pmatrix}$$

We can then find an expression of $(\hat{\xi},\hat{\zeta},\hat{\eta})$ depending on $(\hat{F}_\xi,\hat{F}_\zeta,\hat{F}_\eta)$:

$$\hat{\xi}(k,\ell)=\frac{1}{\det M}[(\nu(\nu-i\sqrt{\Phi_0}k)+\mid\sigma\mid^2)\hat{F}_\xi(k,\ell)+\bar{\sigma}(\nu-i\sqrt{\Phi_0}k)\hat{F}_\zeta(k,\ell)-\bar{\sigma}^2\hat{F}_\eta(k,\ell)],$$

$$\hat{\zeta}(k,\ell)=\frac{1}{\det M}[-\sigma(\nu-i\sqrt{\Phi_0}k)\hat{F}_\xi(k,\ell)+(\nu^2+\Phi_0k^2)\hat{F}_\zeta(k,\ell)-\bar{\sigma}(\nu+i\sqrt{\Phi_0}k)\hat{F}_\eta(k,\ell)],$$

$$\hat{\eta}(k,\ell)=\frac{1}{\det M}[-\sigma^2\hat{F}_\xi(k,\ell)+\sigma(\nu+i\sqrt{\Phi_0}k)\hat{F}_\zeta(k,\ell)+(\nu(\nu+i\sqrt{\Phi_0}k)+\mid\sigma\mid^2)\hat{F}_\eta(k,\ell)],$$

that is $\hat{U}=\begin{pmatrix}\hat{\xi}\\ \hat{\zeta}\\ \hat{\eta}\end{pmatrix}=M^{-1}\begin{pmatrix}\hat{F}_\xi\\ \hat{F}_\zeta\\ \hat{F}_\eta\end{pmatrix}$.

Calling (ξ_1,ξ_2,ξ_3), $(\zeta_1,\zeta_2,\zeta_3)$, (η_1,η_2,η_3) the first, second, and third lines of $(\det M)M^{-1}$, we obtain for instance for ξ :

$$\hat{\xi}(k,\ell)=\frac{\xi_1}{\det M}F_\xi(k,\ell)+\frac{\xi_2}{\det M}F_\zeta(k,\ell)+\frac{\xi_3}{\det M}F_\eta(k,\ell). \tag{3.17}$$

In order to achieve the proof of surjectivity it remains to verify that the (ξ, ζ, η) that have been found (defined by their Fourier coefficients) are in D(A); we thus have to verify that the serie $\sum_{(k,\ell)\in\mathbb{Z}}(1+k^2+\ell^2) \mid \hat{\xi}(k,\ell) \mid^2$ converges and similarly for $\hat{\zeta}$ and $\hat{\eta}$.

But $\hat{F}_\xi, \hat{F}_\zeta, \hat{F}_\eta \in \ell^2(\mathbb{Z}^2)$, thus using (3.17), it suffices to show that there exists $c > 0$ such that for $i = 1, 2, 3$,

$$(1+k^2+\ell^2)\frac{\mid \xi_i \mid^2}{\mid \det\, M \mid^2} \leq c$$

at least for k and ℓ large (and so for ζ and η).
For this, we find a lower bound on $\mid \det\, M \mid^2$:

$$\begin{aligned}
\mid \det\, M \mid^2 &= \mid \nu \mid^2 \mid \nu^2 + \Phi_0(k^2+\ell^2) + f^2 \mid^2 \\
&= [\mu^2 + (u_0k + v_0\ell)^2)] \mid \mu^2 + f^2 + \Phi_0(k^2+\ell^2) - (u_0k+v_0\ell)^2 \\
&+ 2i\mu(u_0k+v_0\ell) \mid^2 \\
&= (\mu^2 + (u_0k+v_0\ell)^2)[[\mu^2 + f^2 + \Phi_0(k^2+\ell^2) - (u_0k+v_0\ell)^2]^2 \\
&+ 4\mu^2(u_0k+v_0\ell)^2]
\end{aligned}$$

Using the Cauchy-Schwartz inequality,

$$(u_0k+v_0\ell)^2 \leq (u_0^2+v_0^2)(k^2+\ell^2)\ \forall k, \ell \in \mathbb{Z},$$

and we obtain the following lower bound :

$$\mu^2 + f^2 + \Phi_0(k^2+\ell^2) - (u_0k+v_0\ell)^2 \geq \mu^2 + f^2 + \tilde{\Phi}_0(k^2+\ell^2),$$

where $\tilde{\Phi}_0 = \Phi_0 - (u_0^2+v_0^2) > 0$.
This yields

$$\begin{aligned}
\mid \det\, M \mid^2 &\geq [\mu^2 + (u_0k+v_0\ell)^2)]\{[\mu^2 + f^2 + \tilde{\Phi}_0(k^2+\ell^2)]^2 + 4\mu^2(u_0k+v_0\ell)^2\} \\
&\geq [\mu^2 + (u_0k+v_0\ell)^2)][\mu^2 + \tilde{\Phi}_0(k^2+\ell^2)]^2
\end{aligned}$$

It remains to estimate $\mid \xi_1 \mid, \mid \xi_2 \mid$ and $\mid \xi_3 \mid$:

$$\begin{aligned}
\mid \xi_1 \mid^2 &= \mid \nu(\nu - i\sqrt{\Phi_0}k) + \bar{f}^2 + \ell^2\Phi_1^2 \mid^2 \\
&= \mid (\mu + i(u_0k+v_0\ell))(\mu + iu_0k + iv_0\ell) + \bar{f}^2 + \ell^2\Phi_1^2) \mid^2 \\
&\leq C_\infty \mid 1 + k^2 + \ell^2 \mid
\end{aligned}$$

where C_∞ is independant of k and ℓ, but depends on μ, u_0, v_0, and Φ_0.
And similarly we have :

$$\begin{aligned}
\mid \xi_2 \mid^2 &= (\bar{f}^2 + \ell^2\Phi_1^2) \mid \mu + iu_0k + iv_0\ell \mid^2 \\
&\leq C_\infty \mid 1 + k^4 + \ell^4 \mid
\end{aligned}$$

$$\begin{aligned} \mid \xi_3 \mid^2 &= \mid \bar{\sigma}^2 \mid^2 = \mid \bar{f}^2 - \ell^2\Phi_1^2 - 2i\bar{f}\Phi_1\ell) \mid^2 \\ &\leq C_\infty \mid 1 + \ell^4 \mid \end{aligned}$$

We thus have :

$$\frac{\mid \xi_1 \mid^2}{\mid \det M \mid^2} \leq C_\infty \frac{\mid 1 + k^2 + \ell^2 \mid}{[\mu^2 + (u_0 k + v_0 \ell)^2)][\mu^2 + \tilde{\Phi}_0(k^2 + \ell^2)]^2},$$

$$\frac{\mid \xi_2 \mid^2}{\mid \det M \mid^2} \leq C_\infty \frac{\mid 1 + k^4 + \ell^4 \mid}{[\mu^2 + (u_0 k + v_0 \ell)^2)][\mu^2 + \tilde{\Phi}_0(k^2 + \ell^2)]^2},$$

$$\frac{\mid \xi_3 \mid^2}{\mid \det M \mid^2} \leq C_\infty \frac{\mid 1 + \ell^4 \mid}{[\mu^2 + (u_0 k + v_0 \ell)^2)][\mu^2 + \tilde{\Phi}_0(k^2 + \ell^2)]^2}.$$

So we can see that when k and ℓ are large, the desired quantities remain bounded.
We thus have proved that there exists $\mu_0 > 0$ such that $\forall \mu > \mu_0$, $A + \mu I$ is surjective.

Thus the operator A satisfies the hypothesis of the Hille-Yosida Theorem which we can apply. Then for every $U_0 \in D(A)$ and every $F \in L^1(0,T;H)$, there exists a unique $U \in L^\infty(0,T;D(A)) \cap C([0,T],H)$, with $U' \in L^\infty(0,T;H)$ which satisfies (3.1).

Acknoledgements : This work was partially supported by the NSF grant DMS-0305110, and by the Research Fund of Indiana University. The author is very thankful to Professor Roger Temam for suggesting this problem and for his helpful advice in its resolution.

Bibliographie

[1] H. Brezis. Opérateurs maximaux monotones et semigroupes de contractions dans les espaces de Hilbert, *North Holland Publishing Company*, 1973

[2] N. Burcq, P. Gérard. Contrôle optimal des équations aux dérivées partielles, *Ecole Polytechnique, Palaiseau, France.* 2003

[3] P. D. Lax, R.S. Phillips. Local boundary conditions for dissipative symmetric linear differential operators. *Comm. Pure Appl. Math.* , 13, 1960, 427–455

[4] J. L. Lions, E. Magenes Problèmes aux limites non homogènes et applications, *Dunod*, 1968

[5] A. McDonald. A step toward transparent boundary conditions for meteorological models. *Monthly Weather Review*, 130 :140–151, 2001.

[6] A. McDonald. Transparent boundary conditions for the shallow-water equations : testing in a nested environment. *Monthly Weather Review*, 131 :698–705, 2002.

[7] A. Pazy. Semigroups of operators in Banach spaces. In *Equadiff 82 (Würzburg, 1982)*, volume 1017 of *Lecture Notes in Math.*, pages 508–524. Springer, Berlin, 1983.

[8] J. Pedlosky. Geophysical Fluid Dynamics, *Springer, second edition*, 1987.

[9] W. Rudin. Functionnal Analysis, *International series in Pure and Applied Mathematics*, McGraw-Hill Inc., New York, second ed., 1991.

[10] R. Temam. *Navier-Stokes equations.* AMS Chelsea Publishing, Providence, RI, 2001. Theory and numerical analysis, Reedition of the 1984 edition.

[11] K. Yosida. Functionnal Analysis, *Springer-Verlag, reprint of the sisth edition, 1995*

Chapitre 4

Une méthode multi-niveaux pour la résolution des équations de Saint Venant

Soumis pour publication.

K. ADAMY[♯], S. FAURE[♯], J. LAMINIE[♯,*], R. TEMAM[♭]

[♭]The Institute for Scientific Computing and Applied Mathematics Indiana University, Bloomington, IN 47405, USA.

[♯]Laboratoire de Mathématiques, Université Paris-Sud, CNRS UMR 8628, Bâtiment 425, 91405 Orsay, France.

*GRIMAAG Guadeloupe, Université des Antilles et de la Guyane, Campus de Fouillole, 97157 Pointe à Pitre, France.

Abstract : In this article we propose and implement a multilevel method for the resolution of the two dimensionnal nonlinear Shallow Water equations. The multilevel method is based on a central-upwind finite volume scheme and uses new incremental unknowns which enable to preserve the numerical conservativity of the scheme. The method is tested and analyzed on two and three levels of discretization on different test cases and turns out to furnish a good resolution of the problems while reducing the CPU time.

4.1 Introduction

Multilevel methods were introduced to improve calculation speed in the simulation of complex physical phenomena while maintaining an accurate resolution of problems. They were originally developped for the study of turbulent flows ([8], [9] [10], [19], [20]) but can be interesting in other domains.
In this article we are concerned with the resolution of the two dimensionnal non linear Shallow Water equations by a multilevel method for finite volume discretizations. This work is intended at exploring the implementation of such methods for such a hyperbolic system. This system being hyperbolic, there is no diffusive term in the equations which could stabilize the scheme, however the multilevel method we present turns out to furnish a good and efficient resolution of the problem.
Incremental unknowns were introduced in the context of finite differences in [19] for the approximation of inertial manifolds. For references on parabolic or elliptic problems treated with multilevel methods in the context of finite differences or finite elements see [3]-[6], [20], in the context of pseudo-spectral methods or wavelets, see [7]-[10]. The implementation of finite volume multilevel schemes for the resolution of the Burgers equations with a diffusive term was made in [12]. The general principle is to split the unknowns in two terms : a "large scale" component y and a "small scale" component z and to treat differently y and z. The decomposition of the unknowns that we employ in this article is purely algebric but enables to preserve the numerical conservativity of the scheme. The decomposition of the variables is here done globally but it can be done locally in certain parts of the domain.

The Shallow Water equations describe the propagation of surface waves of long wavelength and of relatively big amplitude, which gives rise to strongly nonlinear flows. Multilevel methods for the Shallow water equations supplemented with a hyperdissipative operator were studied in [10] in the context of spectral methods for the simulation of turbulence. Our study covers a general framework but we are particularly interested in the modelisation of oceanic or atmospheric flows, from this perspective we present a simulation based on initial conditions dragged from [10]. Our multilevel method allows to resolve accurately the problems studied while reducing the CPU time and preserving the numerical conservativity of the scheme.

For the spatial finite volume discretization, the hyperbolicity of the system obliges to consider schemes that are well adapted for such problems. Recently, several different reliable finite volume schemes have been developped for the resolution of the Shallow Water equations ([1], [2], [14], [18]) in order to study some particular properties (preservation of steady states, positivity of the height of the water).
Here we apply a multilevel method on central-upwind type schemes which were constructed to solve numerically nonlinear conservation laws, [16]-[18]. These Godunov-type schemes are based on exact evolution and averaging over Riemann fans and do not need employ of Riemann solvers and characteristic decomposition, which render them simple and efficient; moreover they can be reduced to a very simple semi-discrete form. More particularly we will work with the schemes presented in [17], [18] : they are based on the one-sided local speeds of propagation and constitute less dissipative generalisations of the first semi-discrete central-upwind schemes;

they also allow to work on nonstaggered grids. However any finite volume scheme which can be written in a semi-discrete form can be used, provided that it is adapted to the hyperbolicity of the system; our method has for example been tested with central leap frog fluxes and the results were bad.
For the time discretization we need to use a TVD method which preserve the spatial accuracy : in the simulations we employ a Runge Kutta method of order two. The small scale components of the variables can be impelled through a simple time scheme; in our experimentations we choose to freeze them.

In Section 4.2 we present the Shallow Water system and the problem we are interested in : the resolution of the system on a rectangular domain with periodic boundary conditions. In Section 4.3 we detail the principle of the multilevel method. For the sake of simplicity, we present the method on two levels of discretization, but the method can become easily extended to three and more levels. First we define the incremental unknowns, then we explain the multilevel algorithm and how the method can help reducing the CPU time; then we describe the central-upwind finite volume scheme we use. In Section 4.4 we expose the results of the numerical simulations that we have done. We first sudy in details the behaviour of the method on an analytical test case and show that it provides an accurate resolution while reducing the CPU time; we then apply the method on a more physical case using initial data from [10]. The results are again very good and the numerical conservativity is displayed. The method is here used on two and three levels of discretization and it shows its most efficiency when solving on a very fine mesh on three levels. Finally we outline in an Appendix the important role of the decomposition and of the small scale component by showing the bad results obtained when they are ommitted or taken to zero.

4.2 Presentation of the problem

We are interested in implementing a finite volume multilevel scheme for the discretization of the non linear two-dimensionnal Shallow Water system on a rectangular domain $\Omega = [0, L_x] \times [0, L_y]$, with periodic boundary conditions. This system is the following :

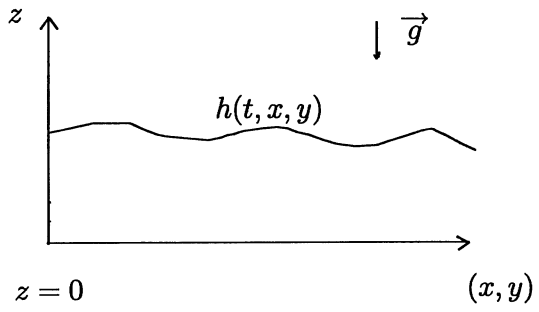

$$\begin{cases} \dfrac{\partial h}{\partial t} + \dfrac{\partial uh}{\partial x} + \dfrac{\partial vh}{\partial y} = S_h \\ \dfrac{\partial uh}{\partial t} + \dfrac{\partial hu^2}{\partial x} + \dfrac{\partial huv}{\partial y} + \dfrac{g}{2}\dfrac{\partial h^2}{\partial x} = S_U \\ \dfrac{\partial vh}{\partial t} + \dfrac{\partial huv}{\partial x} + \dfrac{\partial hv^2}{\partial y} + \dfrac{g}{2}\dfrac{\partial h^2}{\partial y} = S_V \end{cases} \tag{4.1}$$

Here h is the fluid depth above the bottom which is supposed flat, u and v are the x and y components of the velocity, and g denotes the gravity; $S = (S_h, S_U, S_V)^t$ represent a source term that can be taken to zero. We will write $U = uh$ and $V = vh$ and :

$$Q = \begin{pmatrix} h \\ U \\ V \end{pmatrix}, \; F(Q) = \begin{pmatrix} U \\ \frac{U^2}{h} + \frac{gh^2}{2} \\ \frac{UV}{h} \end{pmatrix}, \; G(Q) = \begin{pmatrix} V \\ \frac{UV}{h} \\ \frac{V^2}{h} + \frac{gh^2}{2} \end{pmatrix},$$

which permits us to write the system in the conservative form

$$\begin{cases} \dfrac{\partial h}{\partial t} + \nabla.(U, V) = 0 \\ \dfrac{\partial U}{\partial t} + \nabla.(uU, uV) + \dfrac{g}{2}\nabla_x(h^2) = 0 \\ \dfrac{\partial V}{\partial t} + \nabla.(vU, vV) + \dfrac{g}{2}\nabla_y(h^2) = 0 \end{cases} \tag{4.2}$$

or equivalently :

$$\frac{\partial Q}{\partial t} + \frac{\partial F(Q)}{\partial x} + \frac{\partial G(Q)}{\partial y} = 0. \tag{4.3}$$

The discretization of Ω is done using rectangular finite volumes $K_m = [x_{m/w}, x_{m/e}] \times [y_{m/s}, y_{m/n}]$ of centers (x_m, y_m), see Figure 4.1 and of dimensions $\Delta x \times \Delta y$, with $N_x \Delta x = L_x$ and $N_y \Delta y = L_y$:

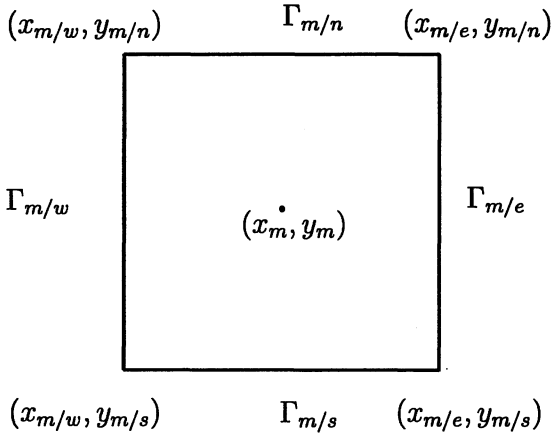

FIG. 4.1 – A cell K_m

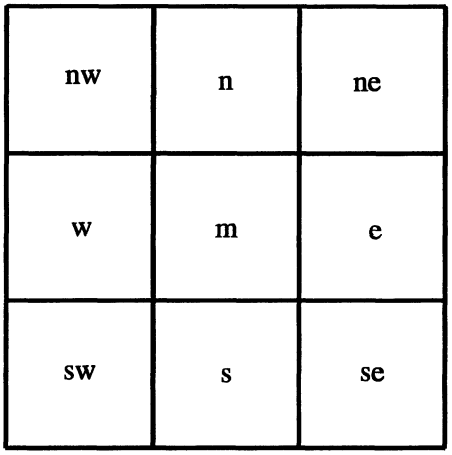

FIG. 4.2 – The NSWE stencil

We use a NSWE (North-South-West-East) stencil which is presented in Figure 4.2 to identify the unknowns.

The unknowns will be approximations of the cell averages :

$$Q_m(t) = \frac{1}{\Delta x \Delta y} \int_{K_m} Q(t,x,y) dx dy,$$

where $Q_m(t) = (h_m(t), U_m(t), V_m(t))^T$.
For the space discretization, we integrate the system (4.2) on each cell K_m, and we obtain :

$$\frac{d}{dt} Q_m(t) = -\frac{H^x_{m/e}(t) - H^x_{w/m}(t)}{\Delta x} - \frac{H^y_{m/n}(t) - H^y_{s/m}(t)}{\Delta y} + S_m(t), \tag{4.4}$$

S_m representing the contribution of the source term.
Here $H^x_{m/e}(t)$ and $H^y_{m/n}(t)$ for example are respectively the horizontal and vertical fluxes on the edges between K_m and K_e, and between K_m and K_n, and similarly for the other terms (see Figure 4.1), for example :

$$H^x_{m/e}(t) = \frac{1}{\Delta x} \int_{\Gamma_{m/e}} F(Q(t,x,y)) dy$$

These fluxes depend on the method employed; we will consider central-upwind fluxes, which are explicited in Section 4.3.3, see [15]-[18] but the multilevel method can also be based on other fluxes.

4.3 Presentation of the multilevel method

The domain is discretized by two levels of rectangular finite volume meshes : the fine mesh $\mathcal{M}_1$ counts $N_x \times N_y$ control volumes of dimensions $\Delta x \times \Delta y$, with $N_x \Delta x = L_x$, $N_y \Delta y = L_y$;

and the coarse mesh $\mathcal{M}_2$ has $\frac{N_x N_y}{9}$ control volumes of dimensions $3\Delta x \times 3\Delta y$.
Here we use small letters for the fine mesh and capital letters for the coarse mesh : we denote by K_m a control volume of the fine mesh and by K_M a control volume of the coarse mesh (see Figure 4.3).

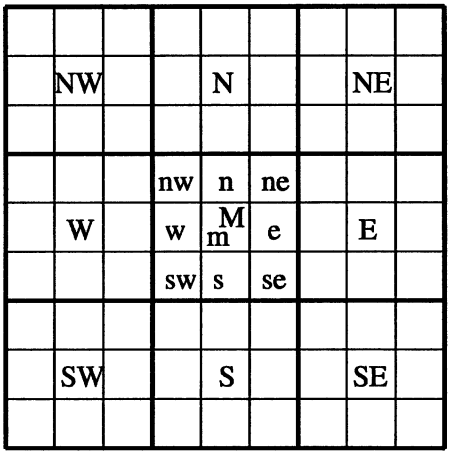

FIG. 4.3 – The NSWE stencil with coarse and fine cells

4.3.1 Incremental unknowns

We define the incremental unknowns for the conservative variables of the Shallow Water system, that is the three components of Q. We split each of the unknowns in a large scale component Y and a small scale component Z, which is meant to be frozen during a certain number of time steps. By large scale and small scale, we mean that the Y contain the major information on the solution and that the Z represent a correcting term which is comparatively small, as explained in Lemma 3.1. For incremental unknowns defined by physical decompositions like Fourier or wavelets, see [3]-[10], [19]-[20].

Definition 4.3.1. *Suppose that $Q = (h, U, V)^T$ is known on the fine mesh $\mathcal{M}_1$.*
Then on the control volume K_M, the large scale component $Y_M = (y_h, y_U, y_V)^T$ and the small scale components Z_e, Z_w, Z_n, Z_s, Z_{ne}, Z_{se}, Z_{nw}, Z_{sw} are defined as follows (see Figure 4.4) :

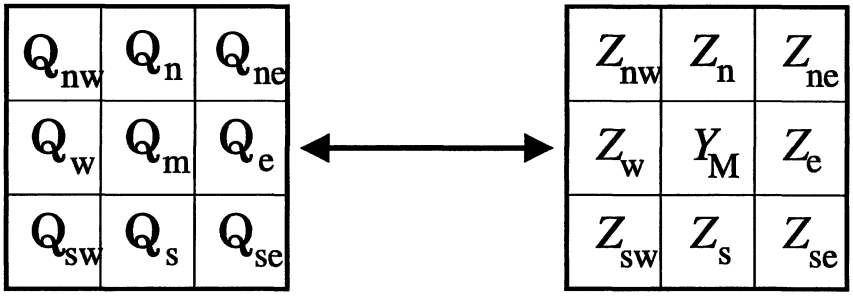

FIG. 4.4 – The Finite Volume Incremental Unknowns

$$
\begin{aligned}
&Y_M = \frac{1}{9}(Q_m + Q_e + Q_w + Q_n + Q_s + Q_{ne} + Q_{nw} + Q_{se} + Q_{sw}),\\
&Z_e = Q_e - \frac{1}{3}(Y_E + 2Y_M), \quad Z_w = Q_w - \frac{1}{3}(Y_W + 2Y_M),\\
&Z_n = Q_n - \frac{1}{3}(Y_N + 2Y_M), \quad Z_s = Q_s - \frac{1}{3}(Y_S + 2Y_M),\\
&Z_{ne} = Q_{ne} - \frac{1}{3}(Y_E + Y_M + Y_N), \quad Z_{se} = Q_{se} - \frac{1}{3}(Y_S + Y_M + Y_E),\\
&Z_{nw} = Q_{nw} - \frac{1}{3}(Y_W + Y_M + Y_N), \quad Z_{sw} = Q_{sw} - \frac{1}{3}(Y_S + Y_M + Y_W),
\end{aligned}
$$

Remark 4.3.1. *Notice that the definition of the large scale components Y differs from the works prevently done on such incremental unknowns (see [12]). In the definition of the small scale components in a coarse cell are needed the values of the variable in the cell but also in the neighbour coarse cells, which is unusual. The large scale component on a coarse cell K_M is defined by taking the mean of the 9 fine cell components of Q, taking the mean on the 9 cells is crucial to ensure the numerical conservativity of the scheme.*

Remark 4.3.2. *The correspondance between the solution on the fine mesh Q and its large scale and small scale components is bijective; that is knowing the component Y on the coarse mesh and the components Z on the fine mesh, we can compute Q on the fine mesh, here are the*

recomposition formulas :

$$
\begin{aligned}
&Q_M = 5Y_M - Y_E - Y_W - Y_N - Y_S - (Z_e + Z_w + Z_n + Z_s + Z_{ne} + Z_{se} + Z_{nw} + Z_{sw}),\\
&Q_e = Z_e + \frac{1}{3}(Y_E + 2Y_M),\ \ Q_w = Z_w + \frac{1}{3}(Y_W + 2Y_M),\\
&Q_n = Z_n + \frac{1}{3}(Y_N + 2Y_M),\ \ Q_s = Z_s + \frac{1}{3}(Y_S + 2Y_M),\\
&Q_{ne} = Z_{ne} + \frac{1}{3}(Y_E + Y_M + Y_N),\ \ Q_{se} = Z_{se} + \frac{1}{3}(Y_S + Y_M + Y_E),\\
&Q_{nw} = Z_{nw} + \frac{1}{3}(Y_W + Y_M + Y_N),\ \ Q_{sw} = Z_{sw} + \frac{1}{3}(Y_S + Y_M + Y_W),
\end{aligned}
$$

Remark 4.3.3. *This definition of the incremental unknowns is recursive : once the Y and Z corresponding to the second level coarse grid have been calculated, we can split Y by the same means to find the Y and Z corresponding to a coarser level of discretization.*

We can show that the small scale components Z are small compare to the large scale components, which are of the same order as Q.

Lemma 4.3.1. *The small scale components Z_e, Z_w, Z_s, Z_n, Z_{ne}, Z_{se}, Z_{nw}, Z_{sw} are of order $\Delta x^2 + \Delta y^2$.*

Proof. Using Taylor's formula, we have for example for Z_s :

$$
\begin{aligned}
Z_s &= Q_s - \frac{1}{3}(Y_S + 2Y_M)\\
&= Q_s - \frac{1}{27}\Big[Q_{Sm} + Q_{Se} + Q_{Sw} + Q_{Sn} + Q_{Ss} + Q_{Sne} + Q_{Snw} + Q_{Sse}\\
&+ Q_{Ssw} + 2(Q_m + Q_e + Q_w + Q_n + Q_s + Q_{ne} + Q_{nw} + Q_{se} + Q_{sw})\Big]\\
&= \frac{1}{27}\Big[25Q_s - (Q_s - 2\Delta y\partial_y Q_s) - (Q_s - \Delta x\partial_x Q_s - 2\Delta y\partial_y Q_s)\\
&- (Q_s + \Delta x\partial_x Q_s - 2\Delta y\partial_y Q_s) - (Q_s - \Delta y\partial_y Q_s) - (Q_s - 3\Delta y\partial_y Q_s)\\
&- (Q_s - \Delta x\partial_x Q_s - \Delta y\partial_y Q_s) - (Q_s + \Delta x\partial_x Q_s - \Delta y\partial_y Q_s)\\
&- (Q_s - \Delta x\partial_x Q_s - 3\Delta y\partial_y Q_s) - (Q_s + \Delta x\partial_x Q_s - 3\Delta y\partial_y Q_s)\\
&- 2(Q_s + \Delta y\partial_y Q_s) - 2(Q_s + 2\Delta y\partial_y Q_s) - 2(Q_s + \Delta x\partial_x Q_s + \Delta y\partial_y Q_s)\\
&- 2(Q_s - \Delta x\partial_x Q_s + \Delta y\partial_y Q_s) - 2(Q_s + \Delta x\partial_x Q_s) - 2(Q_s + 2\Delta x\partial_x Q_s)\\
&- 2(Q_s - \Delta x\partial_x Q_s + 2\Delta y\partial_y Q_s) - 2(Q_s + \Delta x\partial_x Q_s + 2\Delta y\partial_y Q_s)\Big]\\
&+ \mathcal{O}(\Delta x^2 + \Delta y^2)\\
&= \mathcal{O}(\Delta x^2 + \Delta y^2)
\end{aligned}
$$

It works similarly for Z_e, Z_w, Z_n, Z_{ne}, Z_{se}, Z_{sw}, Z_{nw}. □

4.3.2 Multilevel scheme

Scheme on the coarse grid

We split each component of $Q = (h, U, V)^T$ into its large scale component $Y = (Y^h, Y^U, Y^V)^T$ and its small scale component $(Z^h, Z^U, Z^V)^T$. To obtain the scheme on the coarse grid of level 2, we write (4.4) on each fine cell $K_m, K_e, K_w, K_n, K_s, K_{ne}, K_{se}, K_{nw}, K_{sw}$ of the coarse cell K_M (see Figure 4.3), and we take the mean value by summing all the equalities and dividing by 9, this results in :

$$\begin{aligned}
\frac{d}{dt}Y_M(t) = \frac{1}{9\Delta x}\Big[&H^x_{m/w} - H^x_{m/e} + H^x_{n/nw}) - H^x_{n/ne} + H^x_{s/sw} - H^x_{s/se} \\
&+ H^x_{We/w} - H^x_{m/w} + H^x_{nw/Wne} - H^x_{nw/n} + H^x_{sw/Wse} - H^x_{sw/s} \\
&+ H^x_{n/ne} - H^x_{Enw/ne} + H^x_{m/e} - H^x_{e/Ew} - H^x_{se/Esw} + H^x_{s/se}\Big] \\
&+ \frac{1}{9\Delta y}\Big[H^y_{m/n} - H^y_{n/Ns} + H^y_{s/m} - H^y_{n/m} + H^y_{s/Sn} - H^y_{s/m} \\
&+ H^y_{ne/e} - H^y_{ne/Nse} + H^y_{e/se} - H^y_{ne/e} + H^y_{se/Snw} - H^y_{se/e} \\
&+ H^y_{nw/w} - H^y_{nw/Nsw} + H^y_{sw/w} - H^y_{w/nw} + H^y_{sw/Sne} - H^y_{sw/w}\Big]
\end{aligned} \tag{4.5}$$

which gives after simplifications the following semi-discrete scheme to be applied on the coarse grid of level 2.

$$\begin{aligned}
\frac{d}{dt}Y_M(t) = &\frac{1}{9\Delta x}\Big[(H^x_{nw/Wne} + H^x_{We/w} + H^x_{sw/Wse}) - (H^x_{Enw/ne} + H^x_{e/Ew} + H^x_{se/Esw})\Big] \\
&+ \frac{1}{9\Delta y}\Big[(H^y_{sw/Sne} + H^y_{s/Sn} + H^y_{se/Snw}) - (H^y_{nw/Nsw} + H^y_{n/Ns} + H^y_{ne/Nse})\Big]
\end{aligned} \tag{4.6}$$

We can thus use different schemes depending on the definition of the fluxes and the resolution on the coarse level can be done locally in certain parts of the domain.
During the iterations on the coarse grid, while the large scale components Y are impelled through this scheme, the Z components are frozen.

Remark 4.3.4. *Formula 4.6 being equivalent to 4.4, this process is completely recursive and can be repeated for simulations on three or more levels of grids.*

Multilevel algorithm

The small scale components Z have an important role to play in the size of the error. Indeed let us explain the multilevel algorithm.
Let us fix the number N_{max} of levels of grids on which we are going to compute. From $t = 0$ until the final time T, we repeat N_{it}/L times (where N_{it} is the total number of iterations) the cycle $n_1 n_2 ... n_L$ where for $1 \leq i \leq L$, n_i stands for an iteration on the level n_i, $1 \leq n_i \leq N_{max}$. For example for a simulation on two levels, we repeat cycles of the form : 111122221111, where 1 correspond to the fine grid and 2 to the coarse one, and at the n^{th} iteration :

- At level 1 we work on the fine mesh $\mathcal{M}_1$ and compute Q^{n+1} with the classical scheme.
- At level 2
  - we calculate explicitly the fluxes needed by the scheme (4.6),
  - we split Q^n into its large scale Y^n and small scale Z^n components,
  - we compute Y^{n+1} with (4.6),
  - we recompose Q^{n+1} from Y^{n+1} and $\mathbf{Z^n}$.

We freeze the small scale components Z during each iteration at level 2, as a result, the more the time variation of the Z is close to Δt, the more the error commited in freezing it is important, and adds up to the classical error (see Section 4.4.1) ; this time variation thus needs to be controlled during the simulations.

Gain of CPU time

It is important to notice that implementing the scheme on the coarse grid requires to calculate the fluxes on the fine grid only on the exterior edges of the coarse cell, as indicated in Figure 4.5.

When implementing such schemes in the context of Shallow Water equations, the more consu-

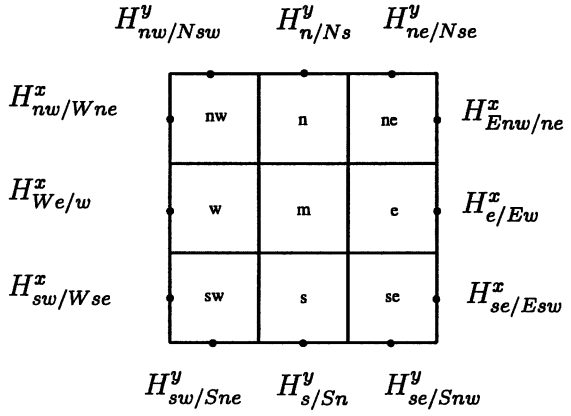

FIG. 4.5 – Fluxes needed for an iteration of the scheme on the coarse grid to calculate Y^{n+1} on K_M

ming step during one iteration is the calculation of the fluxes therefore the multilevel is expected to reduce significantly the CPU time.

Indeed, if we implement the classical finite volume scheme on one level the fine mesh $\mathcal{M}_1$ which has $N_x \times N_y$ control volumes, for each time iteration, we need to calculate the fluxes on $2N_xN_y + N_x + N_y$ edges.

Now with the multilevel method implemented on two levels of grids $\mathcal{M}_1$ and $\mathcal{M}_2$, during an iteration on the coarse grid, the fluxes need to be evaluated on $2N_xN_y/3 + N_x + N_y$ edges. This means that for this iteration, we gain $\mathcal{G}$ computations of fluxes, where

$$\mathcal{G} = \frac{4N_xN_y}{3}.$$

In the particular case of a square mesh (that we will consider in the numerical experiments),

$$\mathcal{G} = 4N_x^2/3,$$

and this corresponds to a computation-saving of

$$\frac{2}{3}\frac{N_x}{N_x+1}\%.$$

For example if we work now on two levels with two grids of 300×300 and 100×100, this means a gain of 66.4% for each iteration on the coarse grid. We can notice that the maximum gain in percent that we can expect is lower than 2/3, and that when the number of cells of the fine mesh increases, it gets closer to this maximal value.

The behaviour of the multilevel method then depends on the number of iterations elapsed on the coarse level : as this number increases, the CPU-time decreases, whereas the error increases. Nevertheless, in order to be sure that we obtain a good approximation of the solution, we need to check that the error when using the multilevel method is ranged between the error made when calculating on the fine level and the one made when calculating on the coarse level. This will ensure that the multilevel method enable us to get a better solution than when calculating on the coarse level, while being faster than the classical one level method on the fine grid. We have to compose with these two aspects.

4.3.3 The multilevel method with central-upwind schemes

The space discretization is done using a semi-discrete central-upwind scheme (presented in [17], [18]) ; we describe here in detail the expression of these central-upwind fluxes. These types of schemes have the advantage to be perfectly adapted to the discretization of hyperbolic systems of conservation laws due to their upwind nature while being robust and simple since they do not require to solve any Riemann problems ; moreover these are nonstaggered schemes. The starting point of the construction of this type of schemes is the equivalent integral formulation of the system. They are based on integration over Riemann fans using the one-sided local speeds of propagation.

Recall that the semi-discrete form of the scheme writes :

$$\frac{d}{dt}Q_m(t) = -\frac{H^x_{m/e}(t) - H^x_{w/m}(t)}{\Delta x} - \frac{H^y_{m/n}(t) - H^y_{s/m}(t)}{\Delta y} + S_m(t),$$

We first use a second order version, and the corresponding numerical fluxes are :

$$H^x_{m/e} = \frac{a^+_{m/e}F(Q^E_m) - a^-_{m/w}F(Q^W_n)}{a^+_{m/e} - a^-_{m/w}} + \frac{a^+_{m/e}a^-_{m/w}(Q^W_e - Q^E_m)}{a^+_{m/e} - a^-_{m/w}} \tag{4.7}$$

and

$$H^y_{m/n} = \frac{b^+_{m/n}G(Q^N_m) - b^-_{m/s}G(Q^S_n)}{b^+_{m/n} - b^-_{m/s}} + \frac{b^+_{m/n}b^-_{m/s}(Q^S_n - Q^N_m)}{b^+_{m/n} - b^-_{m/s}} \tag{4.8}$$

Here, we use a non-oscillatory linear polynomial reconstruction to evaluate the following point values which are present in (4.7), (4.8) :

$$Q_m^E = p_m(t, x_{m/e}, y_m),\ Q_m^W = p_m(t, x_{m/w}, y_m),$$

$$Q_m^N = p_m(t, x_m, y_{m/n}),\ Q_m^S = p_m(t, x_m, y_{m/s}).$$

where $p_m(t, x_m, y_m) = Q_m(t) + s_m^x(t)(x - x_m) + s_m^y(t)(y - y_m)$.
We use a piecewise linear reconstruction in order to obtain a second order scheme. The order of the scheme also comes from the order of the quadrature formula used to approximate the flux integrals coming from the integral formulation.
The slopes of this linear approximation are calculated using a minmod limiter :

$$s_m^x(t) = \text{minmod}(\theta\frac{Q_m(t) - Q_w(t)}{\Delta x}; \frac{Q_e(t) - Q_w(t)}{2\Delta x}; \theta\frac{Q_e(t) - Q_m(t)}{\Delta x}),$$

$$s_m^y(t) = \text{minmod}(\theta\frac{Q_m(t) - Q_s(t)}{\Delta y}; \frac{Q_n(t) - Q_s(t)}{2\Delta y}; \theta\frac{Q_n(t) - Q_m(t)}{\Delta y}),$$

with

$$\text{minmod}(x_1, x_2, ..) := \begin{cases} \min(x_i),\ \text{if } x_i > 0\ \forall i \\ \max(x_i),\ \text{if } x_i < 0\ \forall i \\ 0,\ \text{otherwise.} \end{cases}$$

where $\theta \in [1, 2]$.
An appropriate choice of these approximate derivatives is crucial to ensure that the above reconstruction is non oscillatory in the sense of preventing appearance of new extrema in the solution ; it can be shown that with such approximate derivatives the scheme satisfies the scalar total-variation-diminishing (TVD) property (see [15], [17]). The parameter $\theta \in [1, 2]$ has to be chosen in an optimal way in order to obtain good results ;
The one-sided local speeds of propagation are given by :

$$a_{m/e}^+ = \max[\lambda_{max}(\frac{\partial F}{\partial Q}(Q_e^W)), \lambda_{max}(\frac{\partial F}{\partial Q}(Q_m^E)), 0]$$

$$a_{m/e}^- = \min[\lambda_{min}(\frac{\partial F}{\partial Q}(Q_e^W)), \lambda_{min}(\frac{\partial F}{\partial Q}(Q_m^E)), 0]$$

$$b_{m/n}^+ = \max[\lambda_{max}(\frac{\partial G}{\partial Q}(Q_n^S)), \lambda_{max}(\frac{\partial G}{\partial Q}(Q_m^N)), 0]$$

$$b_{m/n}^- = \min[\lambda_{min}(\frac{\partial G}{\partial Q}(Q_n^S)), \lambda_{min}(\frac{\partial G}{\partial Q}(Q_m^N)), 0]$$

where $\lambda_{max}(\frac{\partial F}{\partial Q}(\tilde{Q}))$ and $\lambda_{min}(\frac{\partial F}{\partial Q}(\tilde{Q}))$ (resp. $\lambda_{max}(\frac{\partial G}{\partial Q}(\tilde{Q}))$ and $\lambda_{min}(\frac{\partial G}{\partial Q}(\tilde{W}))$) are respectively the largest and the smallest eigenvalue of the jacobian matrix

of F, $\frac{\partial F}{\partial Q}$ (resp. of G, $\frac{\partial G}{\partial Q}$) at the point $\tilde{Q}$.
This gives a central-upwind scheme of second order.
Recall that we consider periodic boundary conditions, then the quantities on the boundaries are evaluated using periodicity.

For the time discretization, we use a second order Runge-Kutta (or Heun) method. Let $T > 0$ be fixed, denote the time step by $\Delta t = T/N_{it}$, where N_{it} is an integer representing the number of iterations; for $n = 0, .., N_{it}$ we define Q^n as the approximate value of Q at time $t_n = n\Delta t$.
If we rewrite (4.4) as

$$\frac{d}{dt}Q_m = C(Q_m(t), t),$$

we apply the following time discretization :

$$\begin{cases} k_1 = C(Q_m^n, t_n), \\ k_2 = C(Q_m^n + \Delta t k_1, t_n + \Delta t), \\ Q_m^{n+1} = Q_m^n + \frac{\Delta t}{2}(k_1 + k_2). \end{cases}$$

4.4 Numerical simulations

We present here the numerical results obtained by using the multilevel method presented above. For the sake of simplicity, we consider in all the following simulations a square domain $\Omega = [0, L] \times [0, L]$ and we recall that we are interested with periodic boundary conditions.

4.4.1 Study of the method on analytical solutions

In order to study the peformance of the multilevel scheme, we first consider analytical solutions; we solve the Shallow Water system with the initial condition :

$$\begin{pmatrix} h \\ u \\ v \end{pmatrix} = \begin{pmatrix} h_0 \\ u_0 \\ u_0 \end{pmatrix}$$

and with the appropriate source term so that

$$\begin{aligned} h(t,x,y) &= h_0(1 + \epsilon \sin(\frac{2\pi t}{T}) \cos(\frac{4\pi x}{L}) \sin(\frac{4\pi y}{L})) \\ u(t,x,y) &= u_0(1 + \epsilon \sin(\frac{2\pi t}{T}) \cos(\frac{4\pi x}{L}) \cos(\frac{4\pi y}{L})) \\ v(t,x,y) &= u_0(1 + \epsilon \sin(\frac{2\pi t}{T}) \sin(\frac{4\pi x}{L}) \cos(\frac{4\pi y}{L})) \end{aligned} \tag{4.9}$$

is the exact solution of the system to which we can compare the computed solution.
Here we take $L = 10$, the average height and speed of the fluid are respectively $h_0 = 1$ and $u_0 = 0.1$, and ϵ measures the amplitude of the wave, here $\epsilon = 0.2$. The time period of the exact solution is $T = 0.5$ and the time step retained for all the computations is $\Delta t = 10^{-4}$. Let us

introduce the small parameter $\mu = (h_0/L)^2$ which measures the shallowness of the flow; here $\mu = 10^{-4}$ and the Stokes number which measures the comparison between the dispersive effects and the nonlinear effects is $S = \epsilon/\mu = 2000$. We are thus in the frame of a Shallow Water flow : big amplitude and shallowness, which renders the flow strongly nonlinear. The parameter θ is taken to $\theta = 1.6$ and the fine mesh $\mathcal{M}_1$ counts 90000 cells which corresponds to a space step equal to $\Delta x = 10/300$.

First, we make a one level computation on the fine mesh $\mathcal{M}_1$ in order to study the behavior of the small scale and of the large scale components z and y of the conservative variables corresponding to the coarser level of discretization which here is two. We plot the time evolution of the discrete norms of the following quantities for h :

$$|h^n|_2 = \sqrt{\sum_{K_m \in \mathcal{M}_1} (\Delta x)^2 (h_m^n)^2}$$

$$|y^n|_2 = \sqrt{\sum_{K_M \in \mathcal{M}_2} 9(\Delta x)^2 (y_M^n)^2}$$

$$|z^n|_2 = \sqrt{\sum_{K_m \in \mathcal{M}_1} (\Delta x)^2 (z_m^n)^2}$$

where $\mathcal{M}_2$ denotes the coarser mesh, and similarly fo u and v. We also plot the time evolution of their variations

$$|dh^n|_2 = \sqrt{\sum_{K_m \in \mathcal{M}_1} (\Delta x)^2 (h_m^n - h_m^{n-1})^2}$$

$$|dy^n|_2 = \sqrt{\sum_{K_M \in \mathcal{M}_2} 9(\Delta x)^2 (y_M^n - y_M^{n-1})^2}$$

$$|dz^n|_2 = \sqrt{\sum_{K_m \in \mathcal{M}_1} (\Delta x)^2 (z_m^n - z_m^{n-1})^2}$$

The graph we obtain are presented in Figures 4.6 and 4.7. As expected, the norms of h, U and V are respectively of the same order as the norms of y_h, y_U, y_V, and the norms of z_h, z_U, and z_V are small in accordance with Lemma 4.3.1. Moreover the time variation of the large scale components y of the conservative variables h, U, and V are similar to the variation of h, U, and V and the time variation of the small scale components z satisfy $|dz|_2 = \mathcal{O}(\Delta t^{3/2})$; the order of magnitude of this norm is crucial for performance of the multilevel method.
Indeed during an iteration on the coarse grid, the z are frozen which means that $z^{n+1} = z^n$. But effectively,

$$z^{n+1} - z^n = \Delta t \frac{\partial z}{\partial t} + \mathcal{O}(\Delta t^2),$$

that is $z^{n+1} = z^n + \delta$ where $\delta = \Delta t \dfrac{\partial z^n}{\partial t} + \mathcal{O}(\Delta t^2)$.
Consequently if $\dfrac{\partial z^n}{\partial t} = \mathcal{O}(\Delta t)$ then $\delta = \mathcal{O}(\Delta t^2)$ and freezing the z is legitimate whereas $z^{n+1} -$

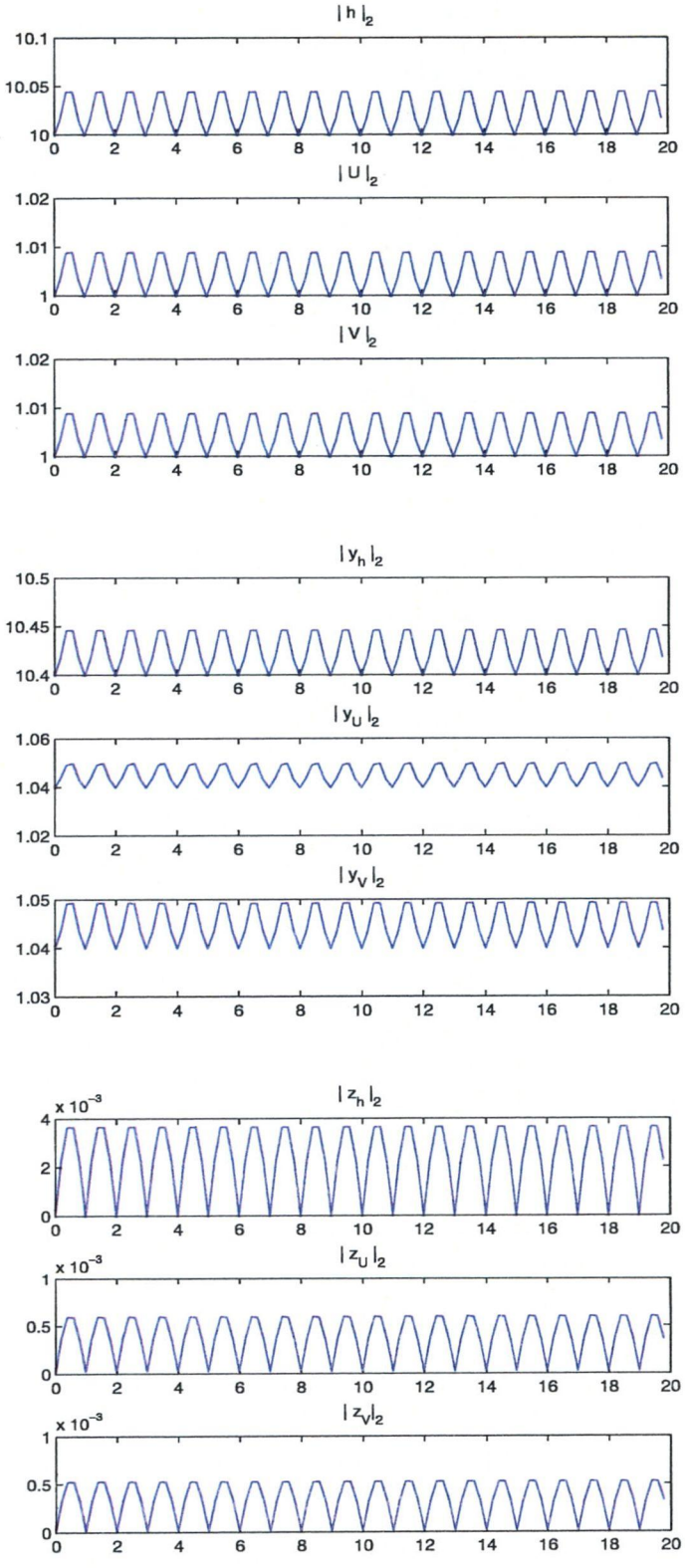

FIG. 4.6 – Time evolution of the discrete L^2-norms of the conservative variables.

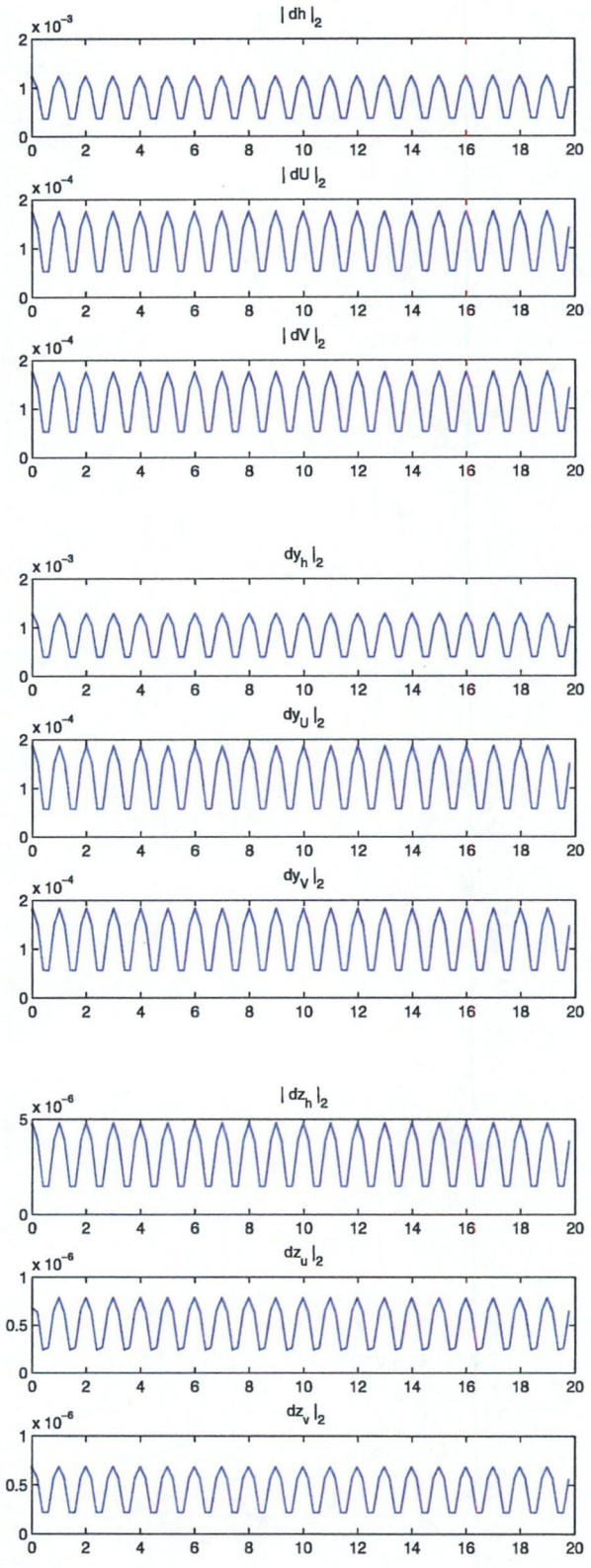

FIG. 4.7 – Time evolution of the discrete L^2-norms of the variations of the conservative variables.

$z^n = \mathcal{O}(\Delta t)$ means that $\delta = \Delta t \dfrac{\partial z^n}{\partial t} = \mathcal{O}(\Delta t)$ or $\dfrac{\partial z^n}{\partial t} = \mathcal{O}(1)$ which cannot allow to freeze the z^n without introducing significative errors.

The quantity $\dfrac{\partial z^n}{\partial t}$ can be computed explicitely and is linked to the space step. Indeed we find using Taylor formula that

$$z_e = -\frac{4}{3}\Delta x^2 \frac{\partial^2 Q_e}{\partial x^2} - \frac{1}{3}\Delta y^2 \frac{\partial^2 Q_e}{\partial y^2},$$

$$z_{ne} = -\frac{4}{3}\Delta x^2 \frac{\partial^2 Q_e}{\partial x^2} - \frac{4}{3}\Delta y^2 \frac{\partial^2 Q_e}{\partial y^2} - \Delta x \Delta y \frac{\partial^2 Q_e}{\partial x \partial y},$$

and

$$\frac{\partial z_e}{\partial t} = -\frac{4}{3}\Delta x^2 \frac{\partial^3 Q_e}{\partial t \partial x^2} - \frac{1}{3}\Delta y^2 \frac{\partial^3 Q_e}{\partial t \partial y^2},$$

$$\frac{\partial z_{ne}}{\partial t} = -\frac{4}{3}\Delta x^2 \frac{\partial^3 Q_e}{\partial t \partial x^2} - \frac{4}{3}\Delta y^2 \frac{\partial^3 Q_e}{\partial t \partial y^2} - \Delta x \Delta y \frac{\partial^3 Q_e}{\partial t \partial x \partial y},$$

and similarly for the other z terms. In a future work, this quantity could be used as a criterion to decide whether a way down on the coarse level is reasonnable in order to control the way downs on coarse levels and the ascents on finer levels instead of following systematic cycles as is done in these simulations.

For the test case we study, the order of magnitude of $\dfrac{\partial z^n}{\partial t}$ can thus be evaluated and we find values which agree with the curves presented in Figure 4.7. To show the importance of the space step we repeat several computations on different fine meshes (with 90×90 and 120×120 control volumes) and plot in Figure 4.8 the evolution of $\dfrac{z^{n+1} - z^n}{\Delta t}$ which is compared to Δt. The multilevel method with 300×300 cells is expected to work well up to a certain point since $\dfrac{\partial z^n}{\partial t}$ is not too far from $\mathcal{O}(\Delta t)$; the bigger the space step is, the larger the value of $\dfrac{\partial z^n}{\partial t}$ will be and the less accurate the multilevel method will be. The multilevel computation with the mesh of 120×120 control volumes is still more precise than the computation on the coarse grid, but with 90×90 cells, $\dfrac{\partial z^n}{\partial t}$ is too much bigger than Δt and the multilevel method provides too big errors : the errors obtained are too close from the ones obtained with a computation on the coarse grid, as displayed in Figure 4.9, for the multilevel method to be profitable.

Consequently the multilevel method is expected to work better the smaller the space step is ; and it enables to descend on coarser levels and to spend more iterations on the coarsers levels, which provides a more important gain in CPU time while preserving the accuracy of the resolution.

In a second step we use the multilevel method to solve the same problem on two levels of discretization. The coarse mesh $\mathcal{M}_2$ counts 100×100 cells with a space step $\Delta x = 0.1$. This computation is made by beginning by a few iterations on the fine mesh, and then repeating cycles of the form 1111122222211111 where 1 corresponds to the fine level and 2 to the coarse one, which means that we spend around 37.5% of the iterations on the coarse grid (see Figure 4.15) ; in the following, we refer to this simulation as the multilevel method at 37% (MM37).

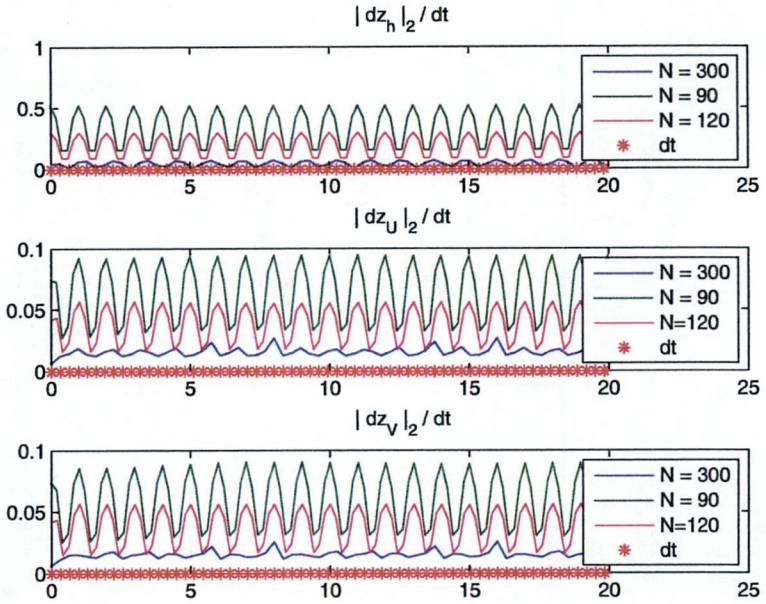

FIG. 4.8 – Time evolution of the L^2-norms of the variations of the variables with different space steps.

We show in Figure 4.10 the solutions obtained at $t = 20$ with the multilevel method on the right, which are visually very same to the reference solutions obtained with the one level computation on the fine mesh and depicted on the left of the figure. For more clearness we also represent the differences between the multilevel solutions and the reference solutions in Figure 4.11 ; they are small and agree with the errors obtained.

Notice that the reconstruction of the solution at each iteration with the frozen small scale component z lead to the appearance of very small peaks on the solutions, a zoom on the solutions is necessary to see them. Indeed suppose that the large scale component Y^n of Q at the n^{th} iteration is exact and suppose that the variation of the Z during this iteration is of order ϵ, namely $Z^n = Z^{n-1} + \epsilon$. After an iteration on the coarse grid, we recompose the solution with Z^{n-1} by freezing the small scale component and find :

$$\begin{aligned} Q_m^n &= 5Y_M^n - Y_E^n - Y_W^n - Y_S^n - Y_N^n \\ &\quad - Z_e^{n-1} - Z_w^{n-1} - Z_s^{n-1} - Z_n^{n-1} - Z_{ne}^{n-1} - Z_{nw}^{n-1} - Z_{se}^{n-1} - Z_{sw}^{n-1}, \end{aligned}$$

$$Q_e^n = \frac{1}{3}(2Y_M^n + Y_E^n) + Z_e^{n-1},$$

and similarly for Q_e^n, Q_w^n, Q_s^n, Q_n^n, Q_{ne}^n, Q_{nw}^n, Q_{se}^n, Q_{sw}^n. But the solution recomposed with the correct Z^n would be :

$$\begin{aligned} Q_m^n &= 5Y_M^n - Y_E^n - Y_W^n - Y_S^n - Y_N^n \\ &\quad - Z_e^{n-1} - Z_w^{n-1} - Z_s^{n-1} - Z_n^{n-1} - Z_{ne}^{n-1} - Z_{nw}^{n-1} - Z_{se}^{n-1} - Z_{sw}^{n-1} - 8\epsilon, \end{aligned}$$

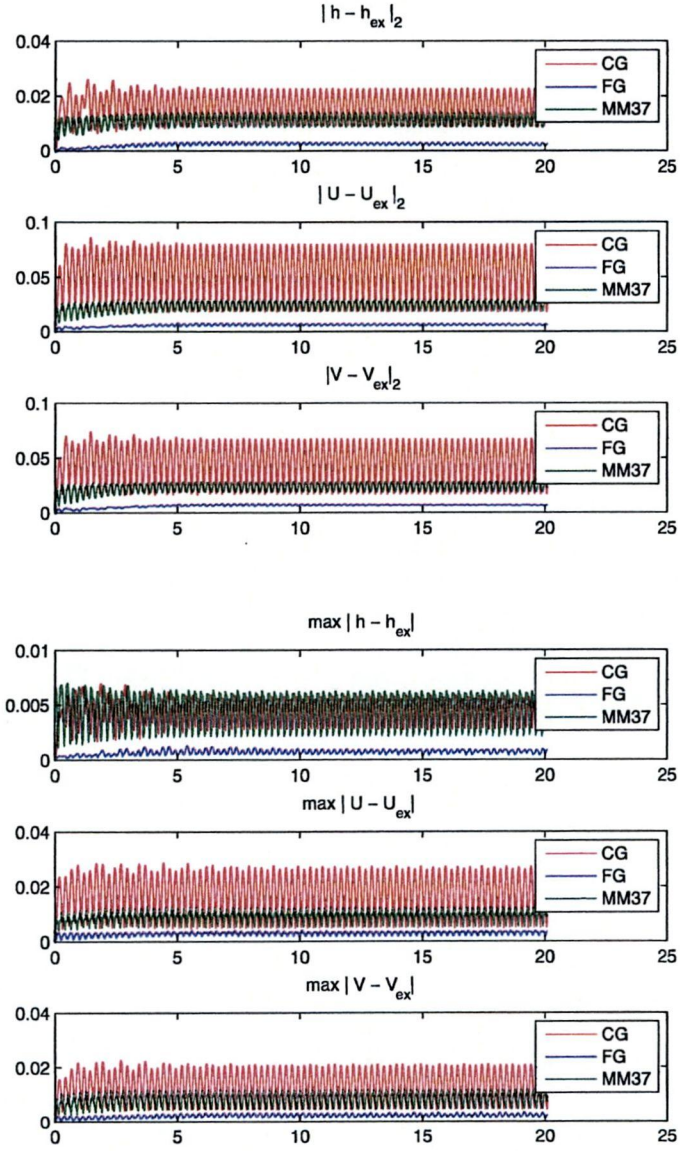

FIG. 4.9 – Time evolution of the L^2 and L^∞ errors obtained with a multilevel computation at 37% and with a computation on the fine grid for a mesh of 90×90 cells.

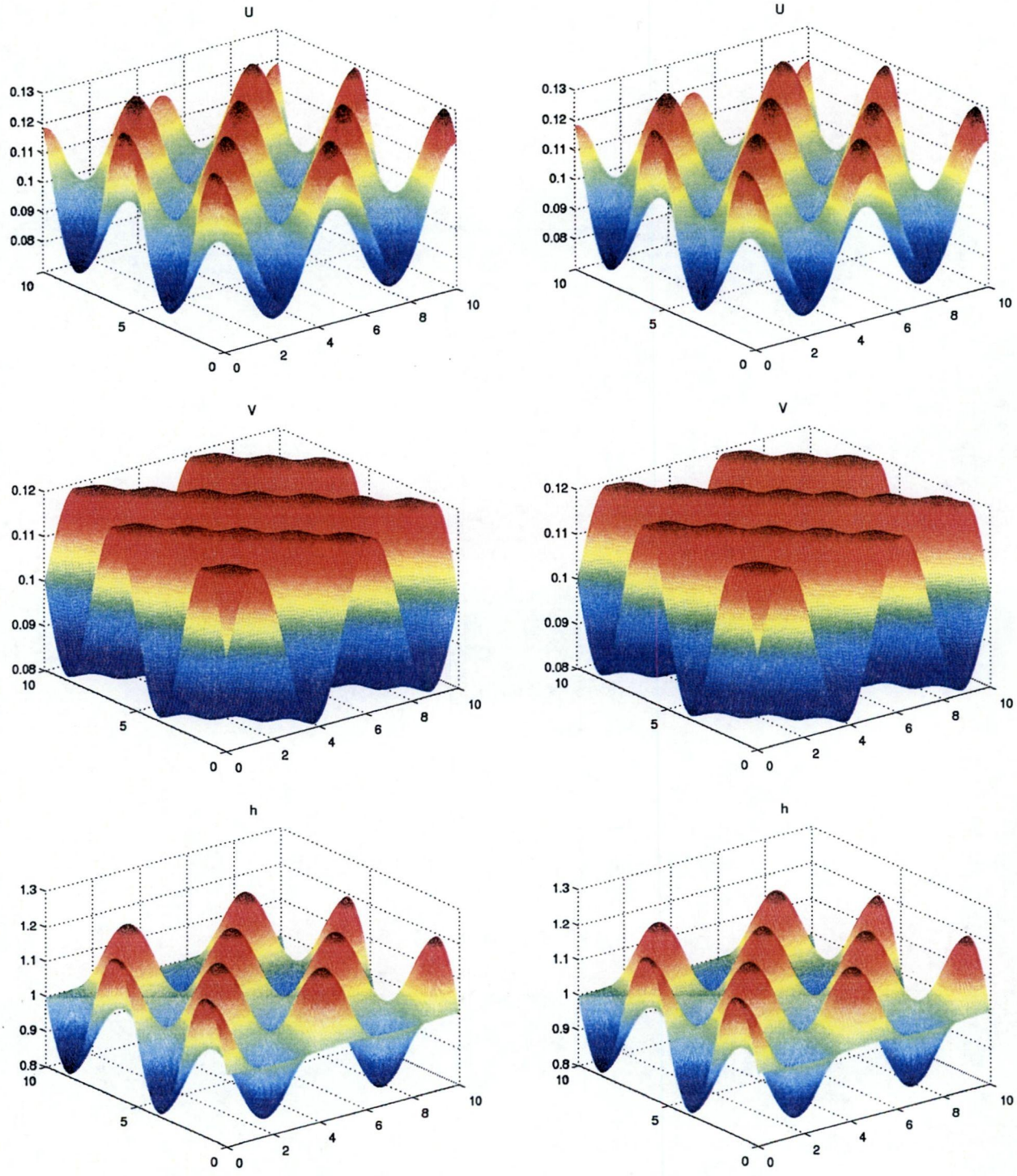

FIG. 4.10 – Solutions obtained at $t = 20$s with a one-level computation on the fine mesh (300×300) (left), and with the multilevel method at 37% (right).

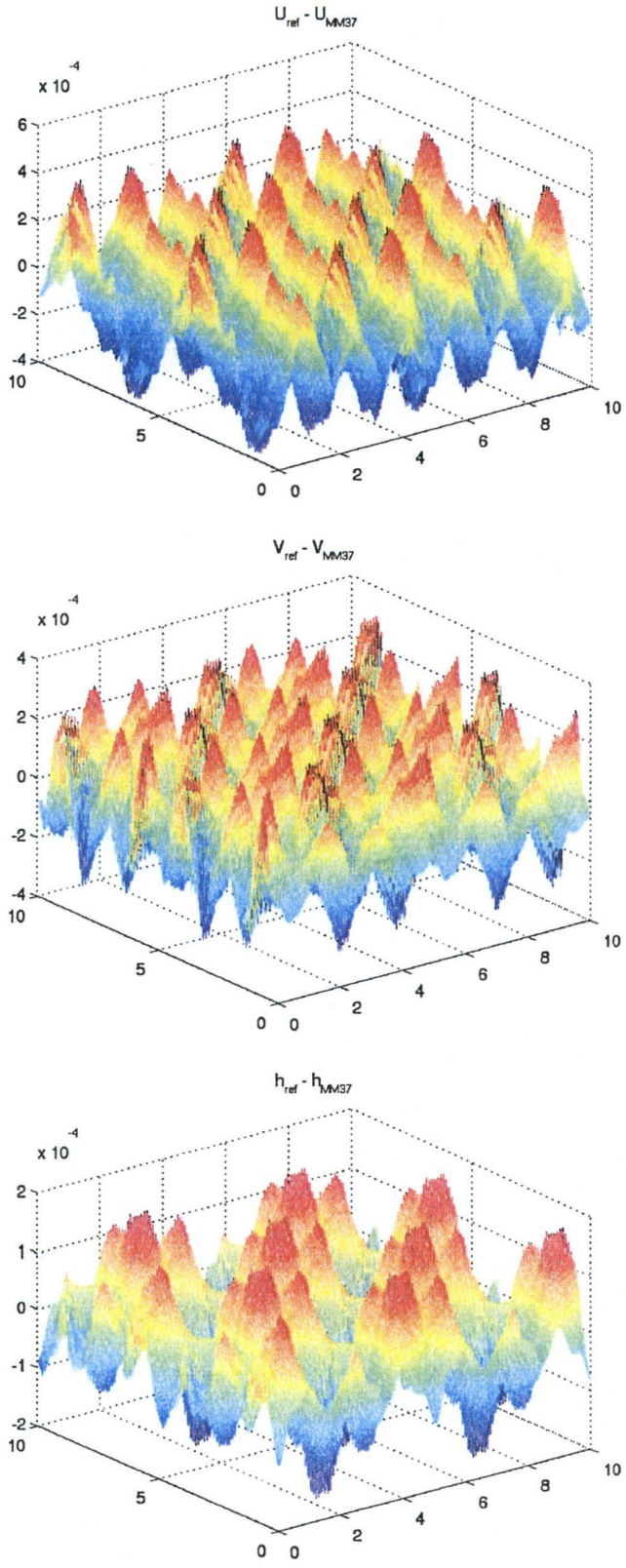

FIG. 4.11 – Differences between the multilevel solutions $(h_{MM37}, U_{MM37}, V_{MM37})$ and the reference solutions $(h_{ref}, U_{ref}, V_{ref})$.

and

$$Q_e^n = \frac{1}{3}(2Y_M^n + Y_E^n) + z_e^{n-1} + \epsilon,$$

and similarly for the other terms. Thus we make an error of ϵ for the solution on the cells K_e, K_w, K_s, K_n, K_{ne}, K_{nw}, K_{se}, K_{sw} and an error of 8ϵ on the cell K_m which results in the formation of these small peaks. If ϵ is small (which is linked to the analysis made in Figure 4.7) this does not spoils the solution.

Remark 4.4.1. *Notice that in one dimension the size of the peaks would be smaller; freezing the Z introduces an error of ϵ on the adjacent fine cells K_e and K_w of a coarse cell K_M and an error of 2ϵ on the cell K_m.*

We also compare the L^2-errors and the L^∞-errors made with this multilevel computation at 37% and with a multilevel computation at 45% to the one made with a one level computation on the coarse and fine meshes on Figure 4.12 and Figure 4.13; Figures 4.12 and 4.13 show that

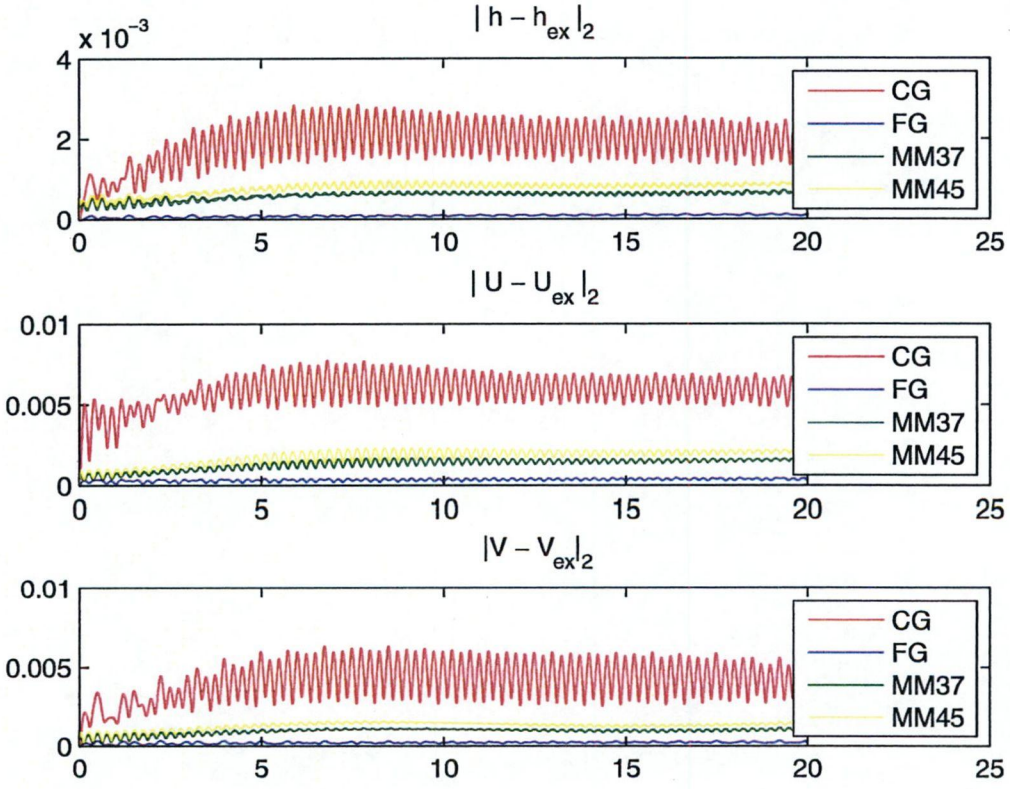

FIG. 4.12 – Time evolution of $||h-h_{ex}||_2$, $||U-U_{ex}||_2$, $||V-V_{ex}||_2$ with the multilevel method at 37% (MM37) and at 45% (MM45), the computation on the fine grid (FG), and the computation on the coarse grid (CG).

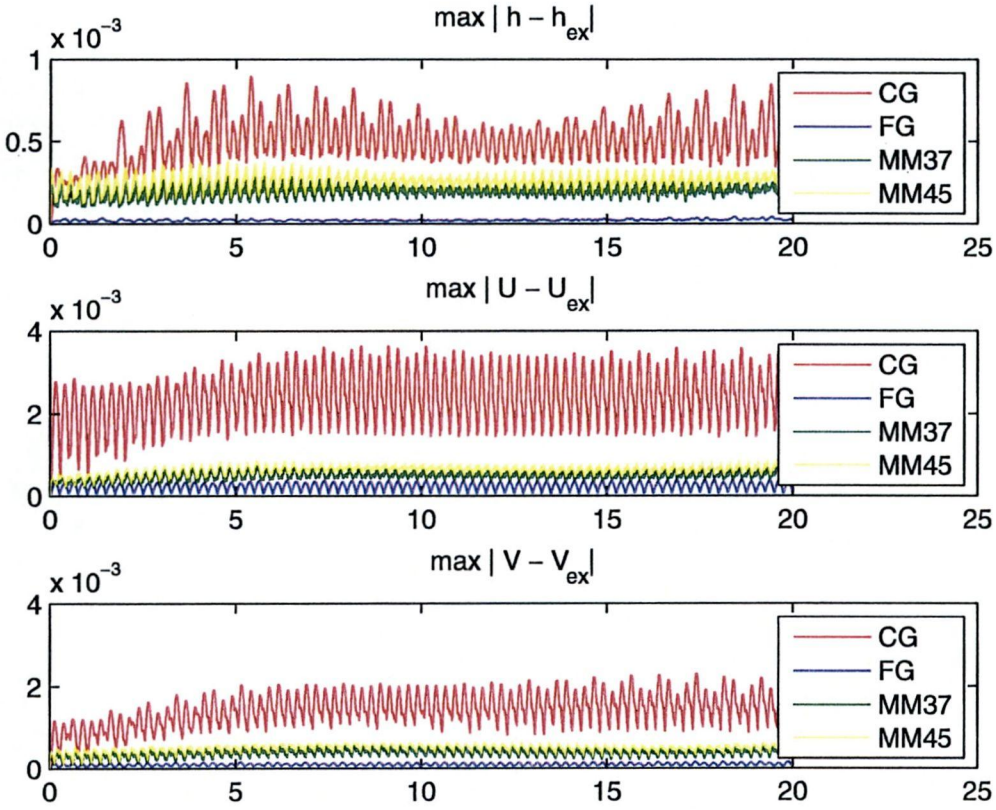

FIG. 4.13 – Time evolution of $||h - h_{ex}||_\infty$, $||U - U_{ex}||_\infty$, $||V - V_{ex}||_\infty$ with the multilevel method at 37% (MM37) and at 45% (MM45), the computation on the fine grid (FG), and the computation on the coarse grid (CG).

the multilevel method at 37% and 45% remain very accurate since the corresponding errors are below the errors made on the coarse grid. The method is also very stable and computations can be pursued in long time. The oscillations observed in the errors are due the strongly oscillating nature of the solution (the time period is 0.5s) and are independant of the multilevel method. We represent in Figure 4.14 a zoom of the comparison of the errors on four periods between $t = 10$ and $t = 12$.

In Figure 4.15 is displayed the scheme of the cycles followed when computing with the multilevel method at 25% (which consists in repeating cycles of the form 1111112222111111 after a few iterations on the fine grid), 37% (cycles of the form 111112222211111) and 45% (cycles of the form 111112222222211111).

Moreover we liken the CPU time consumed with a one level computation made on the fine grid and with the multilevel methods at 37% , at 25% and at 45% in Table 4.1. We also indicate in the second column the gain of CPU time in percent which is made with the multilevel methods in respect to the computation on the fine grid, and in the last two columns the percentage of CPU time spent for iterations on the fine grid and on the coarse grid. Note that the mean CPU time spent for an iteration on the fine grid is of 0.5s and 0.3s for an iteration on the coarse grid.

TAB. 4.1: Comparison of the CPU times consumed with a computation on the fine grid and with multilevel methods with different cycles.

Method	*CPU Time*	*Gain in %*	% IFG	% ICG
FG	26h	-	90%	0%
MM25	24h37	5%	75%	13.5%
MM37	22h21	14%	66%	21%
MM45	21h55	15.6%	61%	26%

The more time is spent on the coarse grid, the faster the computation will be. However if too many iterations are spent on the coarse grid, the method loses its accuracy and can become less precise than the one level computation on the coarse grid. For this test case, a multilevel computation where 50% of the iterations are spent on the coarse grid lead to errors which exceed the errors made on the coarse grid and thus becomes unsatisfactory. Indeed we observe (see Figure 4.16) that with cycles of the form 1111222222221111, the variations $\frac{z^{n+1}-z^n}{\Delta t}$ for h, U and V come very high compared to the time step (and run over 1 for U and V) , and the errors go through the errors made on the coarse grid, as can be seen in Figure 4.17.

An improvement of the multilevel resolution could be made by using a criterion regulating whether a way down on a coarser level is admissible and how many iterations can be spent on this coarse level without spoiling the resolution. A characteristic quantity (see Section 4.4.1) could be evaluated during the multilevel resolution and when it goes too close from a critical value, a way up on a fine level would be done.

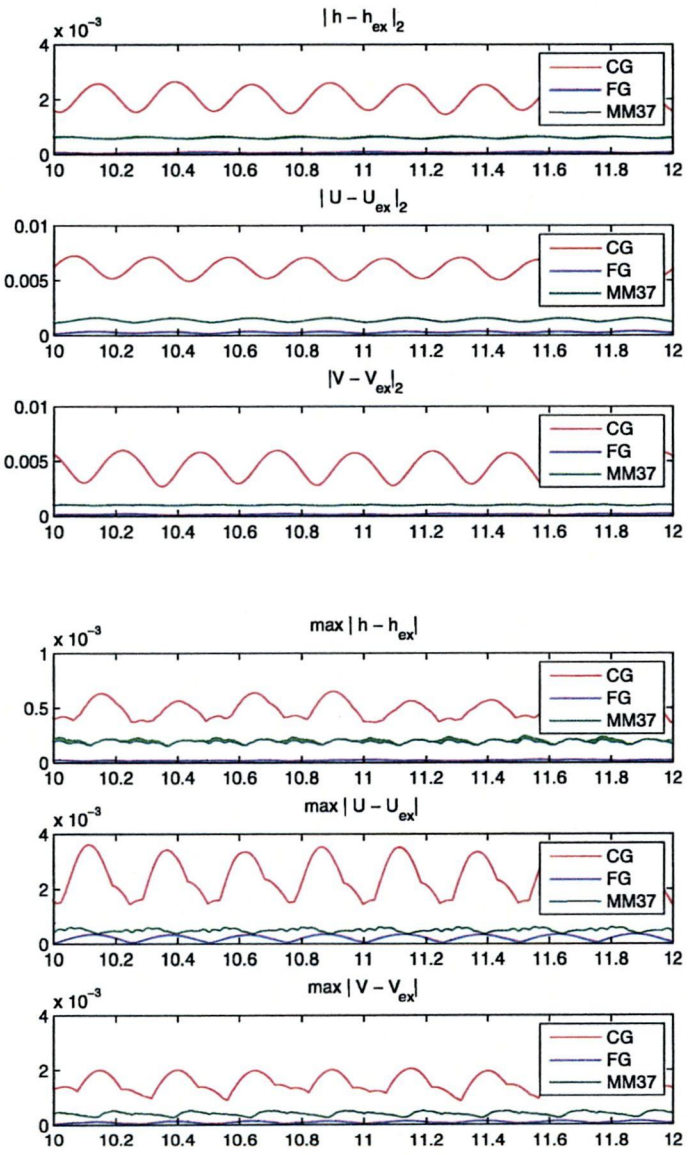

FIG. 4.14 – Time evolution of $||h - h_{ex}||_\infty$, $||U - U_{ex}||_\infty$, $||V - V_{ex}||_\infty$ and of $||h - h_{ex}||_2$, $||U - U_{ex}||_2$, $||V - V_{ex}||_2$ with the multilevel method at 37% (MM37), the computation on the fine grid (FG), and the computation on the coarse grid (CG).

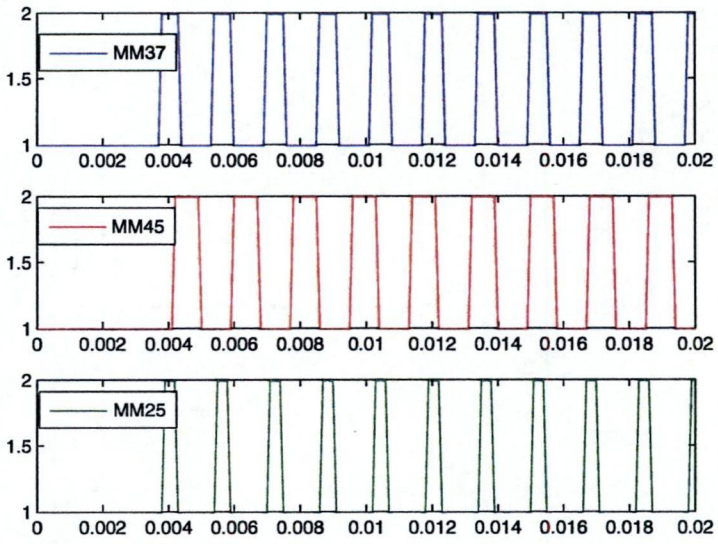

FIG. 4.15 – Evolution of the level of discretization for different multilevel computations.

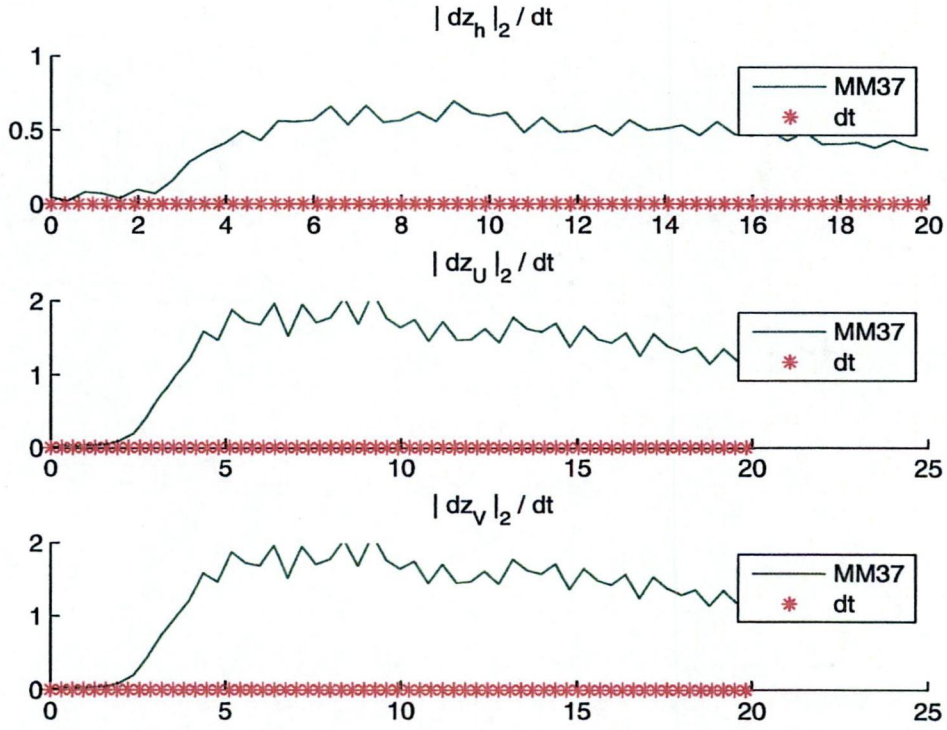

FIG. 4.16 – Time evolution of the discrete L^2-norms of $\frac{z^{n+1}-z^n}{\Delta t}$ for the conservative variables with the multilevel method at 50%.

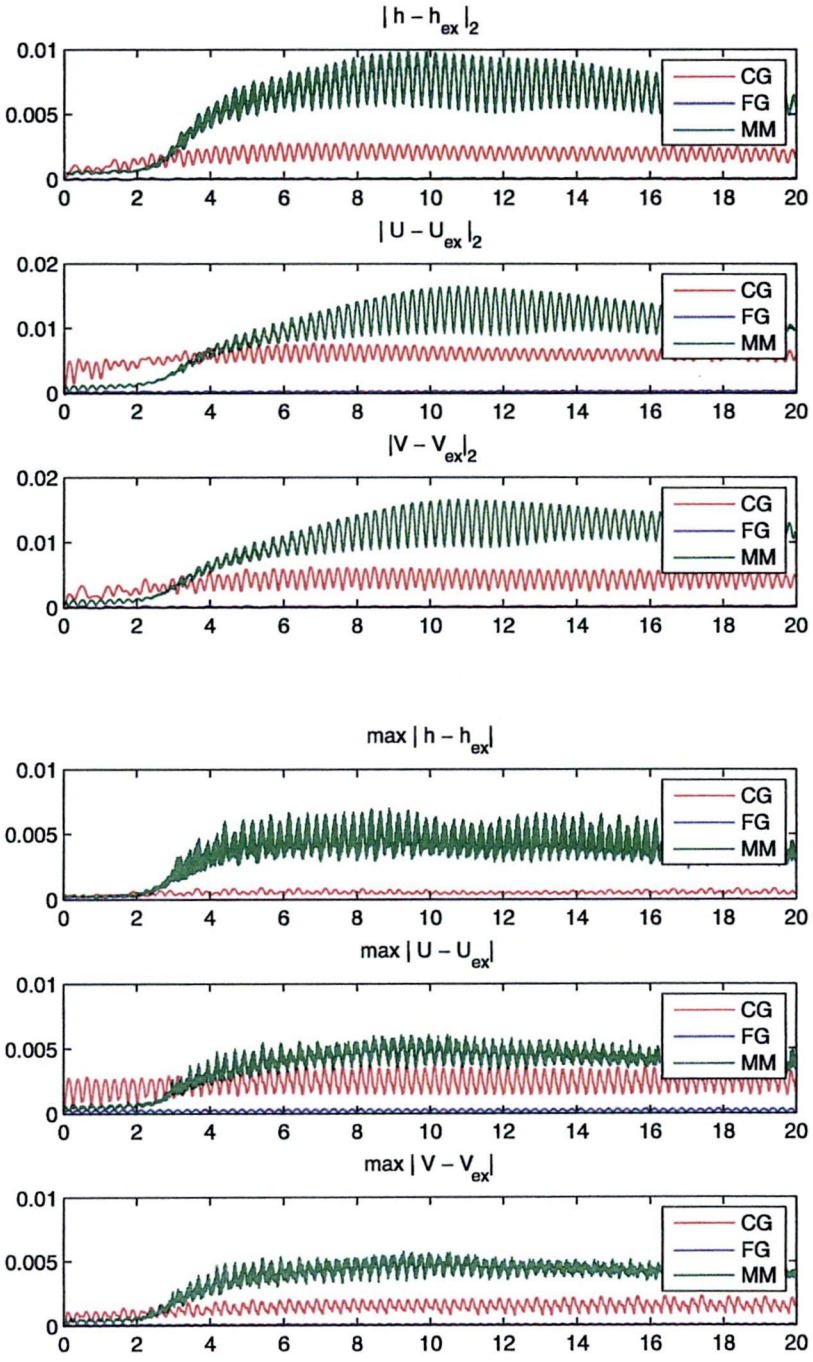

FIG. 4.17 – Time evolution of $||h-h_{ex}||_2$, $||U-U_{ex}||_2$, $||V-V_{ex}||_2$ and of $||h-h_{ex}||_\infty$, $||U-U_{ex}||_\infty$, $||V-V_{ex}||_\infty$ with the multilevel method at 50% (MM50), the computation on the fine grid (FG), and the computation on the coarse grid (CG).

4.4.2 A turbulence model

In this section we test our multilevel scheme on more physical inital data, which were used in [10] to test spectral multilevel methods for the simulation of turbulent atmospheric or oceanic flows with the Shallow Water problem and with periodic boundary conditions. The initial data, the initial vorticity $\partial_x v - \partial_y u$, the initial divergence $\partial_x u + \partial_y v$ and their contour maps are plotted in Figures 4.18, 4.19 and 4.20. The initial divergence and vorticity are very small since it was used for the simulation of atmospheric flows which are quasi-geostrophic (see [10]).
We start by making a computation on a fine grid in order to obtain a reference solution which will play the role of the exact solution. We thus launch a one level computation on a grid counting 500×500 cells up to the time $t = 10000$ seconds with a time step $\Delta t = 0.1$, and $\theta = 1.6$. The computational domain is a square $\mathcal{M} = [0, L] \times [0, L]$ where $L = 6.31.10^6$ (earth radius) is the period in the x and y directions and the mean height is taken to 10^4 (troposphere). The solutions $Q^{ref} = (h^{ref}, U^{ref}, V^{ref})$ obtained with this computation are the reference solutions which we will compare the solutions obtained with the multilevel method to (see Figures 4.24, 4.25, 4.26).
As in [10], we plot in Figure 4.21 some physical characteristic quantities : the maximum velocity $||(u,v)||_\infty$ and the kinetic energy $||(u,v)||_2^2$. As in Section 4.4.1, we also make a one level simulation with a fine mesh of 360×360 cells and represent the evolution of the norms of the conservative variables, of their small and large scale components, and of their variations in Figures 4.22 and 4.23; the problem is here physically dimensional but we also observe that the small scale component are smaller than the large scale component which are of the same order as the variables.

A two-level simulation

Then we study the behaviour of the multilevel method on this problem. The fine mesh counts 360×360 cells and the coarse mesh 120×120 cells. The solutions computed with the multilevel method at 37% (repetition of cycles of the form 1111122222211111) are represented on the right of Figures 4.24, 4.25 and 4.26, they look like perfecly the reference solutions represented on the left of the figures. The differences between the solution Q^{ref} and the solution Q obtained with the multilevel method at 37% are depicted in Figure 4.27, they are small compared to the solutions. We also show the contour maps of the differences between the reference and the multilevel vorticity and divergence in Figure 4.28. For the divergence and the vorticity, the differences seem to be quite big but this is due to the fact that the divergence and the vorticity are here very close to zero since the flow is quasi-geostrophic; since the problem is physically dimensionnal the computer has to deal with very big values and with very small ones (close to zero) thus this is a very steep problem.
In order to test the accuracy of the method, we compare the following errors :

$$E_{max} = ||(u,v)||_\infty - ||(u^{ref}, v^{ref})||_\infty,$$
$$E_{cin} = ||(u,v)||_2^2 - ||(u^{ref}, v^{ref})||_2^2,$$

where (h, uh, vh) denotes the solutions obtained with a multilevel method or with the one level computation on the coarse grid. They are depicted in Figure 4.29; the errors done with the

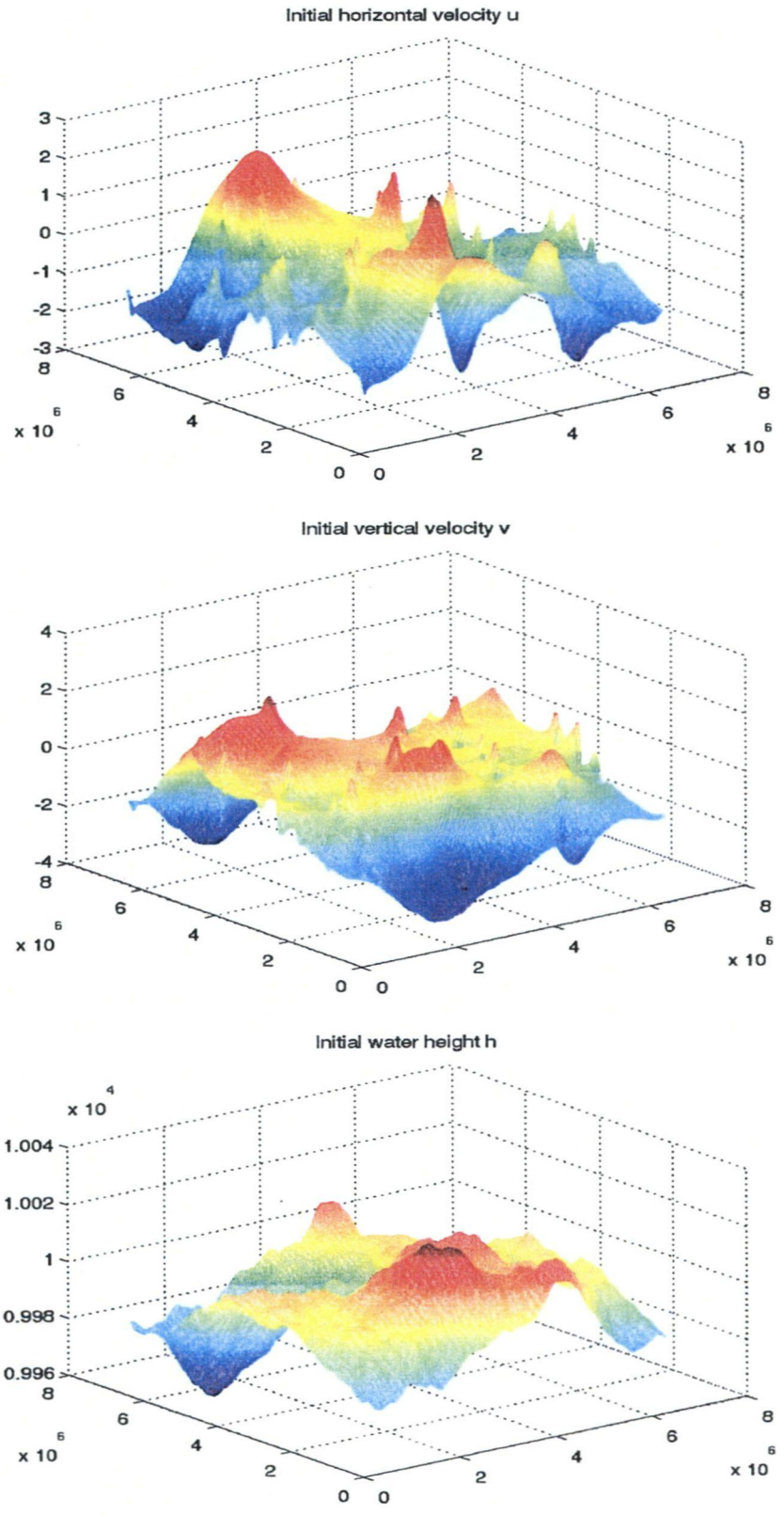

FIG. 4.18 – The initial data.

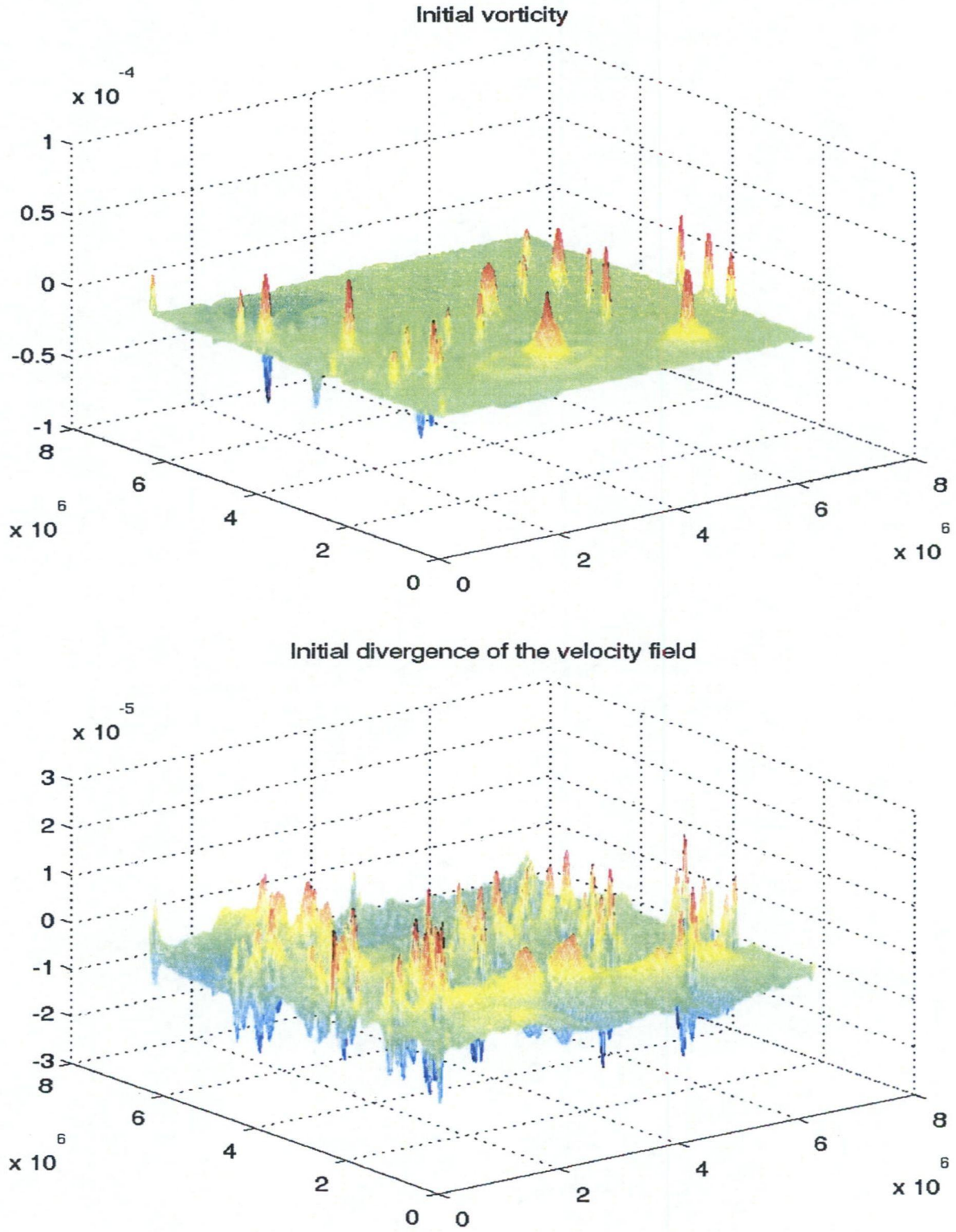

FIG. 4.19 – Initial vorticity and divergence.

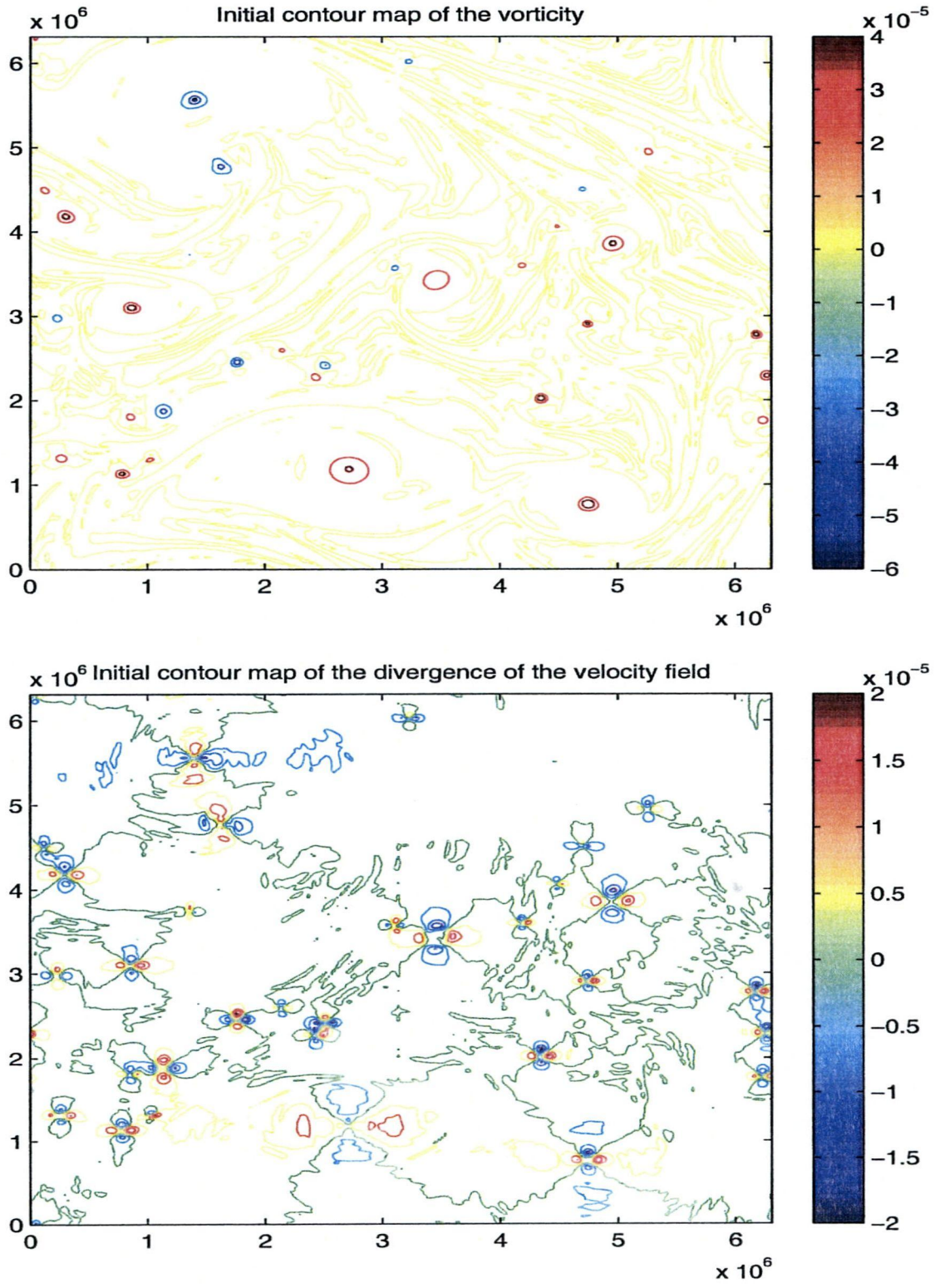

FIG. 4.20 – Contour maps of the initial vorticity and divergence.

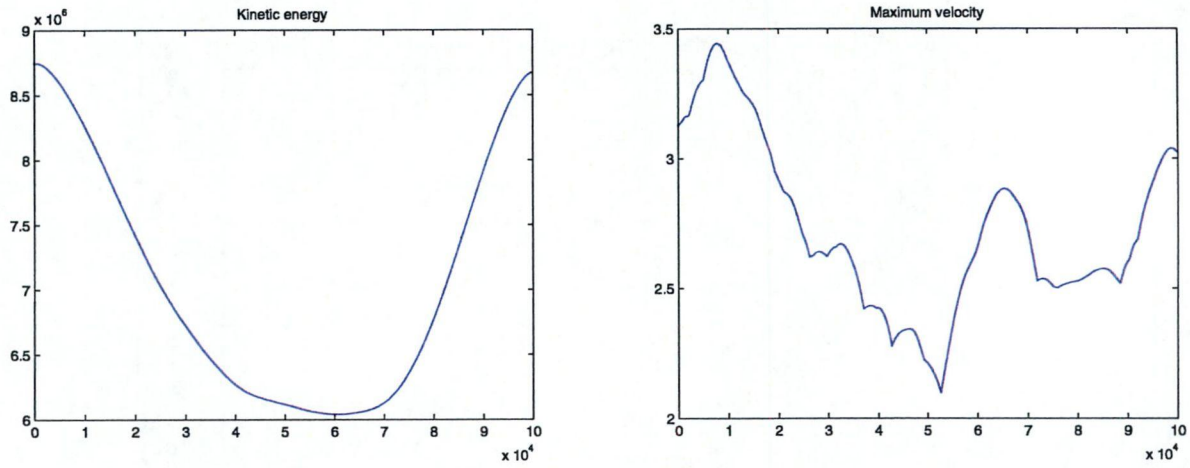

FIG. 4.21 – Reference evolution of the kinetic energy, of the maximum velocity and of the energy norm of h.

multilevel computations follow the error made with the computation on the fine grid and are largely below the errors made with the computation on the coarse grid, which shows the quality of the multilevel resolution. Thanks to our choice of incremental unknowns (particularly the choice of the large scale components Y) the multilevel method also remains conservative. We plot in Figure 4.30 the evolution of $N_h = \int_{\mathcal{M}} h / \int_{\mathcal{M}} h_0$ with a computation on the fine grid and with a multilevel computation (at 37%); because of the absence of a source term and of the periodic boundary conditions, this quantity should be conserved. Figure 4.30 shows that this is the case also for the multilevel method.

Moreover the CPU time needed for the resolution with the multilevel method is smaller than for the one-level resolution on the fine mesh; as in Section 4.4.1, Table 4.2 shows the different CPU time consumed for different computations, the gain observed, and the percentage of CPU time spent for the iterations on the fine grid (% IFG) and on the coarse grid (% ICG). The mean CPU time spent for an iteration on the fine grid is of 0.8s and 0.5s on the coarse grid. Observe that the gains in CPU time are not identical as in Section 4.4.1; the problems studied are very different and the computation of the fluxes in the finite volume mesh may not be equivalent.

TAB. 4.2: Comparison of the CPU times consumed with a computation on the fine grid and with multilevel methods with different cycles.

Method	*CPU Time*	*Gain in %*	%IFG	% ICG
FG	14h10	-	95%	0%
MM25	13h	8%	78%	15%
MM37	12h40	10.5%	70%	24%
MM45	11h20	20%	65%	30%

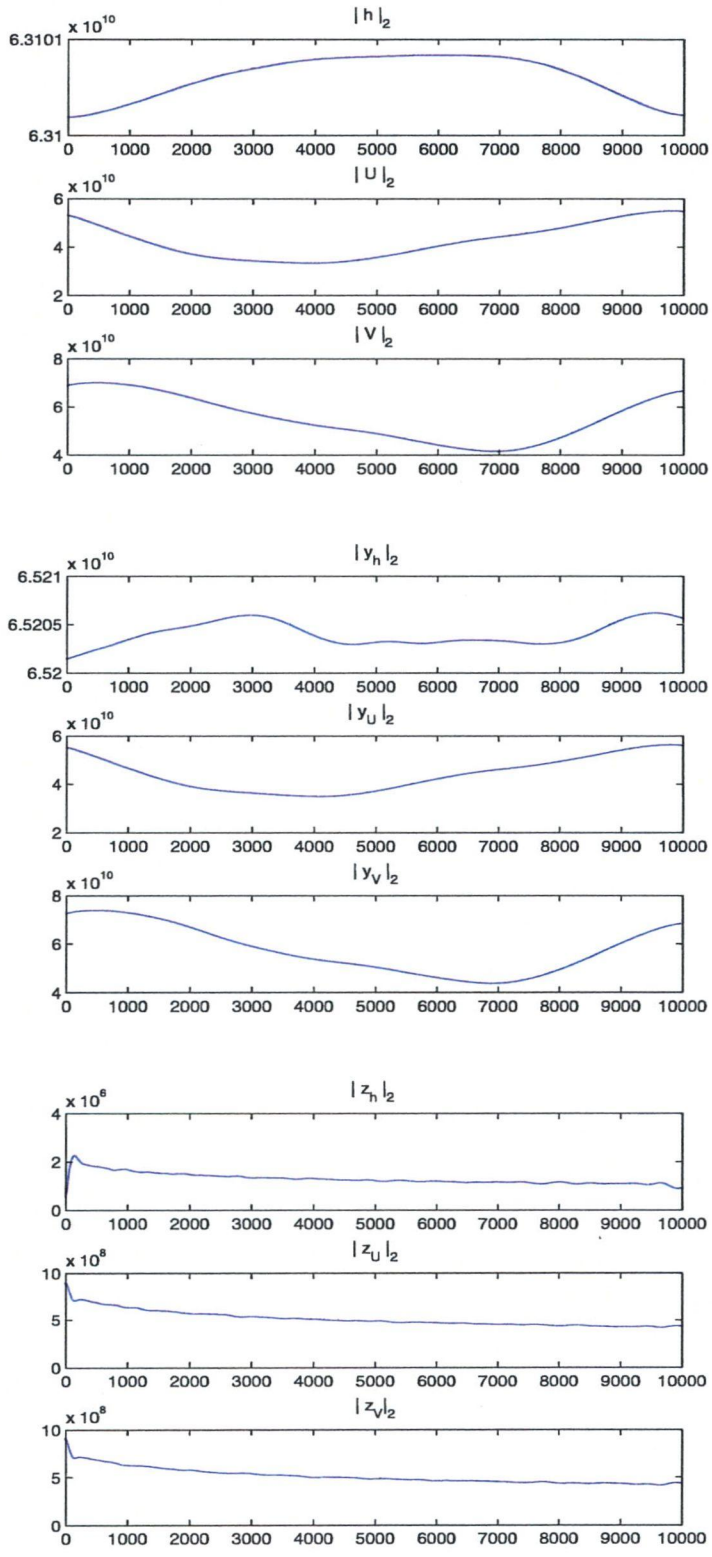

FIG. 4.22 – Time evolution of the discrete L^2-norms of the conservative variables.

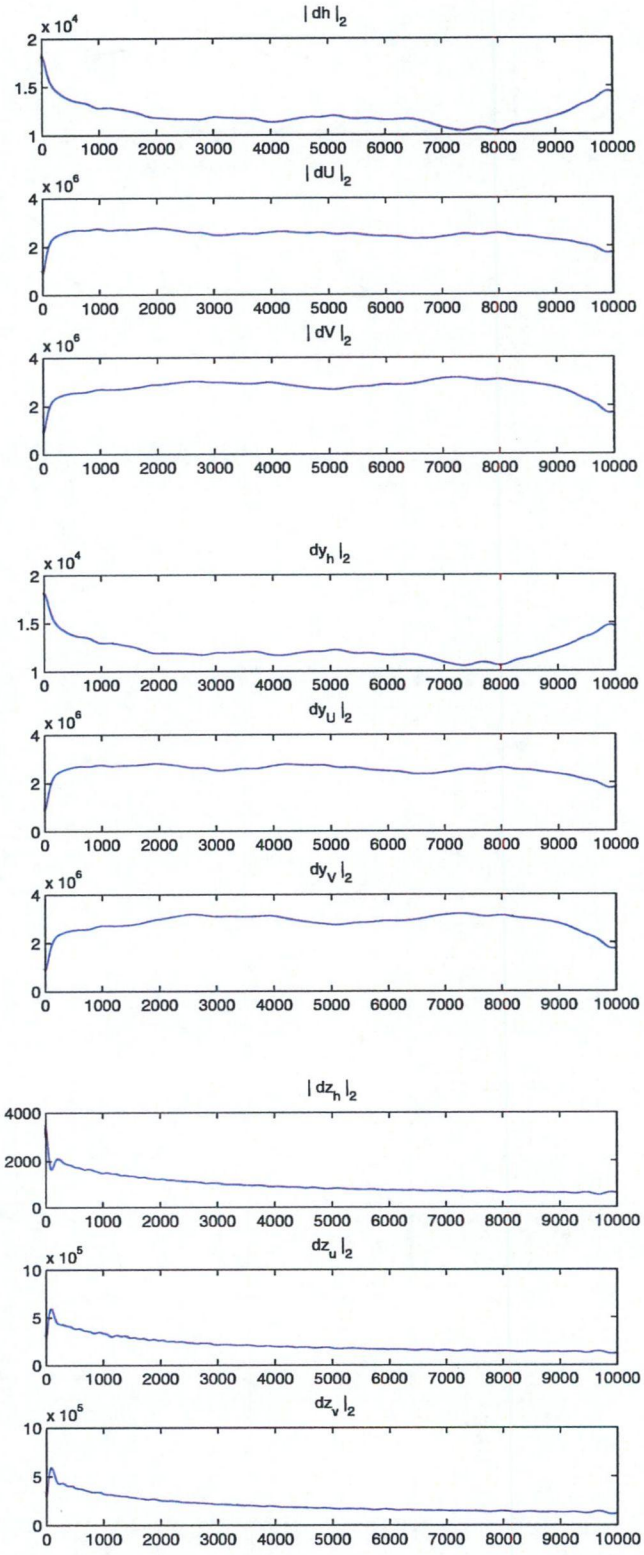

FIG. 4.23 – Time evolution of the discrete L^2-norms of the variations of the conservative variables.

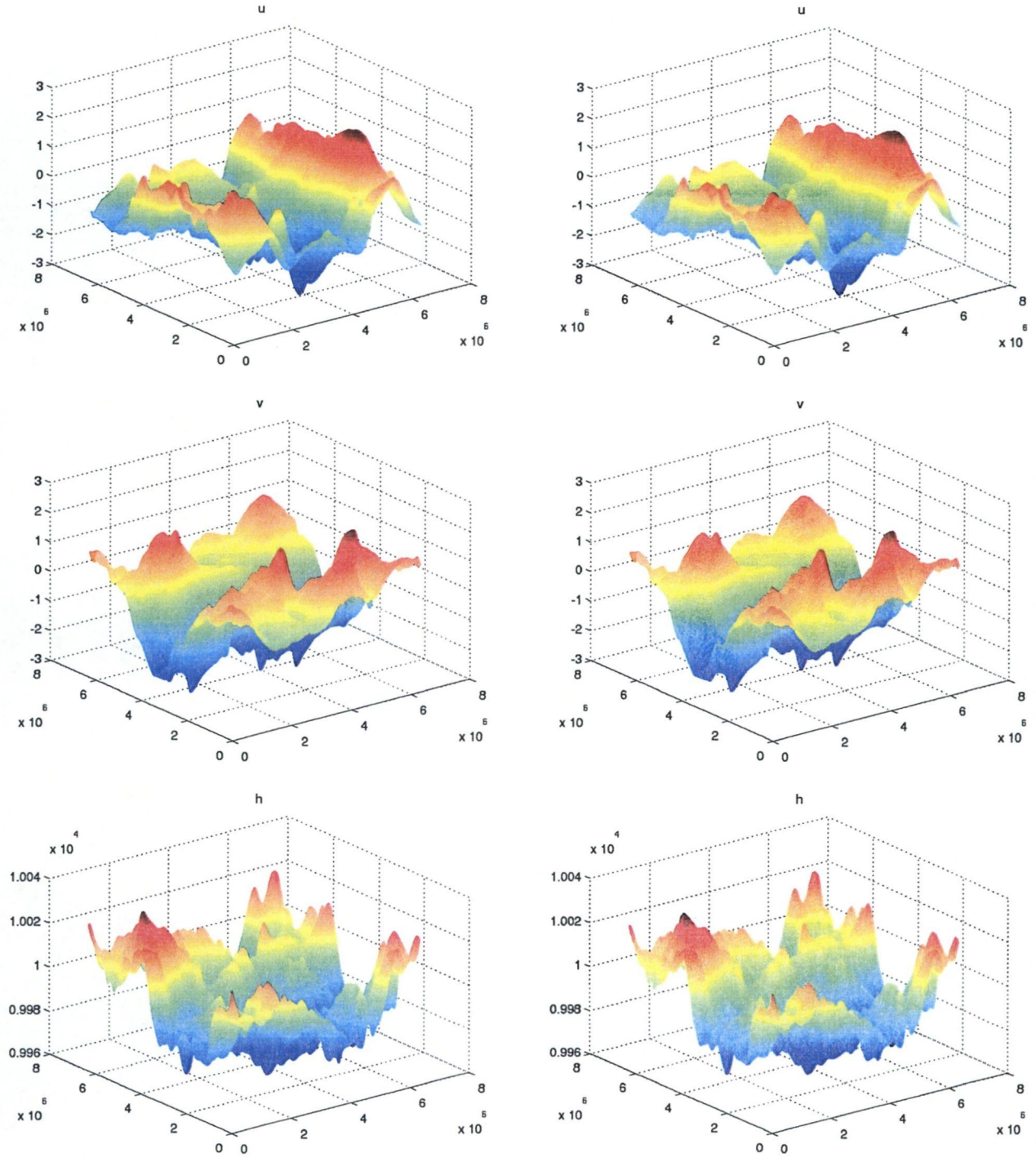

FIG. 4.24 – The reference solutions (left) and the solutions obtained with the multilevel method at 37% (right) at $t = 10000$.
; they show the quality of the resolution.

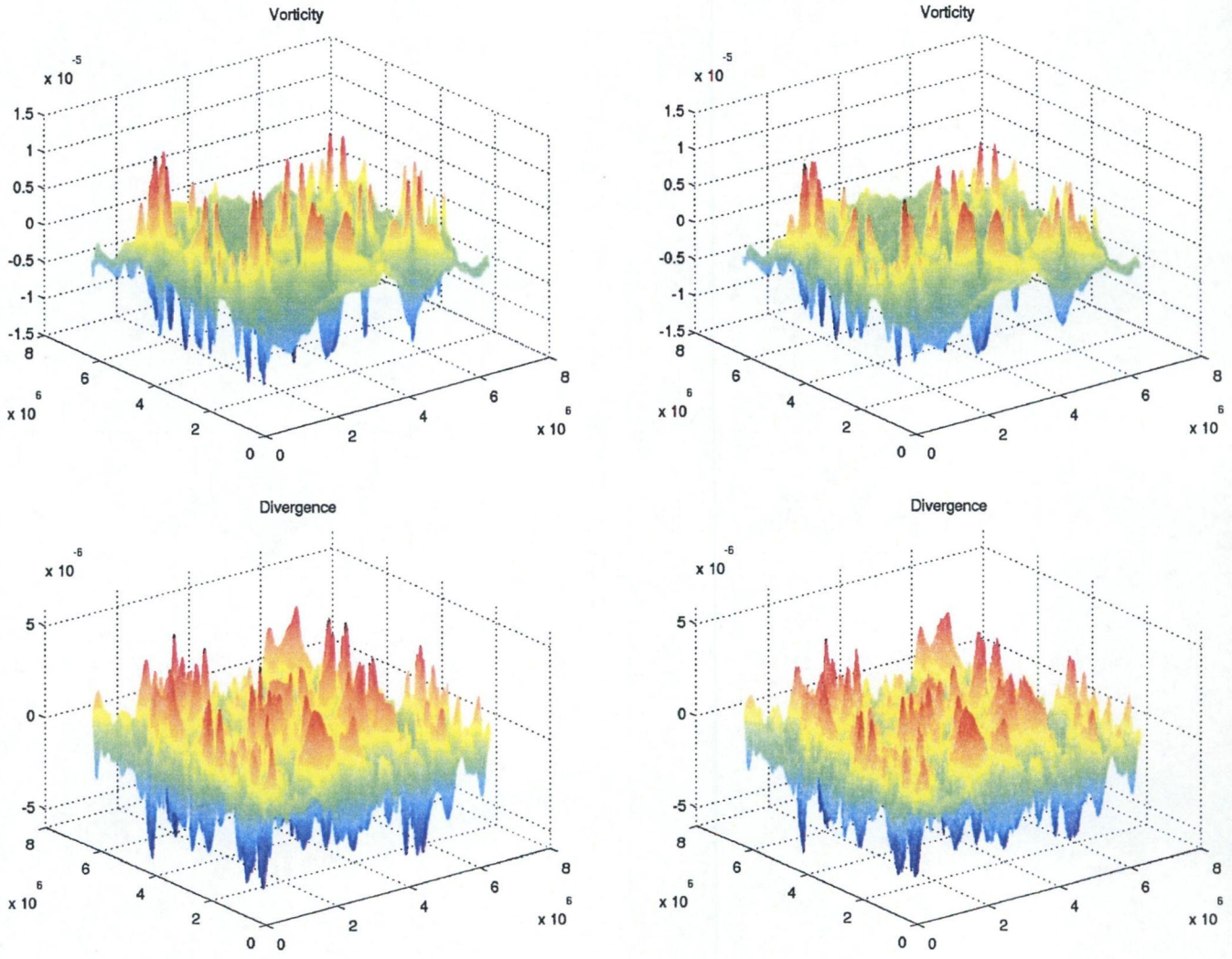

FIG. 4.25 – Reference (left) and multilevel (right) vorticity and divergence at $t = 10000$.

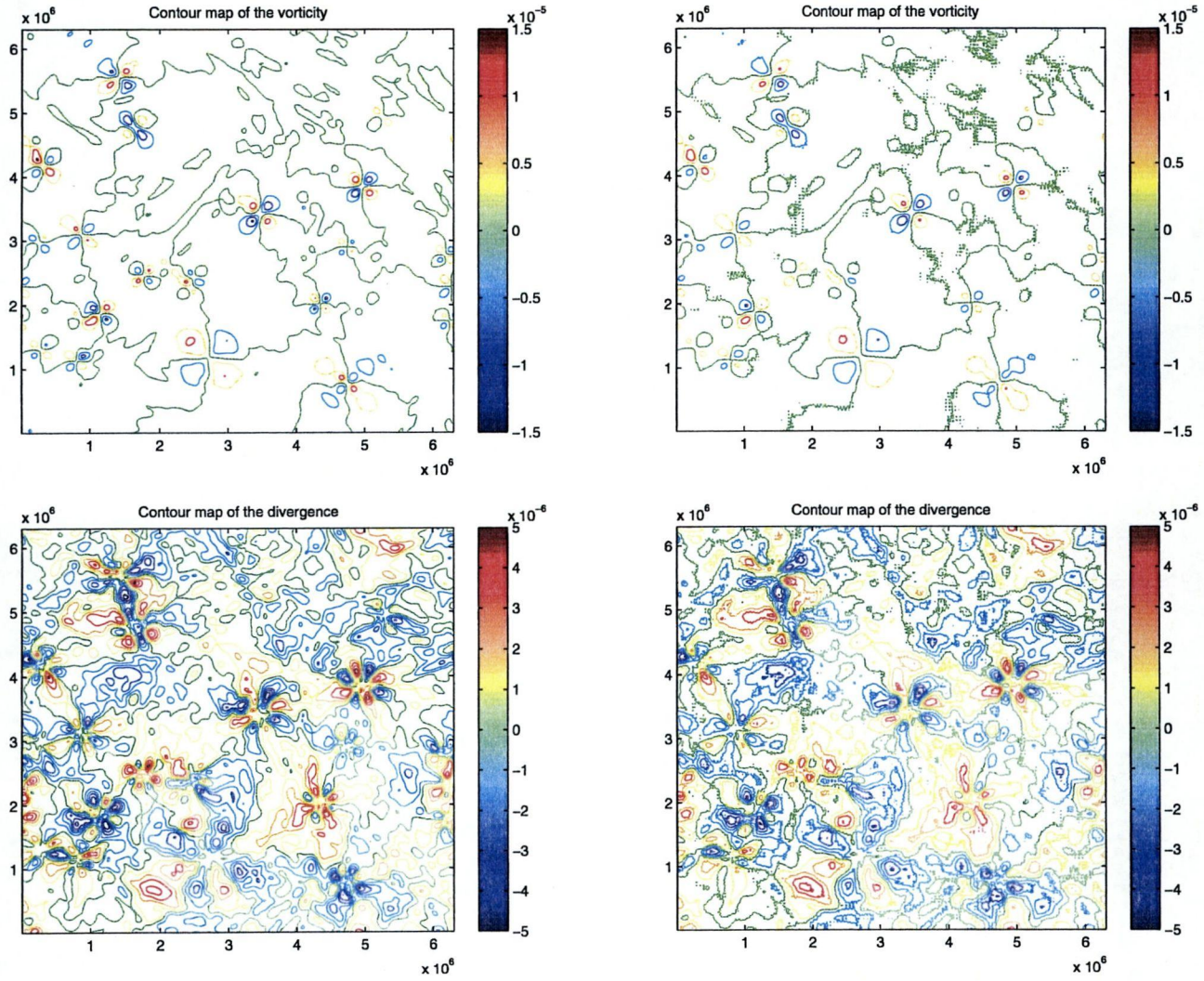

FIG. 4.26 – Contour maps of the reference (left) and multilevel (right) vorticity and divergence at $t = 10000$.

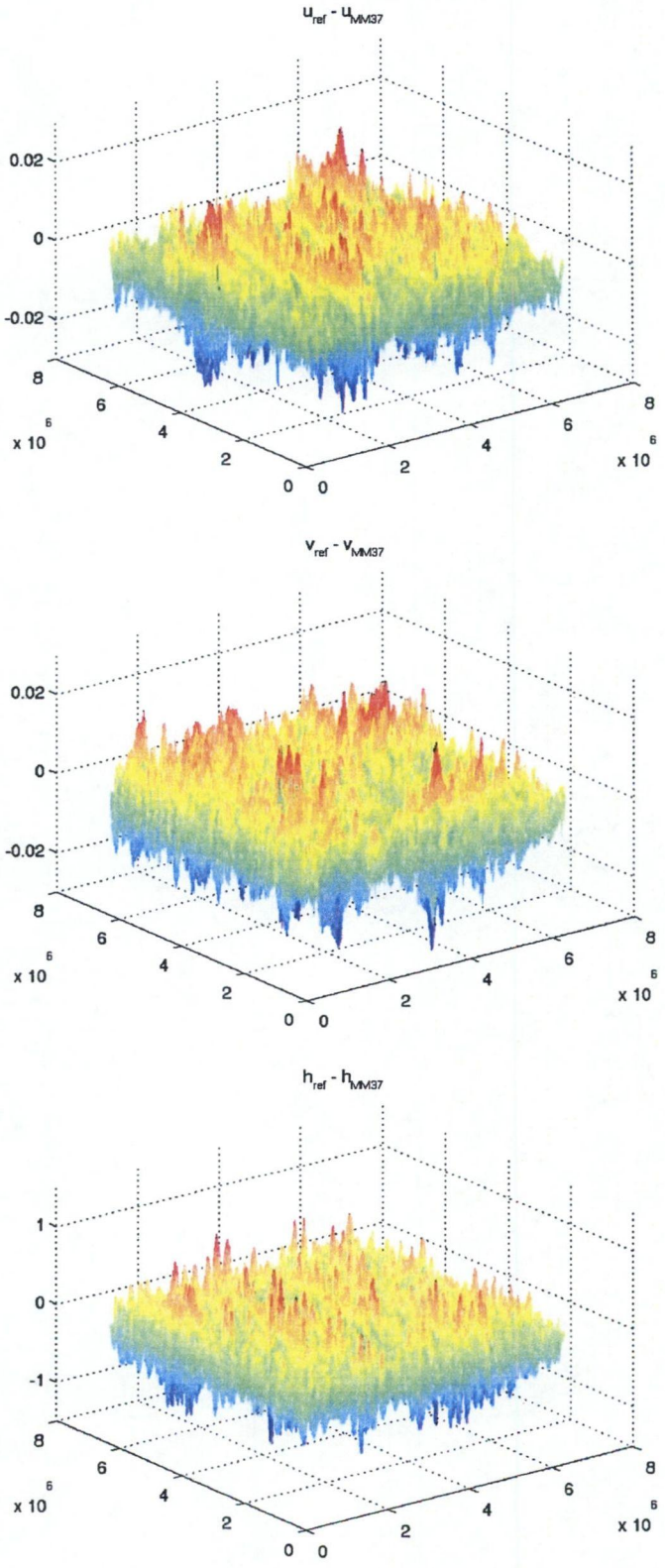

FIG. 4.27 – Differences between the reference and the multilevel solutions at $t = 10000$.

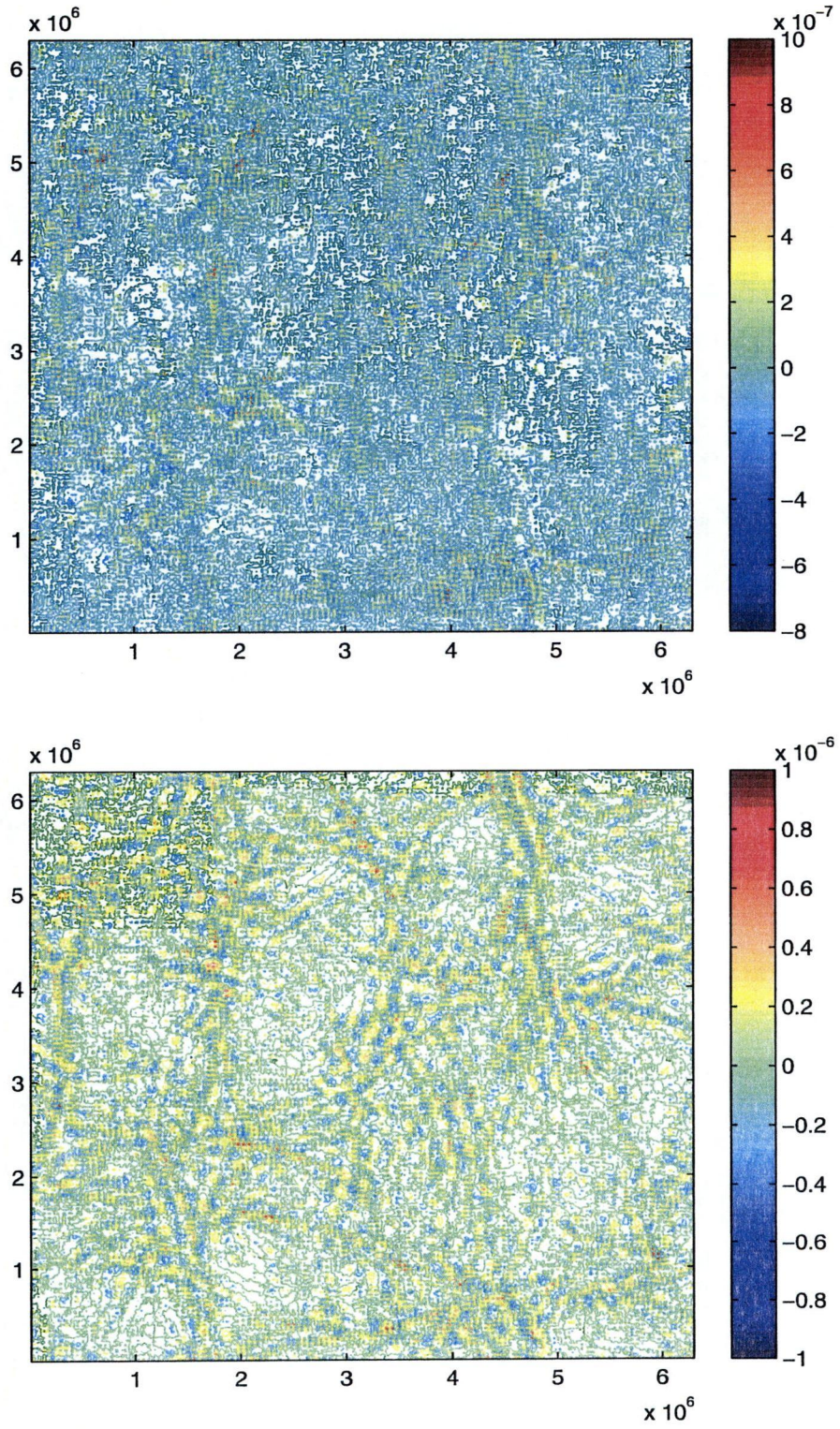

FIG. 4.28 – Contour maps of the difference between the reference and multilevel vorticity and divergence at $t = 10000$.

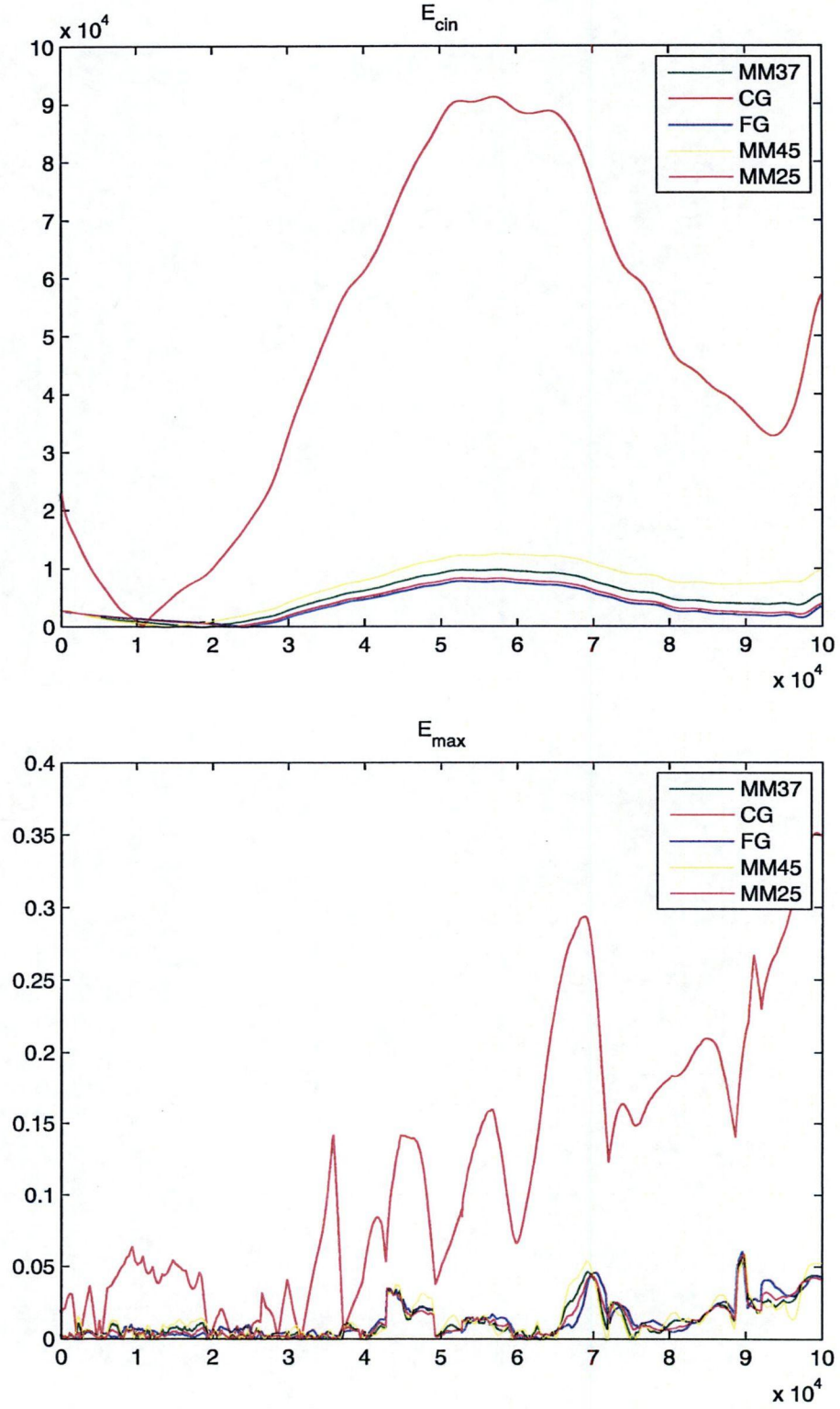

FIG. 4.29 – Evolution of the errors made on the kinetic energy and on the maximum velocity with the multilevel method at 37% (MM37), 45% (MM45) and 25% (MM25), and with the computation on the coarse grid (CG).

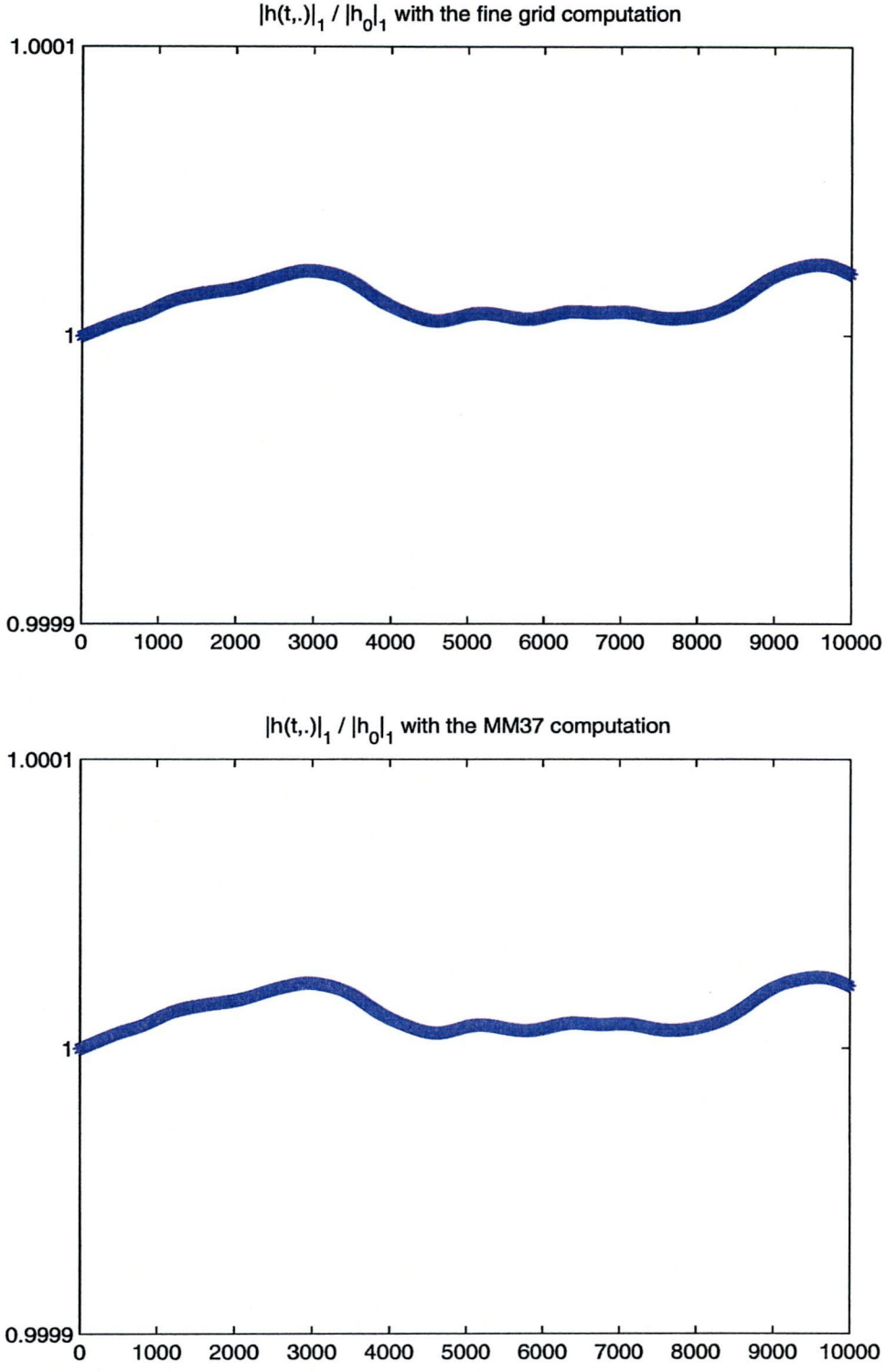

FIG. 4.30 – Evolution of $N_h = \int_{\mathcal{M}} h / \int_{\mathcal{M}} h_0$ during a resolution with the fine grid computation (up) and with the multilevel method at 37% (down).

A three-level simulation

Finally we employ the multilevel method on three levels of discretization for the resolution of this problem. The fine mesh counts 810×810 control volumes, the intermediate mesh 270×270 control cells, and the coarse mesh 90×90 cells. We first make a few iterations on the fine mesh and then repeat as before different cycles of length 40 which determine the level of discretization :

- a multilevel simulation at 10% with cycles of the form : 1..123321..1.
- a multilevel simulation at 15% with cycles of the form : 1..12333321..1.
- a multilevel simulation at 25% with cycles of the form : 1..122333333221..1.

In Figure 4.4.2 are shown the scheme followed for these different cycles.

For these different computations the resolution remaines very accurate : we compare the errors

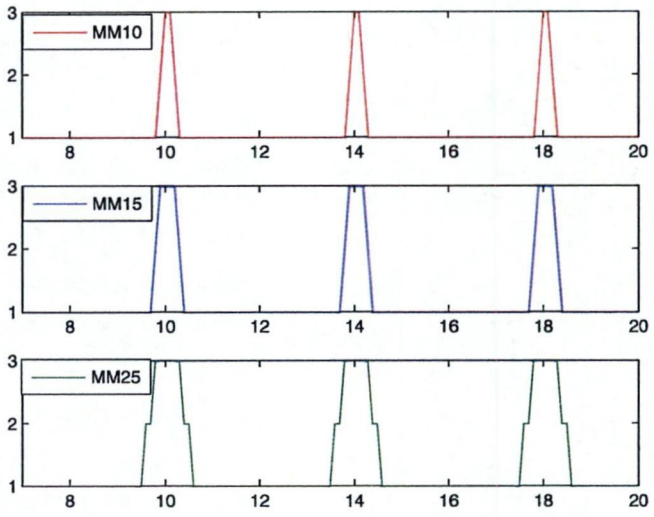

made on E_{cin} and E_{max} with the multilevel methods, the computation on the coarse grid, and the computation on the intermediate grid in Figures 4.31. These errors are evaluated in comparison to the values obtained with the fine computation. The errors made with the above multilevel methods are all largely under the errors corresponding to the coarse and to the intermediate grid.

An iteration on the coarser grid (90×90) is here really faster than an iteration on the fine grid (810×810) ; as a result the gain in CPU time is here very important with the multilevel computations : we observe a gain of 19% with the multilevel method at 10%, a gain of 26% with the method at 15% and a gain of 29.5% for the method at 25%. The multilevel computations are thus here very efficient since they provide a very good resolution and are really faster than the computation on the fine grid. The different CPU times and the gains observed are shown in Table 4.3 along with the percentage of CPU time spent for the iterations on the fine grid (% IFG) and on the coarse and intermediate grids (% ICG).

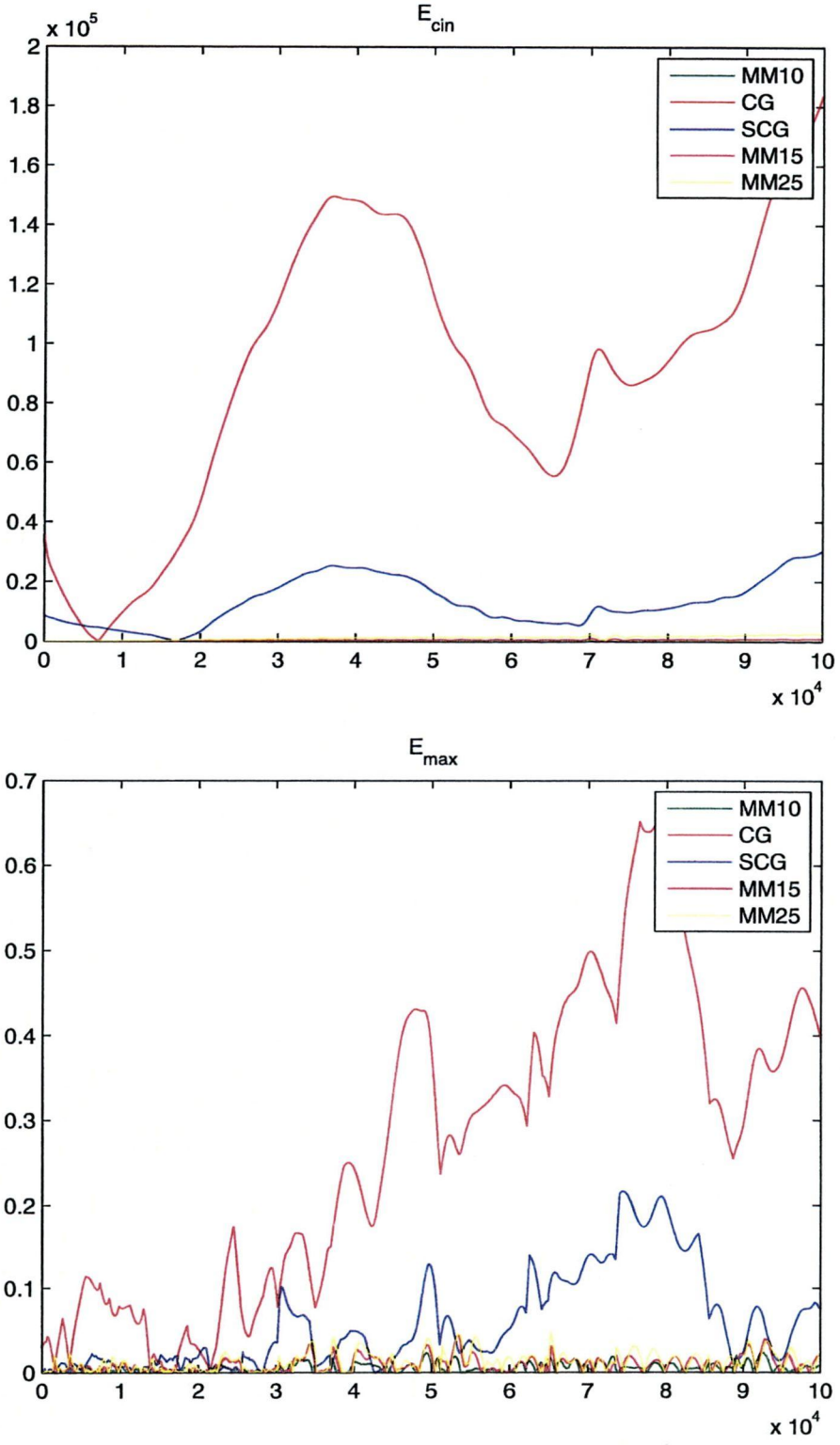

FIG. 4.31 – Evolution of the errors made on the kinetic energy and on the maximum velocity with the multilevel method at 10% (MM10), 15% (MM15) and 25% (MM25), and with the computation on the coarse grid (CG) and on the intermediate grid (SCG).

TAB. 4.3: Comparison of the CPU times consumed with a computation on the fine grid and with multilevel methods with different cycles.

Method	*CPU Time*	*Gain in %*	%IFG	% ICG
FG	81h50	-	92.5%	0%
MM10	66h20	19%	86.7%	4.8%
MM15	60h40	26%	85.1%	6.2%
MM25	57h45	29.4%	77.7%	11.8%

4.4.3 Concluding remarks

In this article we have implemented and studied a multilevel method for the resolution of a hyperbolic system of conservation laws : the Shallow Water equations. We introduced new incremental unknowns which enable to preserve the conservativity of the schemes. The numerical simulations show that the method remains accurate while enabling to decrease the time of resolution when up to a certain number of iterations are spent on the coarse grid. The method shows its best performance for simulations requiring a small space step and very fine meshes. It could be applied at its most efficiency by using a criterion, depending on the problem to be solved (see Section 4.4.1). An improvement of this method could also be done by applying it locally in the spatial domain. These ideas are left to future work.

Acknowledgments : The authors wish to thank T. Dubois and F. Jauberteau for their helpful advice and for making the initial data for the second test case available to them.

4.5 Appendix : Direct recomposition of the variables and recomposition with zero small scale components.

After an n^{th} iteration on the coarse level has been done, the conservative variables h^{n+1}, U^{n+1} and V^{n+1} are recomposed with their small and large scale components y^{n+1} and z^n through the formula described in Definition 4.3.1. We explain here the importance of the small scale components in this recomposition, despite their smallness.
Indeed if the variables are recomposed in the following way :

$$Q_m^n = Q_e^n = Q_w^n = Q_{se}^n = Q_{sw}^n = Q_{ne}^n = Q_{nw}^n = Y_M^n,$$

the results are disastrous, the errors made with the multilevel method with such a recomposition rapidly completely run over the errors made with a computation on the coarse level and some steps appear on the solutions and spoil them. We present in Figure 4.32 the comparison of the errors made with the multilevel method at 37% using this recomposition and made with the computation on the coarse grid (100×100) for the example presented in section 4.1.1.

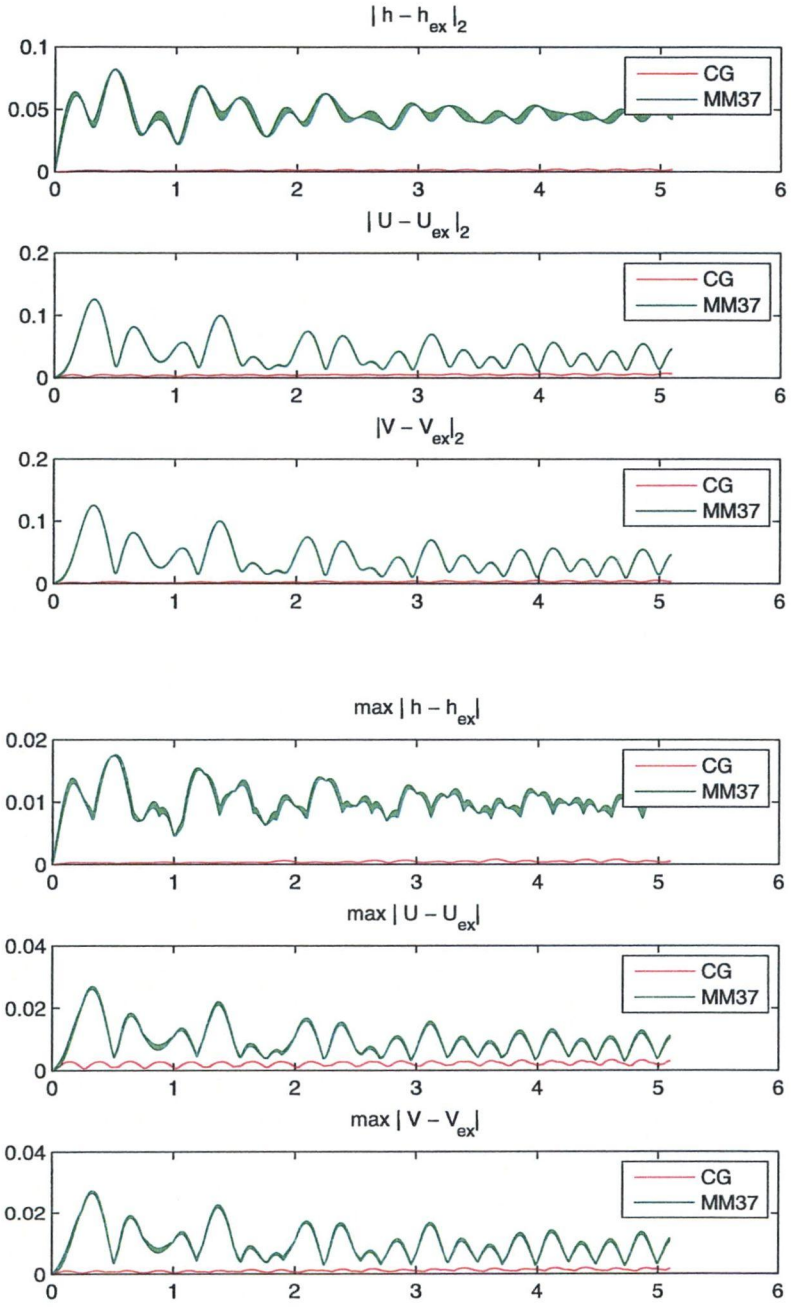

FIG. 4.32 – Time evolution of $||h-h_{ex}||_2$, $||U-U_{ex}||_2$, $||V-V_{ex}||_2$ and of $||h-h_{ex}||_\infty$, $||U-U_{ex}||_\infty$, $||V-V_{ex}||_\infty$ with the multilevel method at 37% (MM37) and the computation on the coarse grid (CG).

What also deserves to be outlined is the important role of the small components z in the multilevel algorithm. They are frozen during each iteration on the coarse cell and are small compared to the other variables; however when the recomposition of the variables is done with scale components equal to zero, the scheme exploses, which shows their crucial role.

Bibliographie

[1] E. Audusse, F. Bouchut, M-O. Bristeau, R. Klein, B. Perthame, A fast and stable well-balanced scheme with hydrostatic reconstruction for shallow water flows *SIAM J. Sci. Comput. 25*, 2004.

[2] E. Audusse, M-O. Bristeau, R. Klein, B. Perthame, Kinetic schemes for Saint-Venant equations sith source terms on unstructured grids *INRIA Report RR-3989*, 2000.

[3] C. Calgaro, J. Laminie, R. Temam, Dynamical multilevel schemes for the solution of evolution equations by hierarchical finite element discretization *Appl. Numer. Math. 23(4)*, 1997.

[4] J. P. Chehab, Incremental unknowns method and compact schemes *RAIRO Model. Math. Anal. Num. 32(1)*, 1998.

[5] M. Chen, R. Temam, Incremental unknowns for solving partial differential equations *Numer. Math. 59*, 1991.

[6] M. Chen, R. Temam, Incremental unknowns in finite differences : condition number of the matrix *SIAM J. Matrix Anal. Appl. 14(2)*, 1993.

[7] A. Debussche, J. Laminie, E. Zahrouni, A dynamical multi-level scheme for the Burgers equation : wavelet and hierarchical finite element *J. Sci. Comput. 25(3)*, 2005.

[8] T. Dubois, F. Jauberteau, R. Temam, Dynamic multilevel methods and the numerical simulation of turbulence *Cambridge University Press, Cambridge*, 1999.

[9] T. Dubois, F. Jauberteau, R. Temam, Incremental unknowns, multilevel methods and the numerical simulation of turbulence *Comput. Methods Appl. Mech. Engrg. 159(1-2)*, 1998.

[10] T. Dubois, F. Jauberteau, R. Temam, J. Tribbia, Multilevel schemes for the shallow water equations *J. Comput. Phys. 207*, 2005.

[11] R. Eymard, T. Gallouet, R. Herbin, Finite volume methods *in Handbook of numerical analysis VII, p.713-1020, North Holland, Amsterdam*, 2000.

[12] S. Faure, J. Laminie, R. Temam, Finite volume discretization and multilevel methods in flow problems, *J. Sci. Comput., 25(1-2)* , 2005.

[13] S. Faure, Méthodes de volumes finis et multiniveaux pour les équations de Navier-Stokes, de Burgers et de la chaleur, *Thèse de Doctorat.*

[14] T. Gallouët, J.M. Hérard, N. Seguin, Some approximate Godunov schemes to compute shallow-water equations with topography *Comput. Fluids 32(4)*, 2003.

[15] A. Kurganov, E. Tadmor, New high-resolution central schemes for nonlinear conservation laws and convection-diffusion equations, *J. Comput. Phys. 160*, 2000.

[16] A. Kurganov, G. Petrova, A third-order semi-discrete genuinely multidimensionnal central scheme for hyperbolic conservation laws and related problems *Numer. Math. 88*, 2001.

[17] A. Kurganov, S. Noelle, G. Petrova, Semidiscrete central upwind schemes for hyperbolic conservation laws and Hamilton-Jacobi equations, *SIAM J. Sci. Comput. 23, no3*, 2001.

[18] A. Kurganov, D. Levy, Central-upwind schemes for the Saint-Venant system,*M2AN, Vol.36, no3*, 2002.

[19] R. Temam, Inertial manifolds and multigrid methods *SIAM J. Math. Anal., 21(1)*, 1990.

[20] R. Temam, Multilevel methods for the simulation of turbulence. A simple model *J. Comput. Phys., 127(2)*, 1996.

Résumé

Cette thèse est composée de quatre chapitres traitant de l'étude théorique et numérique de deux systèmes de mécanique des fluides décrivant la propagation d'ondes de surface : le système de Saint Venant et un système de type Boussinesq.
Dans un premier chapitre intoductif nous présentons les deux systèmes étudiés et leur dérivation ainsi que les résultats obtenus durant la thèse.
Dans le deuxième chapitre nous exposons la résolution de problèmes aux limites sur la demi-droite et sur un intervalle fini pour le système de Boussinesq étudié. Un résultat d'unicité et la preuve de la persistance de réglarité finie pour les solutions du problème de Cauchy pour ce système sont également présentés.
Le troisième chapitre porte sur l'étude d'un problème aux limites pour les équations de Saint Venant bidimensionnelles linéarisées. Nous considérons des conditions aux bords périodiques dans la direction y et nous déterminons les conditions de Dirichlet en x qui rendent le problème bien posé.
Le quatrième chapitre traite de la résolution numérique du système de Saint Venant bidimensionnel à l'aide d'une méthode multi-niveaux basée sur un schéma aux volumes finis. La méthode est présentée puis analysée sur différents cas tests sur un domaine carré avec conditions aux limites périodiques ; elle est d'abord validée sur un test analytique puis expérimentée sur un cas test utilisé pour la simulation d'écoulements atmosphériques ou océaniques turbulents. La méthode s'avère fournir une résolution précise des problèmes tout en préservant la conservativité numérique et en réduisant le temps de calcul.

Mots clés : Système de Saint Venant - Systèmes de Boussinesq - Problèmes aux limites - Méthodes volumes finis - Méthodes multi-niveaux - Systèmes hyperboliques.

Abstract

This thesis is composed of four chapters which deal with the theoretical and numerical study of two systems coming from fluid mechanics which describe the propagation of surface waves : the Shallow Water system and a Boussinesq system.
In a first introduction chapter, we present the two systems and their derivation as well as the results obtained during the thesis.
In the second chapter, we expose in a second chapter the resolution of an initial boundary value problem on the semi infinite space and on a finite intervall for this Boussinesq system. A uniqueness result and the proof of the peristence of finite regularity for the solutions to the Cauchy problem are also presented.
The third chapter is dedicated to the study of a boundary value problem for the linearized two-dimensionnal Shallow Water equations.We consider periodic boundary conditions in the y direction and determine which Dirichlet boundary conditions are to be taken in the x direction to make the problem well posed.
The fourth chapter deals with the numerical resolution of the two-dimensionnal Shallow Water system with a multilevel method based on a finite volume scheme. The method is presented and analysed on different test cases on a square domain with periodic boundary conditions ; it is first validated on an analytical test case, then we experiment it on a test case which was used for the simulation of oceanic or atmospheric turbulent flows. The method tuems out to furnish an accurate resolution of the problems while preserving numerical conservativity and reducing CPU time.

Key words : Shallow Water system - Boussinesq systems- Boundary value problems - Finite volume methods - Multilevel methods - Hyperbolic systems.